UNIVERSITA' DEGLI STUDI DI NAPOLI

FEDERICO II

Chemical Science

XXVIII Cycle

Characterization and biological activity of bacterial glycoconjugates in cold adaptation.

Angela Casillo

Tutor: Prof. Maria Michela Corsaro

Supervisor: Prof. Angela Amoresano

Summary

Results

Colwellia psychrerythraea strain 34H

Psychrobacter arcticus strain 273-4

Pseudoalteromonas haloplanktis TAC 125

Experimental section

Abbreviations

AFGP	**Antifreeze glycoproteins**
AFP	Antifreeze proteins
Ala	Alanine
BacN	2,4-diamino-2,4,6-trideoxy-β-glucopyranose
BSCT-HMBC	Band-Selective Constant Time- HMBC
Cap	Cold acclimation proteins
Col	3,6-dideoxy-L-xylo-hexose
CPS	Capsular polysaccharide
CSP	Cold-shock proteins
DEPT-HSQC	Distortionless Enhancement by Polarization Transfer-Heteronuclear Single Quantum Coherence
DOC-PAGE	Sodium deoxycholate PolyAcrylamide Gel Electrophoresis
DQF-COSY	Double Quantum-Filtered Correlation spectroscopy
EPS	Extracellular polysaccharide
ESI FT-ICR	Electrospray Ionization Fourier Transform-Ion Cyclotron Resonance
Et_3N	Triethilamine
Gal	Galactose
GalA	Galacturonic acid
GalN	2-amino-2-deoxy-galactose
GC-MS	Gas chromatography-Mass spectrometry
GIST	Grid inhomogeneous sovation theory method
Glc	Glucose
GlcA	Glucuronic acid
GlcN	2-amino-2-deoxy-glucose
Gro	Glycerol
HMBC	Heteronuclear multiple bond correlation
HPLC	High Performance Liquid Chromatography
IM	Inner membrane
INA	Ice-nucleating agents
IRI	Ice Recrystallization Inhibition
IRMPD	InfraRed MultiPhoton Dissociation
Kdo	3-deoxy-D-*manno*-oct-2-ulosonic acid
LOS	Lipooligosaccharide
LPS	Lipopolysaccharide
MALDI	Matrix assisted laser desorption

Man	Mannose
MD	Molecular dynamics
MGA	Methyl glycoside per-acetylated
MLGS	Mean largest grain size
NAM	N-Acetylmuramic acid
NMR	Nuclear Magnetic Resonance
NOESY	Nuclear Overhauser enhancement spectroscopy
OM	Outer membrane
PCP	Phenol/Chloroform/Petroleum ethere
PHA	Polyhydroxyalkanoates
PHB	Poly(3-hydroxybutyrate)
PMAA	Partially Methylated Alditol Acetate
Qui2NAc	2-acetamido-2,6-dideoxy-D-glucose
Rha	Rhamnose
RMSD	Root mean squared difference
ROESY	Rotating frame Overhauser effect spectroscopy
ROS	Reactive oxygen species
SOD	Superoxide dismutase
SDS	Sodium dodecyl sulphate
TEM	Trasmission Electronic Microscopy
TFA	Trifluoroacetic acid
Thr	Threonine
TOCSY	Total correlation spectroscopy
TSP	3-trimethylsilyl-propanoate

Abstract

The cryosphere, covering about one-fifth of the surface of the Earth, comprises several components: snow, river and lake ice, sea ice, ice sheets, ice shelves, glaciers and ice caps, and frozen ground which exist, both on land and beneath the oceans (*Vaughan DG, et al. 2013*). All these habitats, combining the low temperature and the low liquid water activity, are challenging for all the forms of life (*Casanueva et al., 2010*). These extreme environments are inhabited by microorganisms of all three domains of life; in particular, cold-adapted microorganisms belong to *Archea* and *Bacteria* domains. To survive in these harsh life conditions, these microorganisms have developed many adaptation strategies, including the over-expression of cold-shock and heat-shock proteins, the presence of unsaturated and branched fatty acids that maintain membrane fluidity (*Chattopadhyay et al., 2006*), the different phosphorylation of membrane proteins and lipopolysaccharides (*Ummarino et al., 2003; Corsaro et al., 2004; Carillo et al., 2013; Casillo et al., 2015*), and the production of cold-active enzymes (*Huston et al., 2004*), antifreeze proteins (AFPs) and antifreeze glycoproteins (AFGPs), and cryoprotectants (*Deming et al., 2009*). Among cryoprotectants, carbohydrate-based extracellular polymeric substances (EPS) have a pivotal role in cold adaptation, as they form an organic network within the ice, modifying the structure of brine channels and contributing in the enrichment and retention of microrganisms in ice (*Krembs et al., 2002; Krembs et al., 2011; Ewert et al., 2013*).

Macromolecules belonging to the external layer are fundamental in adaptation mechanisms, as for example the lipopolysaccharides (LPSs), which constitute the 75% of the outer membrane. LPSs have a structural role since increase the strength of bacterial cell envelope and mediate the contacts with the external environment. The general structure of an LPS is characterized by three distinct portions: the lipid A, composed of the typical glucosamine disaccharide backbone with different pattern of acylation on the two sugar residues, the core oligosaccharide, distinguishable in a inner core and a outer core, and the O-chain polysaccharide built up of oligosaccharide repeating units. This latter moiety can be absent, and in that case LPSs are named lipooligosaccharides (LOSs).

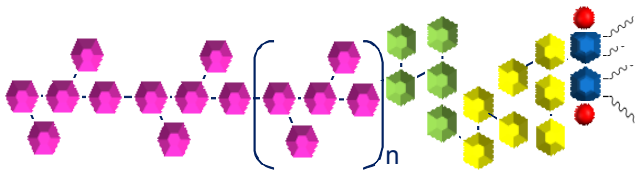

Schematic representation of a lipopolysaccharide.

Since the outer membrane of Gram-negative bacteria is constituted mainly by LPSs, it is reasonable to assume that structural changes could be present in these macromolecules isolated from cold-adapted bacteria.

This work has been focused especially on three different psychrophilic microorganisms, that are considered models for the study of adaptive strategies to subzero lifestyle:

- ✓ *Colwellia psychrerythraea* strain 34H
- ✓ *Psychrobacter arcticus* 273-4
- ✓ *Pseudoalteromonas haloplanktis* TAC125

In particular, LPS molecules from *C. psychrerythraea* 34H grown in different conditions, and from *P.arcticus*, have been purified and analyzed by NMR spectroscopy and mass spectrometry. By comparing the structures obtained, especially for core oligosaccharides, it is possible to speculate that all of them are characterized by high negative charge density. This negative charge is furnished either by phosphate groups, usually linked to Kdo and lipid A saccharidic residues, or by uronic acids. These characteristics have been already found in other LPSs from psychrophilic microorganisms (*Corsaro et al., 2004; Corsaro et al., 2008; Carillo et al., 2011*), suggesting that such structural elements contribute to the tightness of the outer-membrane and to the association of LPS molecules through divalent cations (Ca^{2+} and Mg^{2+}).

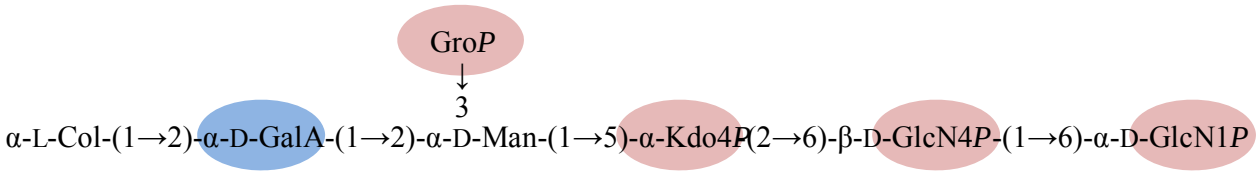

LOS structure from *C.psychrerythraea* 34H.

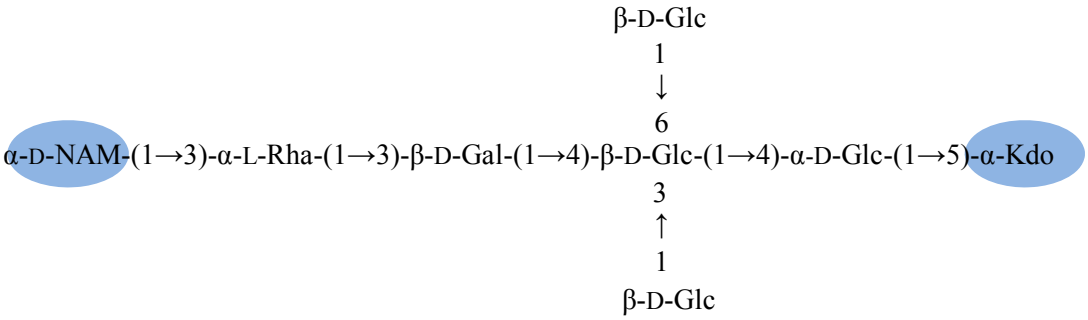

LOS from *P.arcticus* 273-4.

Starting from the core region of LOS from *C. psychrerythraea*, previously characterized (*Carillo et al., 2013*), the structure of lipid A was totally elucidated. The high heterogeneity of this structure, showed by the fatty acids analysis, was confirmed by the complexity of MS and MS/MS spectra. These experiments, indicated a variable state of acylation ranging from tetra- to hepta-acylated glycoforms. The lipid A moiety displayed a structure that is quite new among the LPSs. In fact, it shows the presence of unsaturated 3-hydroxy fatty acids, a feature that up to now is reported only for *Agrobacterium tumefaciens* (*Silipo et al., 2004*) and *Vibrio fischeri* (*Philips et al., 2011*). In particular, the structure of lipid A from *Colwellia psychrerythraea* 34H is very similar to that of *Vibrio fischeri*; in both structures, very intriguing is the presence of an unusual set of modifications at the secondary acylation site of the position 3 of GlcNI consisting of phosphoglycerol (GroP) differently substituted.

The structural characterization of different exopolysaccharides produced by *Colwellia psychrerythraea* have also been reported. The capsular polysaccharide structure from *C. psychrerythraea* is composed of a tetrasaccharidic repeating unit containing two amino sugars and two uronic acids. The unique characteristic of the capsular polysaccharide is the presence of the α-aminoacid, threonine as substituent (*Carillo et al., 2015*). The decoration of the polysaccharide with threonines is particularly intriguing to consider. In fact, amino acid motifs are common and crucial for the interaction with ice in several different kinds of antifreeze proteins (AFPs) and antifreeze glycoproteins (AFGPs) (*Graether et al., 2000*). Then, the molecular mechanic and dynamic calculations were performed, in collaboration with Prof. Randazzo of Department of Pharmacy; the computed model shows that the CPS seems to assume in the space a "zig-zag" flexible arrangement and that the overall structure can be imagined like a spatial repetition of an hairpin-like substructure, where the threonines are placed externally and available to interact with the ice.

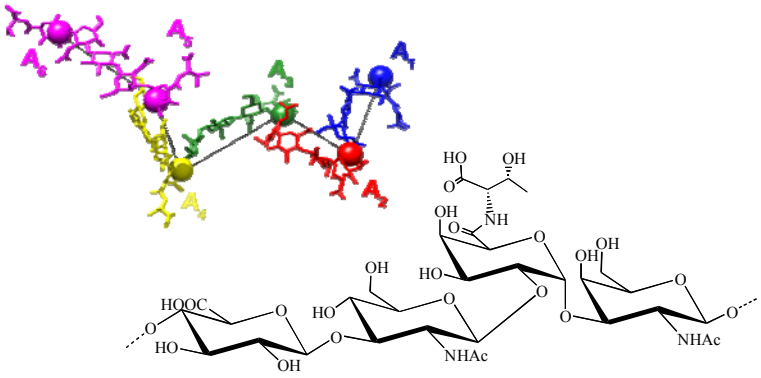

CPS structure from *C.psychrerythraea* 34H.

These results, the resemblance of our CPS structure to that of AFGPs, and the lack of sequence coding for a known AFP in the genome of *C. psychrerythraea* 34H prompted us to assay the purified polymer for ice recrystallization inhibition activity. This analysis, performed by Dr. Bayer-Giraldi, suggest that CPS interacts with ice and that it has an effect on recrystallization (*Carillo et al., 2015*). *Colwellia psychrerythraea* is also involved in the production of other two different exopolysaccharides (EPSs) with cryoprotectant activity: an acidic polysaccharide, named EPS, and a mannan. The EPS structure consists of a trisaccharidic repeating unit containing two galacturonic acids and one residue of 2-acetamido-2,6-dideoxy-D-glucose (Qui2NAc). Again, this structure shows the presence of an α-aminoacid, but in this case the decoration is represented by an alanine linked to the galacturonic acid residue. The chemical nature of the EPS is similar to that of the CPS, as it shows both *galacto-* and *gluco*-configured monosaccharides and aminoacids. Ice recrystallization inhibition activity, performed by Prof. Matthew Gibson, has been tested also for the EPS; the results show that also EPS has an effect on recrystallization, even if less marked with respect to the CPS.

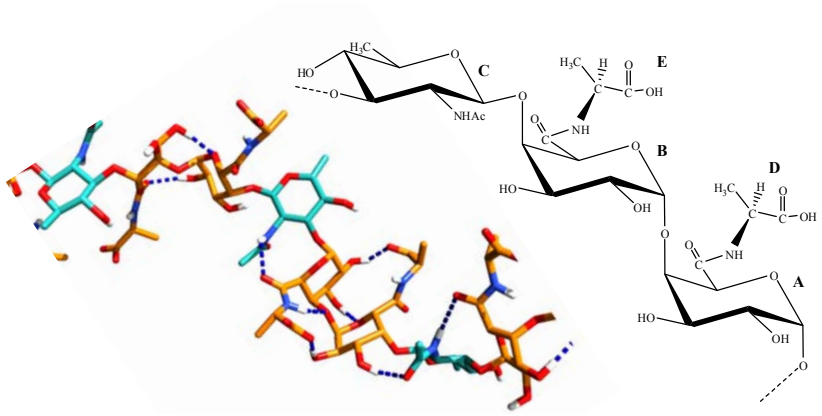

EPS structure from *C.psychrerythraea* 34H.

MD simulation was performed on a simplified model made up by five repeats of the trisaccharide basic unit and clearly revealed that the three central repeats adopt a fairly linear conformation that roughly resembles a left-handed helix. This conformation seems to be stabilized by a series of inter residue H-bond interactions. Of particular interest are three structural features: i) the amide nitrogen of quinovosamine, ii) the specific β-glycosidic linkage of this residue, and ii) the presence of the alanine attached to the galacturonic acid. The last exopolysaccharide produced by *C. psychrerythraea* at 4°C is a mannan, built up of a backbone of mannose α-(1→6) branched at C-2 with oligosaccharidic side chains, a common arrangement of mannans isolated from fungi and yeasts. The peculiarity of these structures is that some of these arms end with a β-glucose residue, and that some arms are cross-linked through phosphodiester bridges. The ice recrystallization inhibition assay showed that it is as active as the CPS produced by the same bacterium. Furthermore, *C. psychrerythraea* has been grown at two temperatures other than 4°C, in order to understand the variations, if any, in the structures of the saccharidic constituents. In particular, -2 and 8°C have been chosen.

The cells extraction confirmed the presence of a rough-LPS (LOS) and sugar analysis suggested that the saccharidic composition is identical to that of the LOS from *Colwellia* grown at 4°C; this result was also confirmed by the MALDI spectrum of the partially deacylated LOS (LOS-OH). In contrast, GC-MS analysis showed a different composition, with a different composition of 3-hydroxy fatty acids, thus suggesting some differences in the lipid A structure.

Furthermore, the presence of the CPS and EPS is confirmed when *Colwellia* is grown at 8 and -2°C, even if at these temperatures, the production of an additional polysaccharide (named CPS_2) has been observed. The last one consists of a trisaccharidic repeating unit and unlike the others, it is not decorated with amino-acids. Interestingly, this polysaccharide displays very low ice recrystallization inhibition.

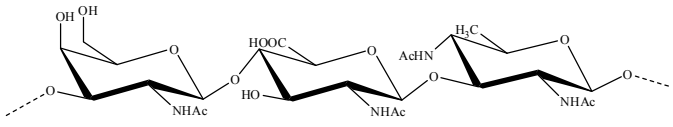

CPS_2 structure from *C.psychrerythraea* 34H.

Numerous prokaryotes, including *Colwellia psychrerythraea* 34 H, are able to accumulate large amounts of lipophilic compounds as inclusion bodies in the cytoplasm. Members of most genera synthesize polymeric lipids such as poly(3-hydroxybutyrate) (PHB) or other polyhydroxyalkanoates

(PHAs). These compounds represent an attractive "green" alternatives to conventional petroleum-based plastics, finding application in various fields. The production of PHAs from *C. psychrerythraea* 34H has been tested in different growth conditions; up to now, the best condition was obtained at 4°C and 72h after inoculation, with the accumulation of 10% PHB and 90% of 3-hydroxyhexanoate.

As *Colwellia psychreeythraea*, *Psychrobacter arcticus 273-4* is involved in the production of a mannan polysaccharide The ice recrystallization inhibition activity has been tested for this polymer, and compared to that of mannans produced by *C. psychreeythraea* and by the yeast *S. cerevisiae*, a commercial product. The activity for *Psychrobacter* is higher than *C. psychreeythraea*, while the mannan produced by the yeast was found to be completely inactive. Intriguingly, the yeast polymer differs from that of *P. arcticus* and *C. psychreeythraea* for the lack of t-Glc residue and phosphates, thus suggesting that these structural features may be connected with the lack of activity. *Psychrobacter arcticus* is known in literature for the production of a capsule, when grown in presence of high salt concentration, that could be an adaptation mechanism (*Ayala-del-Rio et al., 2010*). The preliminary purification, revealed that the capsule polysaccharide is produced in very low amount, thus suggesting that the growth conditions are not so appropriate. Then, it will be necessary to maximize its production in order to fully characterize the CPS.

The last cold-adapted microorganism, is *P. haloplanktis* TAC125, the cell-free supernatant of which presents an anti-biofilm activity against *S. epidermidis* (*Papa et al., 2013*). A purification procedure was set up and the analysis of an enriched fraction demonstrated that the anti-biofilm activity is due to a small molecule, that likely works as signal. The molecule, identified and compared with the corresponding standard, is new among those already reported in the literature.

Part of this PhD thesis was adapted from the following articles co-written by the author of the present thesis:

1. S. Carillo, et a., A unique capsular polysaccharide structure from the psychrophilic marine bacterium *Colwellia psychrerythraea* 34H that mimicks antifreeze (glyco) proteins *J. Am. Chem. Soc.* **2015**, 137(1), 179–189.

2. A. Casillo, et al., Structural Investigation of the Oligosaccharide Portion Isolated from the Lipooligosaccharide of the Permafrost Psychrophile *Psychrobacter arcticus* 273-4 *Mar. Drugs* **2015**, 13, 4539-4555.

3. E. Parrilli, et al., Anti-biofilm activity of *Pseudoalteromonas haloplanktis* TAC125 against *Staphylococcus epidermidis* biofilm: evidences of a signal molecule involvement? *Int. J. Immunopathol and pharmacol.* **2015**, 28(1), 104–113.

4. A. Casillo, et al., A cryoprotectant exopolysaccharide, decorated with alanine, from the marine psychrophilic *Colwellia psychrerythraea* 34H: a strategy for cold lifestyle. (*Submitted*)

Other papers not related to this thesis are:

1. M. Vastano, et a., Production of medium-chain-length polyhydroxyalkanoates from waste oils by recombinant *Escherichia coli Eng. Life Sci.* **2015**, DOI:10.1002/elsc.201500022.

2. E. Parrilli, et al., Large scale biofilm cultivation of Antarctic bacterium *P. haloplanktis* TAC125 for physiologic studies and drug discovery *Extremophiles* **2016**, DOI 10.1007/s00792-016-0813-2

3. C.Pezzella, et al., Production of bioplastic from waste oils by recombinant *Escherichia coli:* A Pit-Stop in Waste Frying Oil to Bio-Diesel conversion race. (*Submitted*)

4. I. Orefice, et al., Light induced changes in the photosynthetic physiology and biochemistry in the diatom *Skeletonema marinoi.* (*Submitted*)

Introduction

Chapter I

Microorganisms at the limits of life

In the fascinating world of microorganisms, the category of extremophiles is the most mysterious on planet Earth (*Rothshild et al., 2001*) and perhaps on other planets as well (*Navarro–Gonzales et al., 2003*). Normal survival may not be possible in environments characterized by extreme conditions of temperature, pressure, salinity, radiation etc.; instead due to extraordinary capacities, some organisms, mostly bacteria, archea and few eukaryotes, can thrive in this habitats. These organisms are called extremophiles (*Singh 2012*). For a long time, extremophiles were considered *terra incognita*, since the environments with aggressive parameters (compared to the human body temperature, pH, mineralization, and pressure) were considered *a priori* as a dead zone. It took time to find out that the environments with extreme physicochemical and climatic parameters are inhabited by a wide spectrum of different microorganisms. Extremophiles were the first representatives of life on Earth and are responsible for the genesis of geological structures during the evolution and for the creation of all currently know ecosystems. Flexibility of the genome probably allowed to adapt to a wide spectrum of extreme environments (*Pikuta et al., 2007*).
Extremophiles, depending on their optimal growth conditions, are named thermophiles, psychrophiles, acidophiles, alcalophiles, halophiles and barophiles. At present, extremophilic microorganisms are exciting thematic of research, both in basic and applied research.

1.1 Psychrophiles

Much of life on Earth has evolved to colonize low-temperature environments. In fact, at temperatures permanently below 5°C, the cold biosphere represents by far the largest fraction of the global biosphere (*Siddiqui et al., 2013*). Permanently cold environments cover about one-fifth of the surface of the Earth including terrestrial ice sheets of Antarctica and Greenland, mountain glaciers and sea ice in Antarctic and Arctic Ocean (Figure 1.1). Sea ice covers a larger area of the Earth than glaciers, approaching 10% of the ocean's surface, but with an average thickness of only 2–3 meter, the global volume of sea ice is much lower than that of the glacial environment.

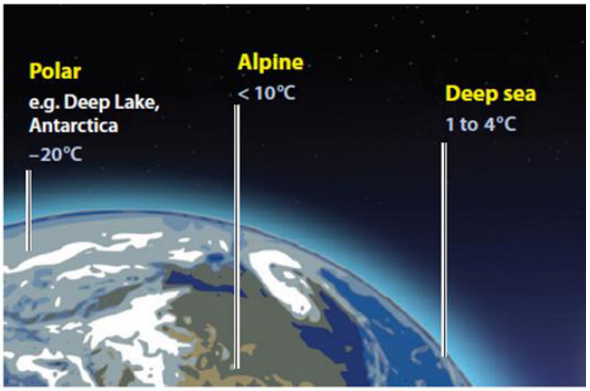

Figure 1.1: Terrestrial cold environments. Representative temperatures are shown.

In these environments, the temperature plays a critical role in the selection and survival of a variety of organisms such as bacteria, archea, yeasts, algae, insects, fishes and plants. These cold-adapted organisms are termed psychrophiles or cold-loving. The term psychrophile (from Gk *psychros* meaning cold and *philes* meaning loving) was first used by Schmidt-Nielsen in 1902 (*Morita 1975*). For many years, cold-adapted organisms have been classified into two partially overlapping groups: psychrophiles, having minimum, optimum and maximum growth temperature at or below 0°C, 15°C and 20°C, respectively, and psychrotolerant, with growth maximum temperature above 25°C, but with the capacity to grow to very low temperatures (*Morita 1975*). Recently, among the additional definition proposed, such as "moderate psychrophiles" (*Helmke et al., 2004*), and "psychro-active" (*Laucks et al., 2005*), the terms "eurypsychrophiles" and "stenopsychrophiles" have been favored (*Feller et al., 2003; Bakermans et al., 2004; Cavicchioli 2006*). Stenopsychrophile, formerly "true psychrophile", refers to a microorganism with a restricted growth-temperature range; in fact they are most frequently isolated from thermally stable cold marine environments. Eurypsychrophile, formerly psychrotolerant, describes a microorganism that prefers cold permanently environment, but can also tolerate a wide range of temperature reaching up into the mesophilic range; these microbes dominate, in fact, cold terrestrial ecosystems (*Helmke et al., 2004*). The genomic differences in cold adaptation between stenopsychrophiles and eurypsychrophiles have yet to be thoroughly investigated (*Bakermans et al., 2004*). However, this distinction is ignored at present and all the cold-tolerant bacteria could be dubbed as psychrophiles (*Chattopadhyay et al., 2014*).

Cold adaptation of microorganisms is the result of intrinsic genome-wide changes that facilitate the growth at low temperatures. Comparative studies of cold-adapted microorganisms are beginning to reveal which adaptations are common to all the psychrophiles and which are specific to the

particular environment each psychrophile inhabits. Cold marine environments are distinctly different from cold terrestrial environments like permafrost; marine environments tend to have high thermal stability as well as stable solute concentrations, while terrestrial environments do not. Consequently, genomic analysis of microorganisms isolated from marine environments likely reflects adaptations to stable low temperatures, while from terrestrial environments may reveal unique mechanism of cold adaptation related to heterogeneous environmental chemistry due to the extreme temperatures fluctuations.

Ecological limiting factors, such as nutrient and water availability, salinity, pressure, UV irradiation and temperature, are all characteristics of cold environments. Psychrophilic microorganisms in glacial ice are restricted to small amounts of unfrozen water inside the permafrost soil or the ice, and to brine channels. In some terrestrial habitats, these stresses dictate that psychrophilic communities develop niches, not only in brine channels, but also frequently associated with lithic habitats, such as cryptoendolithic and chasmolithic environments (*De Maayer et al., 2014*).

1.2 Molecular and physiological adaptation

Cold temperatures impose severe physicochemical constrains on cellular function by negatively influencing cell integrity, water viscosity, solute diffusion rate, membrane fluidity and macromolecular interactions (*De Maayer et al., 2014*). The ability of an organism to survive and grow in cold conditions is therefore dependent on a various number of adaptive strategies (Figure 1.2). The analysis of numerous psychrophilic genomes and metagenomes has indicated the presence of a large number of features contributing to genome plasticity, such as plasmids, transposable and other mobile genetic elements. One of the most obvious disadvantages of life at very low temperatures is the low rates of catalysis: psychrophilic enzymes must therefore be suitable adapted to maintain adequate catalytic rates for cellular function. These enzymes are generally characterized by higher flexibilityand lower thermostability than their mesophilic counterparts. One of the strategy is to reduce the content of amino acids such as arginine and proline; the last ones are involved in the formation of multiple hydrogen bonds and salt bridges and reduce the conformational flexibility.

Following a downshift of temperature from 37°C to 10°C in mesophilic *E. coli*, the synthesis of most of the cellular proteins is repressed for a lag period of 4–5 h. Among these proteins, the most prominently up-regulated genes are those encoding cold-shock proteins (CSPs), a family of small,

single-stranded nucleic acid binding proteins that regulate a variety of cellular process including transcription, translation, protein folding and membrane fluidity (*De Maayer et al., 2014*). These stress proteins have been found to occur both in mesophilic and psychrophilic bacteria. A second class of proteins, called cold acclimation proteins (Caps), is found to be constitutively expressed in psychrophilic bacteria while in mesophiles are expressed in response to cold exposure. The CSPs are believed to facilitate transcription and translation at low temperature in the mesophilic bacteria. However, the exact role of CSPs in cold adaptation of psychrophiles is yet to be elucidated (*Chattopadhyay 2006*).

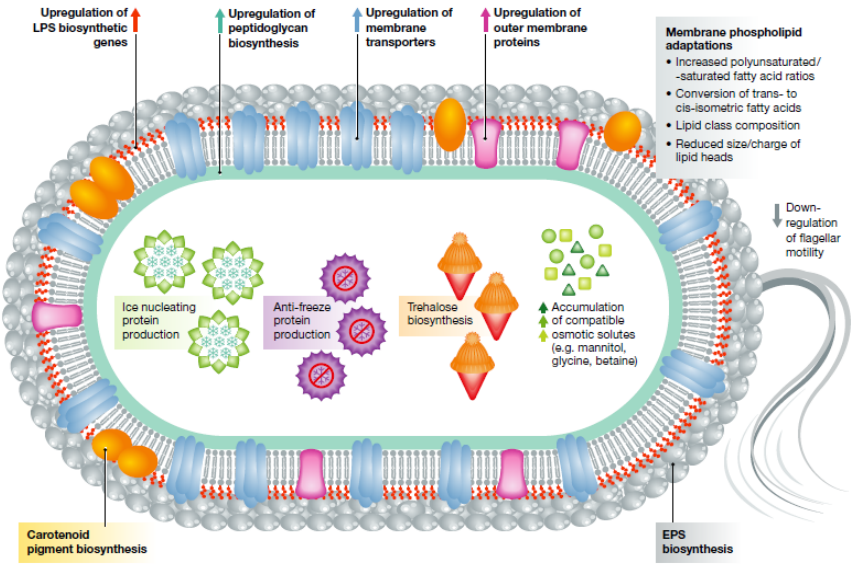

Figure 1.2: Common physiological adaptations in a psychrophilic prokaryote.

Furthermore, the increased solubility of oxygen at low temperatures poses an increased risk from reactive oxygen species (ROS), and different approaches seem to be involved in protecting against free radical damage. *C. psychrerythraea* contains three copies of catalase genes as well as two different superoxide dismutase (SOD) genes, one of which is a nickel-containing SOD never before reported in proteobacteria (*Methe´ et al., 2005*).

It has long been known that one of the most significant impacts of low temperature is on membrane fluidity, essential for its structural integrity and for the cellular functionality. In fact, recent transcriptome analyses have shown that exposure to cold temperatures induces a rapid up-regulation of genes involved in membrane biogenesis, such as fatty acids and LPS biosynthesis, peptidoglycan and outer membrane proteins biosynthesis (*De Maayer et al., 2014*). The lipid composition governs the physical properties of the membranes and hence it is not surprising that this varies with the thermal habitat of the microorganism. In general, a reduction in temperature lead to a higher content

of unsaturated, polyunsaturated and methyl-branched fatty acids, and/or a shorter acyl-chain length. This altered composition is thought to have a key role in increasing membrane fluidity by introducing steric constrains that change the packing order to reduce the number of interaction in the membrane. Lipopolysaccharide (LPS) is a constituent of the bacteria outer membranes that forms a protective barrier around the cell, and is reported that its synthesis is induced by the lowering in temperatures. Some of the genes encoding for enzymes involved in the LPS biosynthesis, as lipopolysaccharide biosynthesis polimerase and lipid A biosynthesis acyltransferase (LpxP) were induced (*Gao et al., 2006*). It is believed that the induction of LpxP is related to the function to enhance the outer membrane fluidity after cold shock with the acylation of lipid A with palmitoleate instead of laureate (*M. Carty et al., 1999*). Carotenoid pigments represent another class of membrane fluidity modulators. Both polar and non-polar pigments are produced by Antarctic bacteria and have been postulated to buffer membrane fluidity and assist maintaining homeoviscosity during temperature fluctuations (*De Maayer et al., 2014*).

One of the main consequences of lowering temperature is the formation and the propagation of cytoplasmic ice crystals, resulting in the destruction of membranes, gas bubbles formation and organelles disruption, determining a total cellular damage (*Fuller 2004*). Psychrophilic microorganisms display the expression of compatible solutes biosynthesis - glycine, betaine, sucros, threalose e and mannitol- during growth at low temperature. Compatible solutes act globally and not specifically, allowing the microorganisms to occupy broader thermal niches and to react quickly to changes in temperature (*Chin et al., 2010*). In particular, the threalose disaccharide may prevent the denaturation and aggregations of proteins, scavenge free radicals and stabilize cellular membranes. To contrast low temperatures, some species of fungi, bacteria, plants and insects produced Antifreeze proteins (AFP) and glycoproteins (AFGPs), also known as thermal hysteresis proteins (Figure 1.3). These possess the ability to inhibit the formation of ice and can lower the freezing temperature of a solution non-colligatively without affecting its melting temperature. A typical AFGP consists of repeating tri-peptide units, the alanyl-alanyl-threonyl (Ala-Ala-Thr)*n* unit, connected to the disaccharide β-D-galactosyl-(1→3)-α-D-*N*-acetylgalactosamine through a glycosidic bond at the second hydroxyl group of the threonine residue, while AFPs possess very different primary, secondary, and tertiary structures (*Bung et al., 2013*).

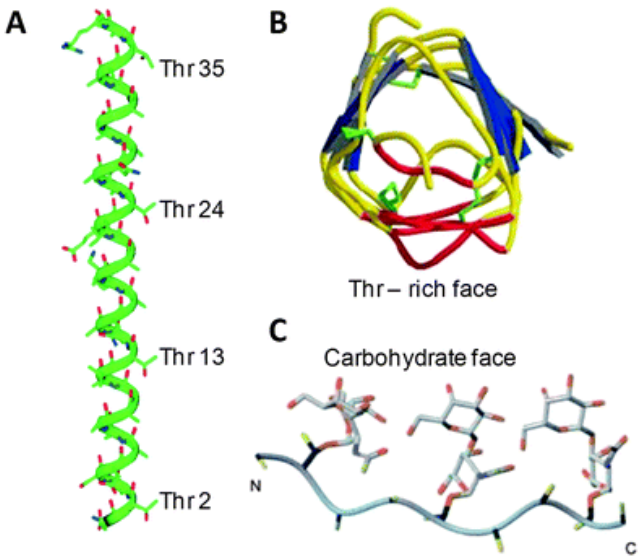

Figure 1.3: 3D structures of antifreeze-active peptides/proteins. (A) X-Ray crystal structure of HPLC 6; (B) X-Ray crystal structure of spruce budworm AFP; (C) Energy optimized solution structure of AFGP mimetic peptide. (Gibson, Polym. Chem., 2010, **1**, 1141-115)

Moreover, is known that some bacteria produce ice-nucleating agents (INAs) that serve as templates for ice crystallization and provide resistance to desiccation. (*Margesin et al., 2007*). Sea ice through its seasonal lifetime is recently known to hold high concentrations of sugar-based exopolymers in its liquid brine inclusions. These exopolysaccharides (EPSs) are understood to serve as natural cryoprotectants not only against potential ice-crystal damage, but also by further depressing the freezing point of the liquid water remains available within the ice matrix (*Marx et al., 2009*). The ability of a microorganism to surround itself with a highly hydrated shell helps to buffer the cell against the osmotic stress of high salt concentrations, may provide it with protection against desiccation, and predation by protozoans (*Kumar et al 2007*). Therefore, EPSs are essential in the aggregate formation, in the mechanism of adhesion to surfaces, in the uptake of nutrient and in the formation of biofilm (*Poli et al., 2010*). EPS is a common component of biofilm and its production is an important feature of the mature biofilm (*Fux et al., 2003*). In addition, EPSs form the matrix that embeds the bacteria, where additional free bacteria can be entrapped (*Costerton et al.,1995; Bianciotto et al., 2001*). The mechanism of adaptation to cold stress have received considerable attention in the last few decades, particularly for the biotechnological potentiality of these organisms and their biomolecules.

1.3 Industrial and biotechnological applications

The scientific interest in cold-adapted molecules has increased substantially in recent years, as evidenced by the growing number of examples recently isolated. The necessity of all components of a microbial cell to adapt to the cold, implies that a broad range of cellular products is available for biotechnological application. The vast majority of studies related to biotechnological applications have focused on cold-adapted enzymes, that possesses high catalytic activity at low temperature and low thermostability at elevated temperatures. Cold-adapted enzymes are of great interest because their employment could avoid heating and consequently save energy. This is very important, especially in food industry since this could prevent heat-sensitive substrates from chemical degradation. Several examples of applications of cold-adapted enzymes are illustrated in the Table 1.1.

Table 1.1: Biotechnological application of cold-active compounds

Enzyme or compound	**Microorganisms**	**Application**	**Reference**
DNA ligase	*Pseudoalteromonas haloplanktis*	Molecular biology	Georlette et al., 2000
RNA polymerase	*Pseudomonas syringae*	Molecular biology	Umma et al., 1999
β-lactamase	*Psychrobacter immobilis*	Antibiotic degradation	Feller et al., 1997
Catalase	*Vibrio rumoiensis*	Food, semiconductor, industries, dairy	Yumoto et al., 1999

In addition to their enzymes, cold-adapted microorganisms have a range of molecules of interest in terms of investigation, patenting and commercial products. For examples, polyunsaturated fatty acids could be used as dietary supplements for use in aquaculture, livestock and human diets; food, pharmaceutical and cosmetic industries are more interested in physical properties of EPS, like high viscosity, gelling capacity or high resistance in wide range of temperature and pH (*Freitas et al., 2011*). Generally, the EPSs produced by microorganism from extreme habitats, show biotechnological promise ranging from pharmaceutical industries, for their biological activity. For example, xanthan, sulphated dextran and sulphated curdlan, are used as antiviral (*Ghosh et al., 2009*) and anticancer agents (*Takeuchi et al., 2009*). Taking into account the increasing impact of bacterial biofilms, the interest in the development of new approaches for the prevention and

treatment of adhesion and biofilm formation capabilities has amplified. Many bacterial biofilms secrete molecules such as quorum sensing signals, surfactants (*Kiran et al., 2010*), enzymes (*Kaplan 2010*), and polysaccharides (*Qin et al., 2009; Valle et al., 2006*) that function regulating biofilm architecture or mediating the release of cells from biofilms during the dispersal stage of the biofilm life cycle (*Kaplan, 2010*). In this context, marine bacteria are also involved in the production of several compounds that have been shown to exhibit anti-biofilm activity against both Gram-positive and Gram-negative bacteria, including *Acinetobacter*, *S. aureus*, *Salmonella typhimurium*, *Shigella sonnei*, *Listeria monocytogenes* and several *Bacillus* species (*Rendueles et al., 2013*).

A variety of cold-adapted microorganisms produces polyhydroxyalkanoates (PHAs) as a storage polymer in response to external stress (*Goh et al., 2012*). These compounds show a wide range of applications from bioplastic, implants biomaterials and biofuels. Among the principal candidates for the production of PHAs, *Colwellia psychrerythraea* 34H and *Photobacterium produndum* SS9 could be consider (*Martin et al., 2002*).

AF(G)Ps can decrease the freezing temperature of solutions and inhibit ice recrystallization during freezing and thawing procedures (*Yeh et al., 1996*). These unique abilities have been tested for potential applications in cryopreservation of a variety of cell lines, reproductive cells, tissues, and organs. In addition, the application of AF(G)P to food preservation may lower the storage temperature and inhibit the growth of bacteria that may have contaminated the food prior to freezing (*Rothwell, 1985*).

Chapter II

Gram-negative bacteria

Since the 1960s, the number and variety of species identified that grow in extreme environments has expanded tremendously (*Kristjansson et al., 1995*). Moreover, more environments have been found in which microorganisms can grow. The organism that grow in these extreme environments belong to two domains of life: *Bacteria* and *Eukarya* (Figure 2.1).

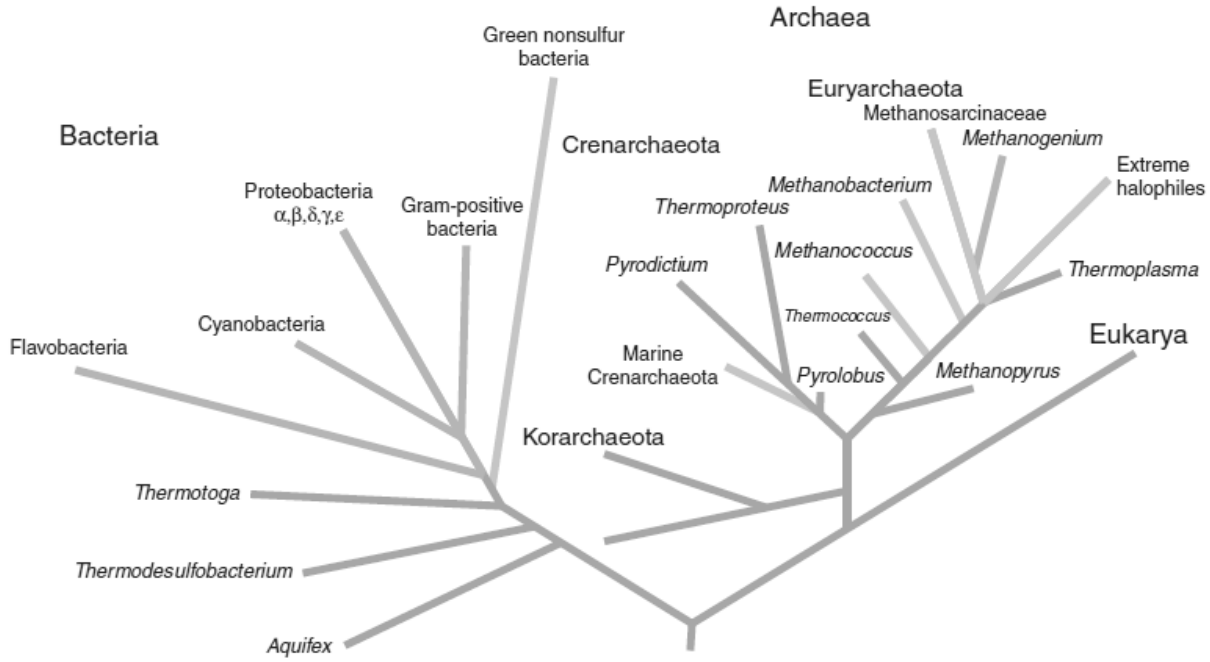

Figure 2.1: Universal phylogenetic tree of life

Despite the enormous difference, all organisms known so far share the same biochemical basis for metabolism and proliferation: the cellular organization, surrounded by a lipid membrane; the DNA contains the inheritable information, coding for RNA that can be translated into proteins. The autonomously replicating living organisms known so far likely originated from one common ancestor (*Woese et al., 1990*). *Bacteria* and *Archea* are prokaryotic organisms and their cells are

about 10 times smaller than eukaryotic cells, typically 0.5– 5.0 micrometers in length. Prokaryotes have a cellular organization different from that of eukaryotes; whereas these latter have a membrane-enclosed nucleus and numerous membrane-enclosed organelles, prokaryotic cells lack these structural features. *Bacteria* comprise a wide group of microorganisms characterized by a bewildering assortment of size, shapes and arrangements reflecting the diverse environments in which they grow and reproduce (*Pommerville 2010*). Despite the high structural variability, *Bacteria* can be divided on the basis of their basic cell morphologies: a bacterial cell with a rod shape is called "bacillus" whereas spherical and curved cells are called "cocci" and "spirilli" respectively (*Raven 2001*). *Bacteria* are classified in two broad groups, Gram-negative and Gram-positive bacteria, depending on their response to a colorimetric assay developed by Christian Gram in 1884. The different reaction in the Gram assay reflects the structural diversity and the different behaviors of bacteria against several antibiotics. The main difference found regards the cell envelope and, in particular, the size of the peptidoglycan layer, that is much thicker in Gram-positive bacteria. Furthermore, Gram-negative bacteria possess an outer membrane, external to their peptidoglycan layer, that is not present in their Gram-positive counterparts (*Beveridge et al., 1991*) (Figure 2.2). In contrast to the thickness of the PG layer, Gram-negative bacteria show much more resistance against antibacterial compounds. The explanation of this phenomenon has been found in the porosity of the PG layer that, despite its mechanical resistance, is not able to resist the diffusion of small molecules like antibiotics (*Demchick et al., 1996*). This means that Gram-negative bacteria outer membrane is more selective in the diffusion of molecules from the environment into the cell.

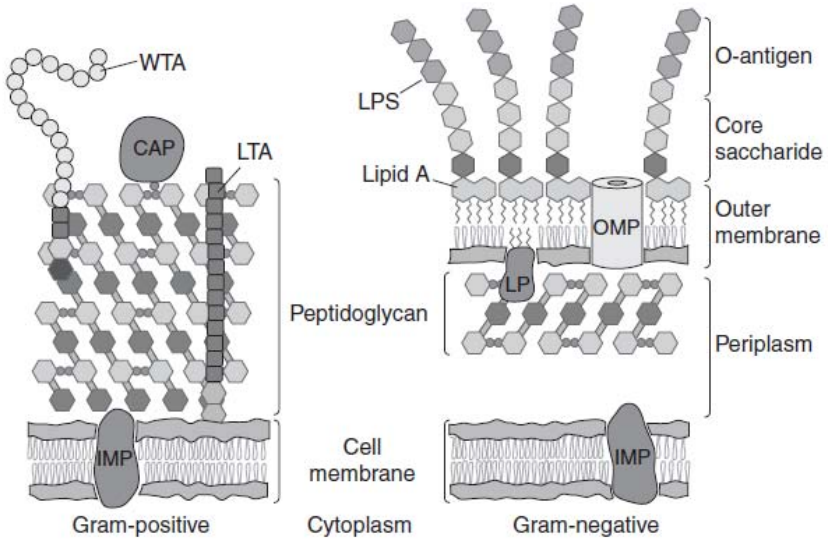

Figure 2.2: Structural organization of Gram-positive and Gram-negative bacteria cell envelops.

2.1 Gram-negative cell membrane: Lipopolysaccharide

To survive, bacteria have evolved a sophisticated and complex system of layers, named cell envelope that protects them and allows selective passage of nutrients from the outside and waste products from the inside. The cell envelope of Gram-negative bacteria is composed from three principal layers: the outer membrane (OM), the peptidoglycan cell wall, and the cytoplasmic or inner membrane (IM) that is a phospholipid bilayer. The two concentric membrane layers delimit an aqueous cellular compartment that Peter Mitchell (1961) first termed as periplasm (*Silhavy et al., 2010*). The OM is a distinguishing feature of Gram-negative bacteria. Like other biological membranes, the OM is a lipid bilayer, but importantly, it is not a symmetric phospholipid bilayer. The OM contain phospholipids that are confined to the inner leaflet of this membrane. The outer leaflet of the OM is composed of glycolipids, principally lipopolysaccharide (LPS) (*Kamio et al., 1976*). LPS is an infamous molecule because it is responsible for the endotoxic shock associated with the septicemia caused by Gram-negative organisms (*Raetz et al., 2002*). An additional feature of many bacteria of diverse genera is the production of extracellular acidic polysaccharides. These polysaccharides may be organized into distinct structures termed capsules, or may be excreted as an extracellular slime. However, this distinction is arbitrary and in practice may be of no functional significance. Encapsulated bacteria are frequently associated with serious diseases in man and animals. This is particularly so for those organisms which are invasive, and encounter the host's immune system in normally sterile tissue. Because of their importance in the virulence of many bacteria and their usefulness as vaccines (*Lee et al., 1987*) for the prevention of bacterial infections, capsules have been the subject of intensive investigation.

The lipopolysaccharides (LPSs) are amphiphilic components present in the cell wall of almost all Gram-negative bacteria; in particular they are localized in the external leaflet of the lipid bilayer constituting the outer membrane in which they represent approximately 75% of the outer surface (Figure 2.3).

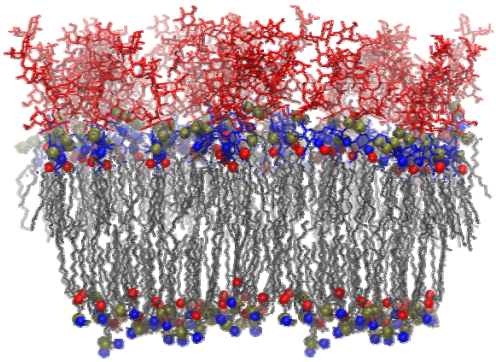

Figure 2.3: Distribution of LPSs molecules.

Lipopolysaccharides are heat-stable complex amphiphilic macromolecules indispensable for the bacterial growth, viability and for the correct assembly of the external membrane. The LPSs, through their negatively charged groups create a highly ordered structure, stabilized by electrostatic interactions of divalent cations (such as Ca^{2+} and Mg^{2+}). Due to their external location, LPSs are involved in all interactions with the external environment; in particular, this monolayer represents a defensive barrier against antimicrobial compounds. LPSs are also called endotoxins because when released, they are involved in the pathogenesis of Gram-negative infection. The LPS is composed of three different domains: a hydrophilic O-specific polysaccharide or O-chain, and a core oligosaccharide that is covalently linked to the third glycolipid domain, the lipid A (Figure 2.4).

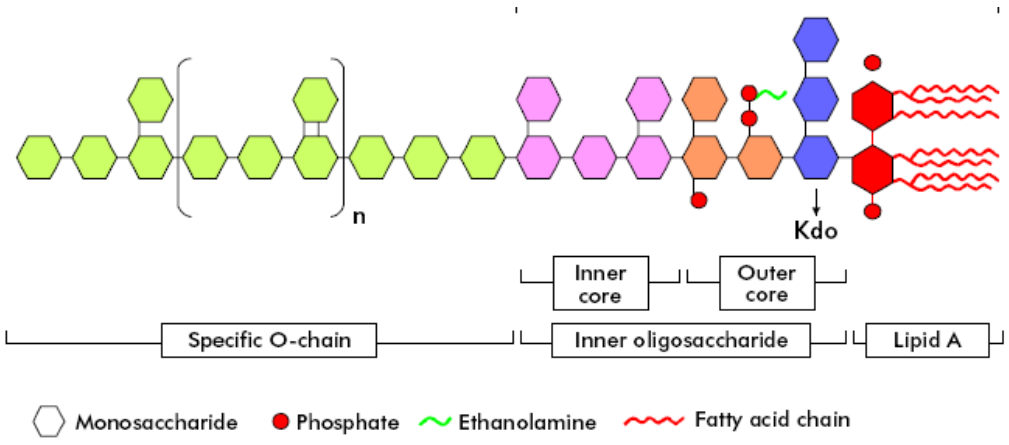

Figure 2.4: Scheme of the general chemical structure of bacterial lipopolysaccharide: lipid A, core oligosaccharide and specific O-chain.

The lipid A moiety is embedded in the outer leaflet of the OM whereas the sugar chain is oriented outwards (*Raetz et al., 2002*). The O-polysaccharide chain is not ubiquitous, as it can be absent or partly truncated in some Gram-negative strains. Bacterial colonies can be identified on the basis of their morphology as *rough* or *smooth* on the basis of the occurrence of the O-side chain, being absent in the former and present in the latter (*Lüderitz et al., 1966*). The terminology currently used to designate the different LPS types, namely with or without the O-polysaccharide portion, is S-LPS or R-LPS (or lipooligosaccharide, LOS, Figure 2.5), respectively (*Raetz et al., 2002*).

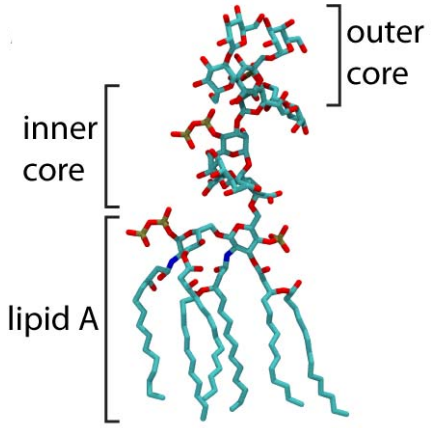

Figure 2.5: Scheme of the general chemical structure of bacterial LOS:
lipid A, inner core and outer core

The lipid A represents the endotoxic principle of the LPS molecule, since it acts as a potent stimulator of the host innate immune system, by interaction with the complex toll-like receptor 4 (TLR4)/myeloid differentiation factor 2 (MD-2). Otherwise, the presence of a large amount of LPS results in more dangerous symptoms even the septic shock. Therefore, the immune-activity and the modality of interaction of lipid A and immune system is related to the primary structure of lipid A.
Lipid A possesses a quite conservative structure usually consisting of a of a β-D-GlcN-(1→6)-α-D-GlcN (GlcN, 2-amino-2-deoxy-glucopyranose) disaccharide backbone that bears 3-(R)-hydroxy fatty acid residues, linked as ester at 3 and 3' positions, and amide-linked at 2 and 2' positions, which are indicated as primary fatty acid residues. The 3-OH, in turn, can be esterified by secondary fatty acids. Generally, the α-anomeric position of the reducing GlcNI residue (reducing

unit) and the hydroxyl at position 4' of the non-reducing GlcNII residue (non reducing unit) are linked to polar heads, phosphate groups (Figure 2.6). Phosphate groups can link other phosphate groups to give a pyrophosphate or additionally be substituted by 2-amino-ethanol group (EtN) or 4-amino-4-deoxy-L-arabinopyranose (arabinosamine, Ara4N). In few cases, the phosphate group can be displaced by acid monosaccharides such as galacturonic acid (GalA) as reported for the lipid A of *Aquifex pyrophilus* (*Plotz et al., 2000*).

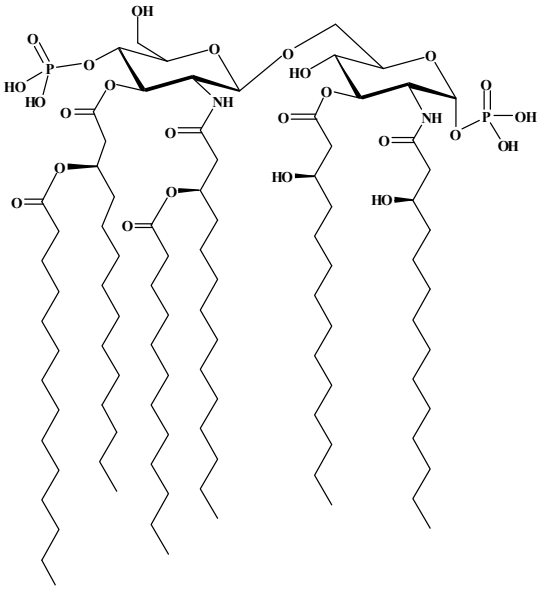

Figure 2.6: *E.coli* lipid A

Despite this general structure, lipid A could present chemical differences that are responsible of the variation among bacterial species and among the same species; this variability has been linked to a variety of biological functions, including the survival under hostile conditions. In fact, LPSs from psychrophilic microorganisms, contribute to the fluidity of membranes to contrast low temperatures. The presence of phosphate groups and charged residues in the core oligosaccharides, allowed the binding of divalent cations which probably help in stabilizing the outer leaflet of the membrane. The alteration in the outer membrane property and related compositional change in LPS, is well known to be related to the lipid A portion. At lower temperatures, in bacteria that are not naturally adapted to cold (mesophiles such as *E.coli* and *B.subtilis*), cold shock induces homeoviscous adaptation of phosholipid acyl structure in order to preserve membrane integrity (*Sweet et al., 2014*). This response is related to the incorporation of an increased amount of hydroxylate fatty acids compared to that of fatty acids of LPS from higher temperature grown cells

(*Kumar et al., 2002*). Even though only few LPS structures from cold-adapted bacteria have been characterized (*Corsaro et al., 2004; Corsaro et al., 2008; Carillo et al., 2011; Carillo et al., 2013*), their attractive feature is the production of rough lipopolysaccharides.

2.2 Bacterial extracellular polysaccharides (CPSs and EPSs)

Many microorganisms, including bacteria, archea, fungi and algae, are known to produce extracellular polysaccharide material or EPSs. This term was used for the first time by Sutherland in 1972 to describe carbohydrate polymers produced by marine bacteria (*Sutherland 1972*). EPSs, by coating the outside of bacterial cell, play an intimate role in mediating interactions between the bacterium and its immediate environment. The ubiquitous expression of EPSs in a different range of bacteria genera suggests that the EPS expression represents an advantage in several situations. For example, these compounds make up a substantial component of extracellular polymers in microbial cells that populate extreme environments as Antarctic ecosystems, saline lakes, or geothermal springs. Bacterial EPSs usually occur in two forms: capsule and slime polysaccharides. The capsule is a discrete structure that is defined as a layer of polysaccharide that is either physically attached to, or remains tightly associated with the cell surface. On the contrary, slime remains loosely bond to cell surface and in most cases, is shed in large amounts in the surrounding environment (*Poli et al., 2010*).

Exopolysaccharides synthesized by microbial cells vary in their composition and consequently in their chemical and physical properties. Chemically, EPSs are rich in high-molecular mass polysaccharides, that very often carry a net negative charge at physiological pH (*Corbett 2010*). Some are neutral macromolecules, but the majority are polyanionic due to the presence of amino sugar, uronic acids (D-glucuronic acid being the commonest, although D-galacturonic and D-mannuronic acids are also found) or ketal-linked pyruvate. These polyanionic polymers with high levels of acetyl groups has been shown to bind a wide range of metal cations, such as Fe^{2+}, Zn^{2+}, Cu^{2+} and Co^{2+}, indicating an helpful role in concentrating metal ions to the surface of the strain in the microenvironment around the cell. It has been demonstrated that EPSs produced by sea-ice isolates possesses a molecular weight 5-50 times larger than the average of the other isolated marine EPSs (*Decho 1990*). The increasing demand of natural polymers for various industrial application

led to an incessant interest in EPSs production by microorganisms, that might have innovative uses as emulsifiers, stabilizers, and gelling or texture-enhancing agents (*Sutherland 2001*).

An additional number of function have been assigned to exopolysaccharides when occur as capsule; it plays an important role not only in protection and communication of the cell with the external environment, but also in adhesion, resistance to the host's adaptive immune response, chemokine and cytokine induction and intracellular survival (*Corbett 2008*). There is great potential for structural diversity amongst capsular polysaccharides both within and between bacterial species. The basis of this diversity is a consequence of differences in both the repeat monosaccharide components but also in the glycosidic linkage between the different repeating monosaccharide units. This peculiarity is exemplified by *Streptococcus pneumonia* with over 90 different capsule serotypes (*Henrichsen 1995*) and *E. coli* with over 90 capsules or K antigens (*Whitfield 2006*). The diversity of capsular polysaccharides within a single bacterial species such as *S. pneumoniae*, which is a highly adapted human respiratory pathogen and will not have to grow outside the host, raises the obvious question regarding the function of this diversity. In fact, capsular polysaccharides are considered as virulence factor because they enhance the ability of bacteria to cause disease, preventing phagocytosis and enhancing cell adhesion to host tissues. In marine environments, bacterial exopolysaccharides provide protection and ecosystem stability. The enhanced production of a high-molecular-weight polyanionic EPS at suboptimal incubation temperatures lends support to theories that EPS may serve as a cryoprotectant both for organisms and their enzymes. The cryoprotectant role of EPS was established in the psychrophilic Gamma Proteobacterium *Colwellia psychrerythraea* grown at increased pressure or temperatures from −8 to −14 °C (*Marx et al., 2009*). The EPS from the psychrotolerant bacterium *Pseudoalteromonas* could enhance the stability of the cold-adapted protease secreted by the same strain through preventing its autolysis, avoiding enzyme diffusion, and helping the strain in enriching the proteinaceous particles and trace metals in the deep-sea environment (*Qin et al., 2007; Nicolaus et al., 2010*).

2.3 Biofilm

It is very interesting to note that microorganism aggregates are ubiquitous and abundant in the world's oceans. Marine bacteria benefit from living in aggregates since their proximity to other cells and surfaces provides opportunities for interaction and nutrient uptake. Biofilm on surface have a characteristic structure consisting of microcolonies enclosed in a hydrate matrix of proteins, nucleic acids and polysaccharides. The development of biofilm in vitro involved different stages

(Figure 2.7), and the EPSs excreted by bacteria are polymeric substances displaying an important role in biofilm matrix in regard to the biochemical interactions between bacteria and surrounding cells (*Decho 1990; Logan, et al., 1987*).

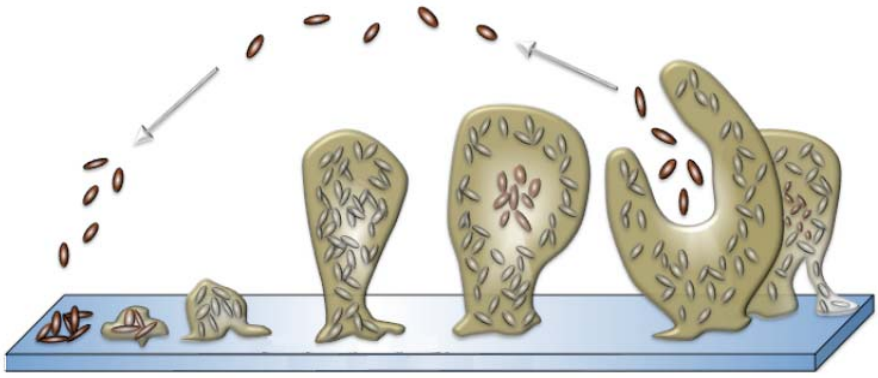

Figure 2.7: Biofilm maturation cycle.

The hydrated biofilms offer a stable micro-environment in which extracellular enzymes can find storage and at the same time facilitating cellular uptake of small molecules (*Decho et al., 1995*). Biofilms were also estimated to be responsible in humans for a large proportion of persistent infections, such those derived from orthopedic implants or indwelling catheters (*Francolini et al., 2010*). Indeed, pathogens embedded in biofilm matrix appear to be more resistant to many physical or chemical treatments, therefore even a well-designed anti biocidal cure often results in the selection of persistent pathogens cells, which are responsible for recurrent infections. However, issues derived from biofilm formation are not only relevant in medicine but in a wide range of sectors such as food industry (*Lequette et al., 2010*), marine and industrial equipment (*Holmstrom et al., 2002*). Staphylococci are recognized as the most frequent causes of biofilm associated human infections. This exceptional status among biofilm associated pathogens is due to the fact that staphylococci are frequent commensal bacteria on the human skin and mucous surfaces. Indeed, staphylococci are among the most likely bacteria to infect any medical devices that penetrates those surfaces, such as when being inserted during surgery (*Otto 2008*). *Staphylococcus epidermidis* contributes to making infections chronic and particularly difficult to eradicate. The interest in the development of new approaches for the prevention and treatment of adhesion and biofilm formation capabilities has increased. A viable approach should target adhesive properties without affecting bacterial vitality in order to avoid the rapid appearance of escape mutants. Molecules implicated in

active biofilm dispersal include glycosidases and proteases. There is a notable effort towards finding small available molecules that should “break up” the “tangled matrix” of the biofilm.
Marine bacteria are a resource of biologically active products (*Debbab et al., 2010*). Cold adapted marine bacteria represent an untapped reservoir of biodiversity endowed with an interesting chemical repertoire. A preliminary characterization of molecules isolated from cold adapted bacteria revealed that these compounds display antimicrobial, anti-fouling and various pharmaceutically relevant activities (*Bowman 2007*). The ability of polar marine bacteria, belonging to different genera/species, to synthesize bioactive molecules might represent the result of the selective pressure to which these bacteria are subjected. One of the developed survival strategies may be represented by the production of metabolites with anti-biofilm activity.

2.4 Polyhydroxyalkanoates (PHAs)

Many prokaryotes are able to accumulate large amounts of lipophilic compounds as inclusion bodies in the cytoplasm. Member of most genera synthesize poly(3-hydroxybutyrate) (PHB) or other polyhydroxyalkanoates (PHA) (*Steinbuchel 2001*), whereas the accumulation of triacylglicerols (TAGs) and wax esters (WEs) is a property of only a few prokaryotes (*Alvarez et al., 2002*). All these compounds act as carbon reserve material in response to the availability of excess carbon source when growth is limited owing to starvation of other nutrients such as nitrogen and phosphorus. The terminology for PHAs is based on the chain length, and refers to PHA_{scl}, short-chain-length PHAs (C3 to C5), and PHA_{mcl}, with medium-chain-length PHAs (C6 to C14).
Accumulation of PHA was first reported nearly 90 years ago in *Bacillus megaterium* (*Lemoigne 1926*), and the best-characterized bacterium with respect to PHA metabolism is *Ralstonia eutropha*. This bacterium accumulates intra-cytoplasmatic inclusions with a diameter of up 500 nm and amounting to up to 90% of the cell dry weight (Figure 2.8) (*Anderson et al., 1990*).
These polyesters have aroused interest because they are biodegradable (*Ho et al., 2002; Lenz et al., 2005; Lim et al., 2005*), biocompatible (*Zinn et al., 2001; Hazer et al.,2007*) and exhibit a crystallinity ranging from 30% to 70% and a melting temperature of 50 °C to 180 °C. These thermoplastic material properties make PHAs commercially relevant as renewable and biodegradable alternatives to oil-based plastics.

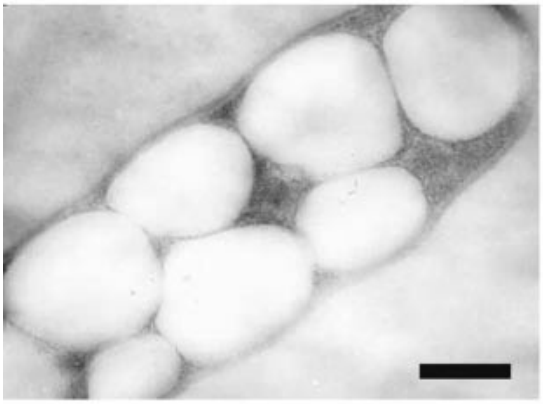

Figure 2.8: Cell of *Ralstonia eutropha* H16 accumulating PHB inclusions

For the past decades, the production of PHA by bacteria and their PHA biosynthesis pathways have been extensively studied. However, there is scarce information about the diversity of PHA producing bacteria in Antarctic regions, the properties of these PHA and the enzymes involved in their biosynthesis. Therefore, the accumulation of PHA in cold-adapted bacteria might also increase the survival capabilities of these bacteria in the extreme environments and poor nutrient availability. Ayub et al had suggested that PHA methabolism in *Pseudomonas* sp 14-3 was an adaptation mechanism to withstand oxidative stress and drastic changes in temperature, which are common stress factors encountered in Antarctic environment. More studies on PHA production by Arctic and Antarctic bacteria would be useful to demonstrate the possible association between PHA accumulation and stress tolerance (*Gohn et al., 2012*).

Chapter III

Methodology

3.1 Extraction and purification of LPS

The first approach aimed to the structural elucidation of LPS/LOS is represented by their extraction from intact microbial cells. This is conventionally achieved through two complementary procedures, that lead to the selective isolation of *rough*-type LPSs, extracted with a phenol-chloroform-petroleum ether procedure (PCP) (*Galanos et al., 1969*) and *smooth*-type LPSs, extracted with the hot phenol-water protocol (*Westphal et al., 1965*). The PCP method uses a mixture of phenol, chloroform and petroleum ether (2:5:8, v:v:v), which allows to extract the more lipophilic lipopolysaccharide molecules (LOS), constituted by the lipid A and core portions. This procedure allows to obtain a sample free from nucleic acids contaminations.

The phenol-water method, instead, had been widely used for lipopolysaccharides extraction (*Westphal et al., 1965*). It uses a mixture of phenol and water (1:1, v/v) at 68°C; after centrifugation, the LPS molecules are generally recovered from the water phase together with nucleic acids, while the phenol phase generally contains proteins. In order to remove nucleic acids from the water extract, an enzymatic treatment, with RNase, DNase and protease, is necessary, followed by dialysis in order to remove digested material.

The screening for detecting the nature of LPS is realized by polyacrylamide electrophoresis gel, by using the denaturing agents sodium dodecyl sulfate (SDS) and sodium deoxycholate (DOC). For visualization of lipopolysaccharides the mostly used method is the silver staining (*Tsai et al., 1982*). The presence of LPS is displayed by the observation of the typical “ladder-like” pattern of the electrophoresis migration, due to the presence of molecules differing in their structure for the number of repeating units composing the O-polysaccharide moiety. Conversely, LOS appears as a dark band that quickly migrates at the bottom of the gel, denoting the lower molecular weight of LOS lacking O-chain domain.

3.2 Chemical analysis and reactions on LPS

Chemical analyses (Figure 3.1) are useful to obtain important preliminary information regarding the primary structure of poly/oligosaccharides. The procedure, usually are performed by GC-MS only after conversion of the monosaccharides into volatiles derivatives.

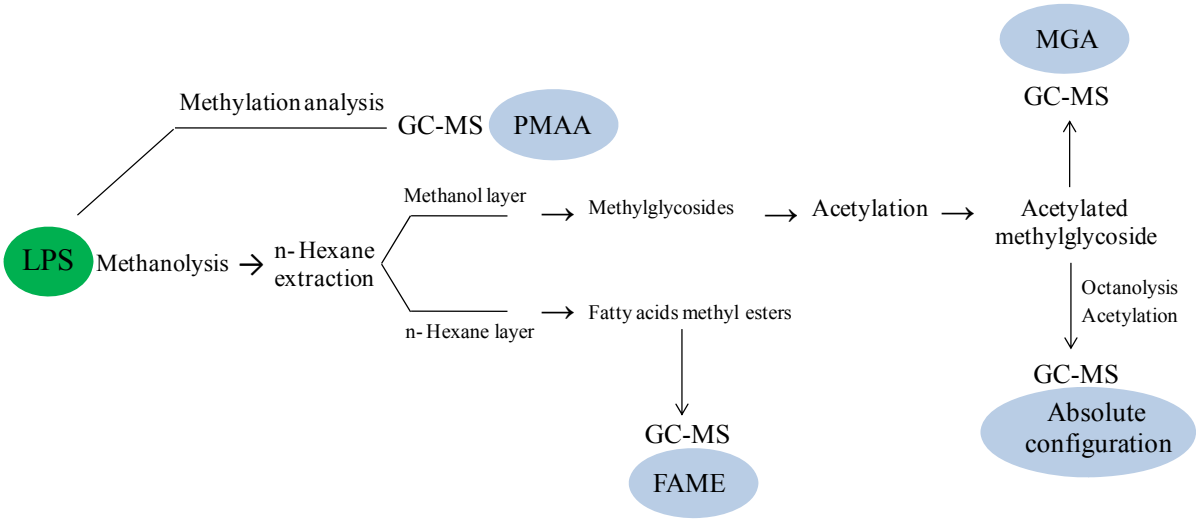

Figure 3.1: Procedures for GC-MS analysis of LPSs.

Typically, the qualitative analysis by GC-MS is achieved by treating the oligo-/polysaccharide with hydrochloric anhydrous methanol that leads to solvolysis of the molecule and to the formation of the *O*-methyl glycoside for each monosaccharide. Subsequent acetylation with acetic anhydride in pyridine produces the per-acetylated *O*-methyl glycosides (MGA), that can be injected and analyzed by GC-MS. By comparison the retention times from the GC analysis and the fragmentation pattern from the MS spectra analysis with opportune standards, is possible the identification of the monosaccharidic residues. Quantification analysis can then be obtained by using an internal standard, that usually is per-acetylated inositol. Since the MGA protocol provides a solvolysis in acid conditions, several isomers for each monosaccharide may form (i.e. pyranose and furanose either α and β anomers) resulting in the occurrence of many peaks in the corresponding chromatogram.

An alternative and complementary approach that can be used, leads to the formation of acetylated alditol derivatives. In this case, after strong acid hydrolysis with trifluoroacetic acid (TFA), the

carbonyl moiety of the free residues is reduced with $NaBH_4$, thus providing a single peak for each monosaccharide.

For the determination of absolute configuration of each monosaccharide, the solvolysis is executed with an optical chiral pure alcohol as 2-(+)-octanol or 2-(+)-buthanol; the disteroisomeric molecules, can be acetylated and analyzed by GC-MS (*Leontein etal., 1978*).

Chemical analysis can provide also the ring size and the glycosilation sites of the monosaccharides. The procedure consists in an extensively methylation of the oligo/polysaccharide with CH_3I in strongly alkaline conditions. Then, the permethylated sample is hydrolysed in acid conditions and reduced with a marked hydride ($NaBD_4$). The alditols so obtained, have a free hydroxyl groups at the positions previously involved in glycosidic linkages and cyclization, that can be acetylated. These partially methylated alditols acetylated (PMAA, Figure 3.2) can be analysed by GC-MS and the fragments observed in the MS spectra are diagnostic for specific substitution patterns of acetyl and methoxyl groups. To obtain desired information it is necessary to consider that position of the acetyl groups in the fragments accounts for the attachment point or for the position of ciclysation of the pyranose or furanose cycle whereas the methyl groups correspond to free positions, not involved in linkages (*Hakomori 1964*). Information obtained from these chemical analyses helps and confirms the interpretation of subsequent NMR and MS experiments.

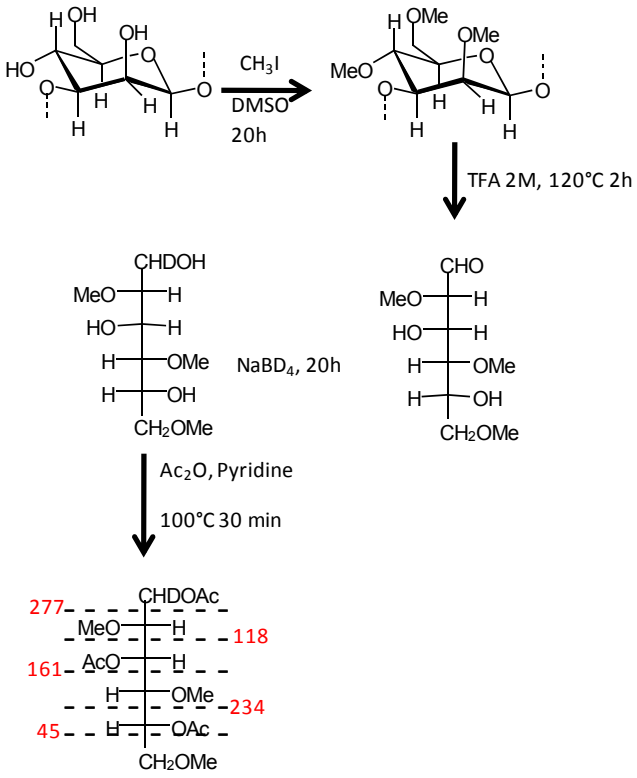

Figure 3.2: AAPM procedure on 3-D-Mannose. Reactions and fragmentation pattern are showed.

Structural investigation of LPS/LOS is a difficult task since their amphiphilic nature determines the tendency to form micelles with low solubility in both aqueous and organic solvents. As a consequence, portion with a different nature are studied separately.

3.2.1 Lipid A structure determination

A mild acid hydrolysis with 1% of acetic acid, allowed the cleavage of the acid-labile glycosidic linkage between Kdo and the saccharidic backbone of lipid A. This kind of procedure allows the isolation of the intact lipid A and of the oligo/polysaccharidic portion (Figure 3.3). The structural approach makes an extensive use of mass spectrometry analysis by ESI MS techniques, as well as NMR spectroscopy and chemical analyses both on the native and selectively degraded lipid A fractions. Fatty acids determination is usually achieved through GC-MS analysis of their methyl ester derivatives. Mass Spectrometry is the most common approach used in lipid A structural determination. MALDI-TOF and ESI-MS data allow gaining insights into the number of lipid A species present in the fraction, the presence of polar heads and the distribution of acyl residues on each GlcN units of the disaccharide backbone (*Que et al., 2000*). The punctual distribution of fatty acids on the disaccharidica backbone is achieved by a study of negative ion mass spectra and positive ions IRMPD-MS/MS spectra of the intact lipid A and NH_4OH treatment product (*Silipo et al., 2002*). This procedure selectively cleaves the ester linked acyloxyacyl groups, leaving untouched the amide-linked acyloxyacil groups. In particular, negative ions mass spectra furnish the acylation and phosfphorylation degree of the molecules and the fatty acids linked at position C2 and C2' when NH_4OH is investigated. Positiveion IRMPD-MS/MS spectra of lipid A can reveal the type of fatty acids linked to the non-reducing glucosamine of disaccharidic backbone in whole lipid A as well as in NH_4OH product.

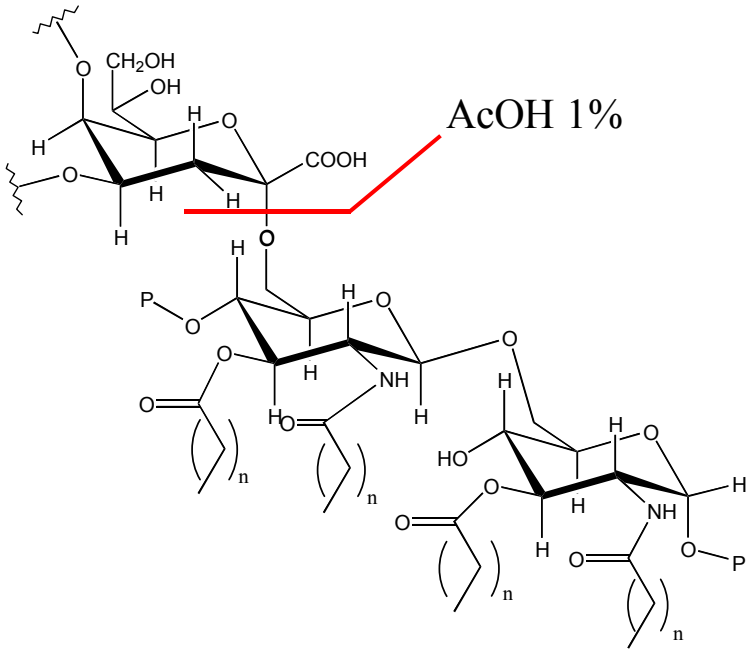

Figure 3.3: Schematic illustration of Kdo cleavage linkage during mild acid hydrolysis

3.2.2 Core region determination

The mild acid hydrolysis reaction conditions lead to dehydration of Kdo with consequent formation of artifacts (*Volk et al., 1972*). This increase the sample heterogeneity and can make difficult the interpretation of NMR spectra, because the artifacts can be present in not negligible amount.

Therefore, this procedure is avoided for the structural characterization of core region or rough-LPS. A complete delipidation of lipid A portion is mandatory for the study of the core oligosaccharidic region. The alkaline treatment lies in a first *O*-deacylation of the LOS, and a successive *N*-deacylation (Figure 3.4), which leads to the isolation of an oligosaccharide containing the glycosidic portion of the lipid A (*Holst 2000*). The first one is a mild alkaline hydrolysis using anhydrous hydrazine that removes the ester linked fatty acids and does not cause the loss of basic-lable substituents. The increased hydrophilic nature of the molecule sometimes allowed to obtain some structural information by NMR. In the majority of cases, a complete deacylation is necessary to obtain a water-soluble oligasaccharide. This is obtained by a strong alkaline treatment with KOH 4M, that leave intact the phosphate groups but remove other substituents.

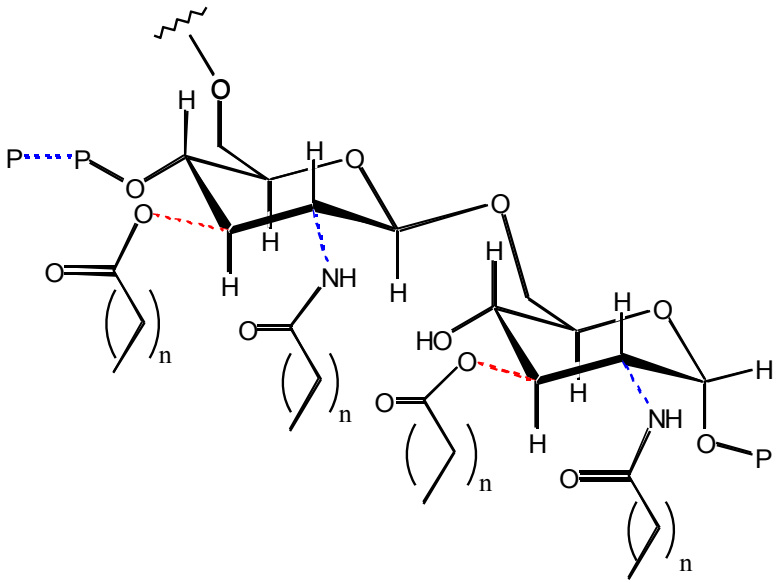

Figure 3.4: Schematic representation of the lipid A. Dotted red and blue lines indicates the linkages hydrolyzed during treatment with hydrazine or KOH, respectively.

3.3 Chromatography in the study of oligo/polysaccharides

Purification of oligo- and polysaccharide mixtures is generally achieved by using chromatographic techniques, as size-exclusion chromatography and ion exchange chromatography.

When the components show different molecular masses, size-exclusion chromatography is suitable for separation. The molecules that are too large to pass through the pores are excluded and traverse the column more rapidly. Smaller molecules instead, because they pass trough gel pores, are eluted later. Different kinds of resins are commercially available, with different range of pore sizes. Moreover, it is possible to elute the sample using water or buffers with high ionic strength.

- Sephacryl: the matrix consists of allyl dextran and N,N'-methylenebisacrylamide. These resins are used to separate polysaccharides with a suitable buffer as eluent.
- Bio-gel P: the matrix is polyacrylamide with either water or a buffer as eluent.
- Sephadex: the matrix consists of allyl dextran. These resins are mainly used to desalt samples.

Ion exchange chromatography can be applied for the separation and purification of many charged or ionizable molecules such as proteins, peptides and polysaccharides.Ion-exchange chromatography

is part of ion chromatography which is an important analytical technique for the separation and determination of ionic compounds, together with ion-partition/interaction and ion-exclusion chromatography. Ion chromatography separation is based on ionic (or electrostatic) interactions between ionic and polar analytes, ions present in the eluent and ionic functional groups fixed to the chromatographic support.
The fractions obtained are suitable for chemical, mass spectrometry and NMR analysis.

3.4 Mass spectrometry of oligo/polysaccharides

Mass spectrometry is widely applied to carbohydrates and lipid A structure elucidation. It provides information about the molecular mass of the samples and, in particular cases, information about the sequence of the monosaccharides. The MALDI and ESI ionization sources are suitable for oligosaccharides structure elucidation. In the standard conditions used to perform the experiments, both the ionization mechanisms do not cause fragmentation of the oligosaccharidic chains. This implies that a MALDI or an ESI mass spectrum can give information about the number of species present in the sample. The main difference between the spectra obtained by the two ionization techniques is that the ESI spectrum can show the presence of multicharged ions.
Among mass analyzers, the FT-ICR gives the best resolving power. In fact, depending on the magnetic field strength, it can achieve a mass resolving power higher than 100000 and a mass accuracy less than 1 ppm. It is usually coupled with an electrospray ionization source and it finds important applications in LPS analysis. In particular it is possible to perform the CSD (Capillary Skimmer Dissociation) experiment, which allows the cleavage of the labile glycosidic linkage between the Kdo and the GlcN4*P* belonging to the lipid A. Thus, analysing the intact LPS, it is possible to obtain information about both the core region and the lipid A. The signals belonging to the core region are, most of the times, easily recognizable, because they are characterized by the loss of 44 u, which is due to the Kdo de-carboxylation (*Kondakov et al., 2005*).
Moreover, when a spectrometer is equipped with a collision cell, it is possible to perform tandem mass spectrometry experiments, selecting an ion and inducing its fragmentation.
Nevertheless, the interpretation of fragmentation spectra of carbohydrates is not always easy, because fragmentation could not occur at each glycosidic linkage. Moreover different fragment types can be formed, the identification of which is sometimes not immediate.
The nomenclature used for fragment types classification was developed by Domon and Costello in 1988 (Figure 3.5).

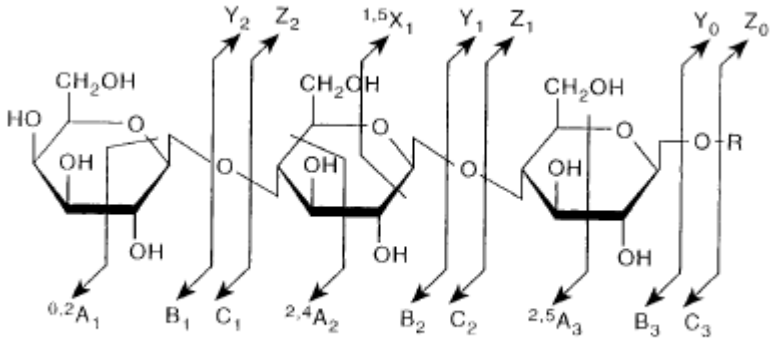

Figure 3.5: Fragments nomenclature by Domon and Costello.

The cleavage of the glycosidic bond can lead to the formation of B, C, Y and Z fragment types. The fragments which contain the reducing end of the oligosaccharide are named Y and Z, while those containing the non reducing end of the molecule are named B and C fragments. Each fragment is also identified by a number, which indicates the number of monosaccharides present in the fragment. A type fragments regard internal fragmentation (*Domon et al., 1988; Spina et al., 2004*).
Mass spectrometry alone is not able to give all the necessary informations for the complete characterization of an unknown oligosaccharide. It is fundamental to combine these results with NMR data.

3.5 Nuclear Magnetic Resonance (NMR)

Nuclear Magnetic Resonance (NMR) represents the most useful and decisive technique in the field of structural investigation of carbohydrates. This is due to the possibility of analysing molecules in solution in a native state, owing to the good solubility observed for oligo- and polysaccharides in aqueous solutions. During the structural study of saccharides, nuclei usually observed are ^{1}H, 13C and ^{31}P, to detect phosphate groups and unusual phosphorous containing substituents.
Analysing a typical monodimensional ^{1}H-NMR spectrum for an oligo-/polysaccharide, it is possible to distinguish three different regions:
The region between 5.5 and 4.6 ppm relative to the anomeric protons signals
The region between 4.6 and 2.6 ppm where the ring proton signals are located
The region between 2.5 and 1.0 ppm that is typical of the deoxy positions signals

While the principal values of ^{13}C resonances are: -104-105 ppm : anomeric carbon atoms involved in a glycosidic linkage

- ✓ 80-60 ppm : oxymethylene or carbinolic carbon atoms
- ✓ 60-45 ppm : carbon atoms linked to nitrogen
- ✓ ~ 30 ppm : aliphatic methylene carbons of deoxy-sugar residues
- ✓ 20-17 ppm : methylene carbon atoms of 6-deoxy-sugar residues and of acetyl residues

Additionally, the values of coupling constants $^{1}J_{C1,H1}$ and $^{3}J_{H1,H2}$ are diagnostic of the anomeric orientation of pyranose rings. In sugar with *gluco* or *galacto* configuration (H-2 axial), a $^{3}J_{H1,H2}$ around 8 Hz is indicative of a β-anomer, whereas below 3 Hz of an α-anomer. On the other hand, *manno* configured sugars (H-2 equatorial) show both $^{3}J_{H1,H2}$ below 3 Hz. The values of $^{1}J_{C1,H1}$ are also indicative of the anomeric configuration, indeed, a $_{1}J_{C1,H1}$ below 165Hz indicates a β-anomer whereas above 170 Hz indicates the presence an α-anomer.

The identification of the sugar moieties is possible by determining the number of the different spin systems corresponding to each sugar moiety, that can be achieved by analysis of COSY, that shows cross-peaks for vicinal scalar coupled protons, and TOCSY spectra. This last one permits the identification of all the protons belonging to the same spin system. COSY and TOCSY experiments, are in turn used to attribute the carbon resonances in the HSQC spectrum. Furthermore, in the HSQC spectrum, the down-field shift of carbon resonances (glycosidation shift) allows to locate the positions of glycosidation. In fatc, glycosidic linkage causes the "glycosilation shift": the carbons involved in the linkage undergo a downfield shift of 8-10 ppm, while the adiacent carbons will be upfield shifted of 1-3 ppm.

NOESY and ROESY spectra are very useful both to confirm the *intra*-residual assignment and the anomeric configuration. Actually, in β-configured sugars, H-1 gives *intra*-residue NOE correlation with H-3 and H-5, while in α-configured only with H-2. In addition, *inter*-residual contacts, together with the long range correlations present in HMBC experiments, are crucial to understand the sugar sequence in the saccharide chain (Figure 3.6)

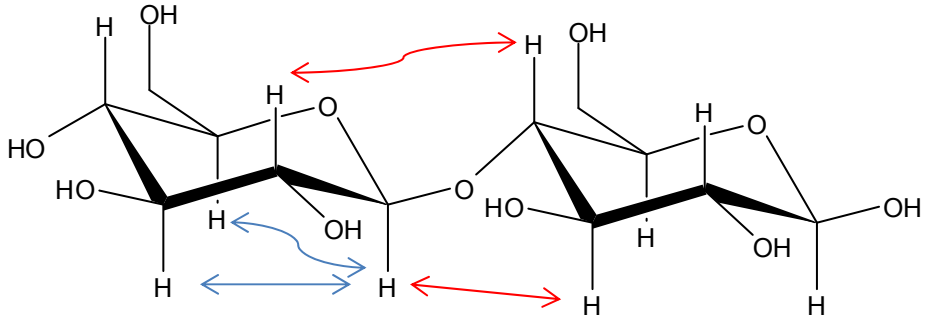

Figure 3.6: *Intra*- (blu) and *inter*-(red) residual NOE contacts.

Results

Colwellia psychrerythraea strain 34 H

The family *Colwelliaceae* is a part of the order of *Alteromonadales*, located within class *Gammaproteobacteria*. It contains twelve psychrophilic or psychrotolerant species (*Deming et al., 1988*), two of which are also barophilic (*Collins et al., 2010*). The species of family *Colwelliaceae* are principally Gram-negative, rod- to curved rod-shaped cells and facultative anaerobic. The genus *Colwellia* was first described by Deming et al. (1988) for a psychrophilic microorganism isolated from Flounder eggs collected in Norway. This name gave in honor of the american microbiologist Professor Rita Colwell. (*Bowman 2014*). *Colwellia* species are ubiquitous present in cold and polar marine ecosystem, including ice brine channels, marine biofilms and aquaculture system. Nowadays, only the genome of the sea ice bacterium *Colwellia psychrerythraea* strain 34H had determined. Analysis of the genome suggests that a collection of synergistic changes in the overall genome content and amino acid composition supports its psychrophilic lifestyle (Methe et al ., 2005). *Colwellia psychrerythraea* strain 34H, isolated from subzero Arctic marine sediments (*Huston et al., 2000*), grows at temperatures as low as -12°C, with optimal and maximal growth temperatures of 8-9°C and 19°C, respectively (*Huston et al., 2000*).

The analysis of *C. psychrerythraea* genome, evidences the types of features that allow to live at freezing temperatures and for this reason, this bacterium is considered a model to study cold adapted life-style. In addition to one of the most important adaptation mechanism, that is the enhanced fluidity of membranes, the genome of *C. psychrerythraea* also encodes for the accumulation of compatible solutes (*Wiggins 2008*), the production of osmoprotectant betaine and glycine betaine (*Mooibroek et al., 2007*) and polyhydroxyalkanoates granules accumulation. *C. psychrerythraea* 34H is also involved in the production of exopolysaccharides that appear to be capable of acting as a cryoprotectant during freezing process in ice brine environment (*Bowman 2014*).

Chapter IV

Colwellia psychrerythraea 34 H grown at 4°C

4.1 Lipopolysaccharide and lipid A structures

LPS molecules were extracted and analyzed during my master degree thesis; here are reported only few information in order to contextualize the results obtained during the PhD thesis work about the lipid A. The cells extracted by the PCP method revealed a rough-LPS (LOS), as already founded for other psychrophilic microorganisms (*Corsaro et al., 2004; Corsaro et al., 2008; Carillo et al., 2011*). The structure, obtained by chemical analysis, NMR spectroscopy and ESI mass spectrometry, is reported below (Scheme 1) (*Carillo et al., 2013*):

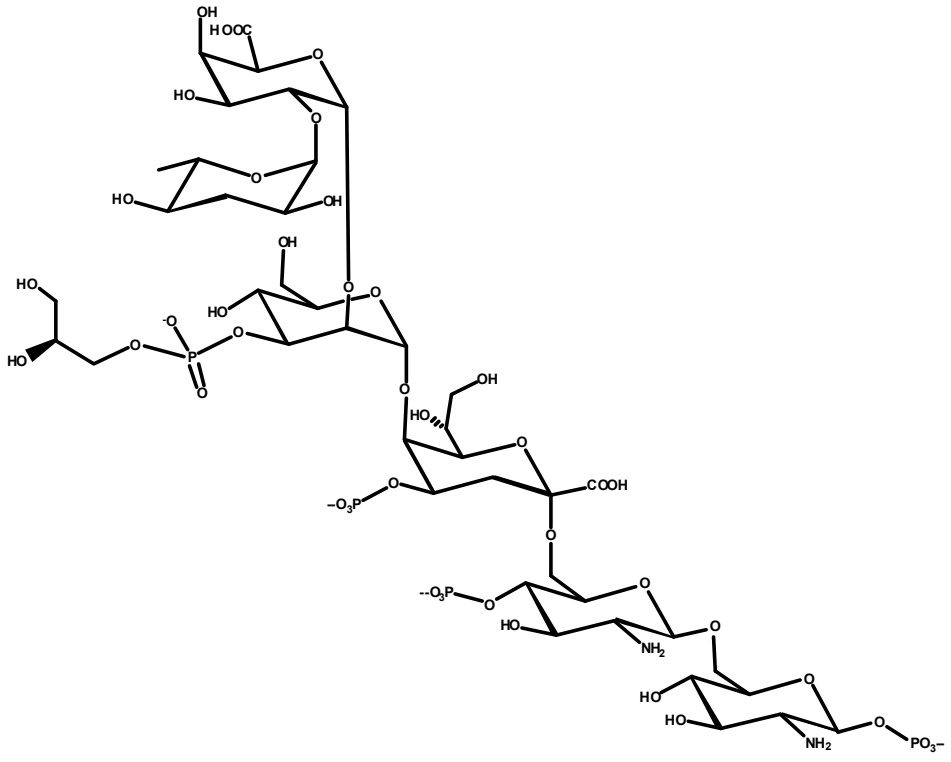

Scheme 1: Core structure of LOS from *C. psychrerythraea* 34H.

The core region is constituted by only few sugar units, some of which are acidic monosaccharides. This structural feature, together with the presence of several phosphate groups, gives to the LOS a high charge density. Furthermore, it is worth noting the lack of heptose residues in the inner core of LOS; in their place, an α-mannose residue is linked to the Kdo. This structural feature is commonly found in *Rhizobiaceae* family, but has never been found in extremophiles. Finally, colitose and phosphoglycerol, already founded in some O-polysaccharides chain (*Silipo et al., 2005; Kenyon et al., 2011*), are present (Scheme 1).

4.1.1 Isolation and purification of lipid A

Extraction of *Colwellia psychrerythraea* 34H dried cells by the phenol/chloroform/light petroleum (*Galanos et al. 1969*) yielded about 1.1% of LOS (*Carillo et al., 2013*). The lipid A fraction was obtained by 1% acetic acid hydrolysis of LOS suspension. The lipid A was recovered as pellet after centrifugation of the crude reaction, washed twice with water and freeze-dried. Sugar analysis revealed the presence of D-glucosamine as unique monosaccharide. Fatty acids methyl esters, obtained after methanolysis of a lipid A sample and extraction with hexane, were recognised in the GC-MS chromatogram by comparison with standards and from their EI-MS spectra. GC-MS analysis revealed the presence of 3-hydroxy-dodecanoic [C12:0(3-OH)] and 3-hydroxy-tetradecenoic acids [C14:1(3-OH)], as hydroxylated species. The presence of an unsaturated hydroxylated species was quite uncommon (ref). The analysis also revealed the occurrence of decanoic (C10:0), dodecanoic(C12:0), dodecenoic (C12:1), tetradecanoic (C14:0), tetradecenoic (C14:1), and hexadecenoic (C16:1) acids. This last abundant signal and the signals attributable to hexadecanoic (C16:0) and octadecanoic (C18:0) acids suggested the presence in the LPS sample of membrane phospholipids. Finally, less abundant signals were attributed to pentadecanoic (C15:0) and pentadecenoic (C15:1) acids.

4.1.2 ESI FT-ICR mass spectrometric analysis of lipid A

To obtain a mass profile of the *Colwellia psycherythraea* 34H lipid A, the mixture was analyzed by ESI FT-ICR mass spectrometry. The charge negative ions ESI FT-ICR mass spectrum showed the presence of several signals clusters $[M-H]^-$ centered on the main species named **K1-K5** (Figure 4.1, Table 4.1), corresponding to a number of glycoforms differing for their acylation as well as their phosphorylation degree. In particular, as shown in the spectrum (Figure 4.1), lipid A sample was found to be highly heterogeneous, displaying a group of major signals in the range 1300-2200 *m/z* that could be assigned to tetra-acylated up to hepta-acylated glycoforms.

The species at 1301.744 m/z (**K1**), with the composition $GlcN_2P_2[C12:0(3\text{-}OH)]_2[C14:1(3\text{-}OH)][C12:0]$ (calculated molecular mass: 1302.762Da), revealed a tetra-acylated lipid A with only three hydroxylated fatty acids. The species **K2** at 1499.905 m/z (calculated molecular mass: 1500.927 Da), was identified as penta-acylated lipid A, suggesting an asymmetric distribution of hydroxylated primary fatty acids.

Table 4.1: Composition of the main species present in the charge negative ions ESI FT-ICR mass spectrum of the lipid A from *Colwellia psychrerythraea* 34H.

Species	Mw calculated	$[M\text{-}H]^-$ observed	Composition
K1	1302.762	1301.744	$(GlcN)_2P_2[C12:0(3OH)]_2[C14:1(3OH)][C12:0]$
K2	1500.927	1499.905	$(GlcN)_2P_2[C12:0(3OH)]_3[C14:1(3OH)][C12:0]$
K3	1654.930	1653.907	$(GlcN)_2P_2[C12:0(3OH)]_3[C14:1(3OH)]GroP[C12:0]$
K4	1809.069	1808.042	$(GlcN)_2P_2[C12:0(3OH)]_3[C14:1(3OH)]GroP[C12:0][C10:0]$
K5	2047.301	2046.287	$(GlcN)_2P_2[C12:0(3OH)]_3[C14:1(3OH)]GroP[C12:0][C10:0][C16:0]$

Moreover, species at 154.002 u higher, indicated as K3, differs from the **K2** for the uncommon presence of a glycerol phosphate residue (GroP). The most abundant **K4** species at 1808.04 m/z (calculated molecular mass: 1809.069 Da) was identified as hexa-acylated species with the following composition: $GlcN_2P_2[C12:0(3OH)]_3[C14:1(3OH)]GroP[C12:0][C10:0]$. Moreover, **K5** species at 2046.28 m/z (calculated molecular mass: 2047.301 Da) dispayed and additional C16:0.
All these species comprise heterogeneity in chain length, due to the substitution of the C14:0 with a C16:1 (+26 u) or a C12:0 (-28 u) fatty acid, respectively.

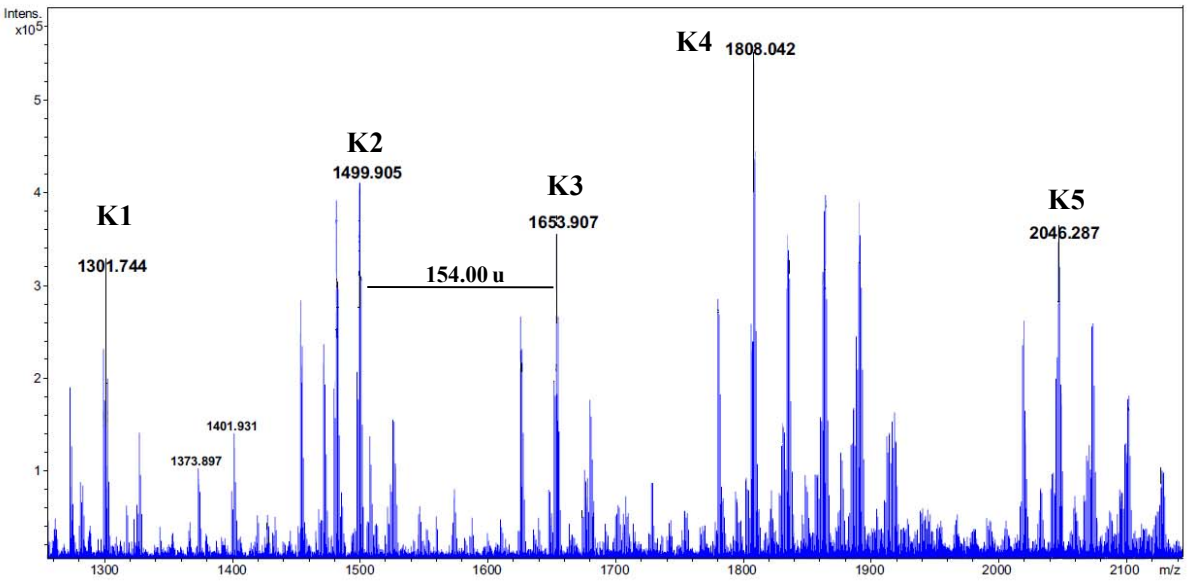

Figure 4.1: Charge negative ions ESI FT-ICR mass spectrum of the lipid A from *Colwellia psychrerythraea* 34H.

The lipid A was then treated with NH_4OH (*Silipo et al., 2002*), that hydrolyses only acyl and acyloxacyl esters, leaving intact acyl and acyloxacyl amides. Lipid A_{NH_4OH} was analyzed by ESI FT-ICR MS (Figure 4.2) and the negative ion mass spectrum showed the presence of two main signals corresponding to species **M1**-**M2** (Table 4.2)

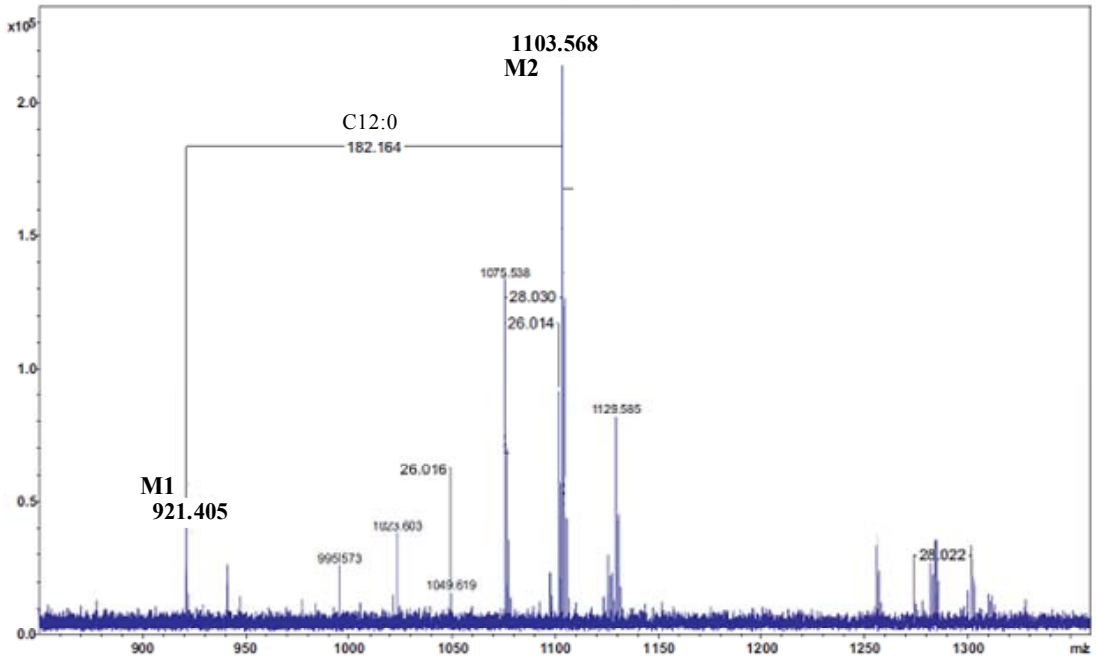

Figure 4.2: Mass spectrum of the Lipid A_{NH4OH} from *Colwellia psychrerythraea* 34H.

Table 4.2: Composition of the main species of the Lipid A_{NH4OH} observed in the ESI FT-ICR mass spectrum.

Species	Observed[M-H]$^-$(Da)	Calculated mass (Da)	Composition
M1	921.405	922.426	$GlcN_2P_2$[C12:0(3OH)][C14:1(3OH)]
M2	1103.568	1104.596	$GlcN_2P_2$[C12:0(3OH)][C14:1(3OH)][C12:0]

M2 species ([M-H]$^-$ signal at 1103.568 m/z, calculated molecular mass 1104.596 Da) corresponds to the species with the following composition: $GlcN_2P_2$[C12:0(3OH)][C14:1(3OH)][C12:0], whereas species **M1** ([M-H]$^-$ signal at m/z 921.405, calculated molecular mass 922.426 Da),lacks C12:0. The positive MS/MS fragmentation spectrum of the selected **M2** species showed for the B1 fragment ion the following composition: GlcNP[C14:1(3OH)][C12:0], thus indicating that the C14:1(3OH) is *N*-linked to the GlcNII and that the C12:0 is linked as acyloxyamide to this residue.
In order to obtain the detailed information on the distribution on the disaccharidic backbone, MS and MS/MS spectra in the positive ion mode were generated. The positive ions mass spectrum of lipid A, performed by a Q Exactive Hybrid Quadrupole Orbitrap, showed the presence of the adduct ions $[M+Et_3N+H]^+$ of species **K1-K5** (Figure 4.3). The spectrum displays the same heterogeneity as already observed with the ESI FT-ICR MS in the negative ions mode, even if a different relative intensity among the signals was detected.

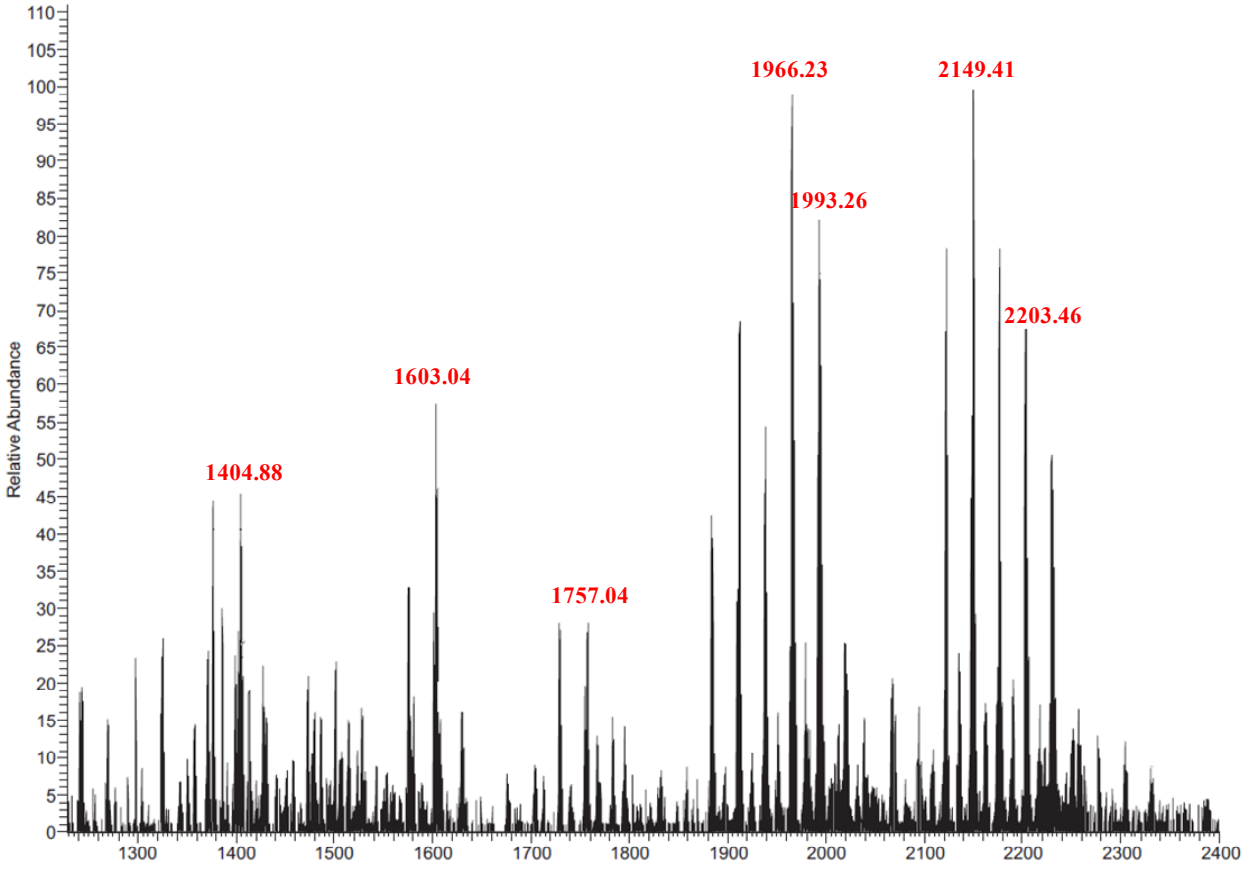

Figure 4.3: Q-Exactive Hybrid-Quadrupole-Orbitrap positive ion spectrum of the lipid A from *Colwellia psychrerythraea* 34H.

In particular, the adducted species at 1603.04 *m/z*, corresponded to the penta-acylated glycoform **K2** (calculated molecular mass 1500.92 Da). The MS/MS spectrum of this signal (Figure 4), obtained by infrared multiphoton dissociation (IRMPD), displayed a **B1** fragment ion (Domon et al., 1988; Kondakov et al., 2005) at *m/z* 846.55 with the following composition: GlcNP[C14:1(3OH)][C12:0(3OH)][C12:0]. Instead, the **Y1** fragment at *m/z* 558.40, indicated only two primary fatty acids [C12:0(3OH)], thus identifying the reported **K2** structure (Figure 4.4).

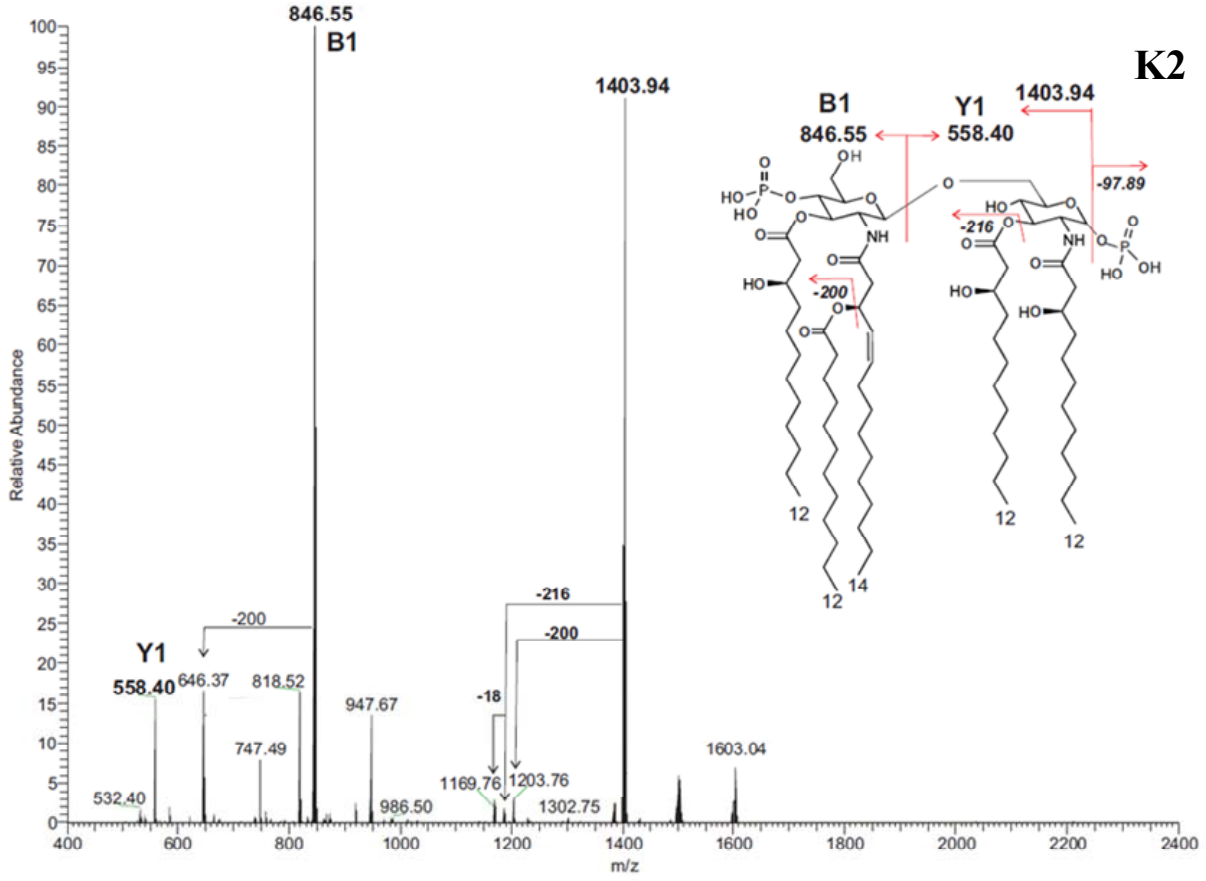

Figure 4.4: MS/MS positive ion mass spectrum of the selected parent ion at *m/z* 1603.00.

This procedures was applied for most of the signals displayed in Figure 4.3, and, from the **B1** and **Y1** fragment ions, the structure of all the glycoforms was obtained. In particular, the signal at *m/z* 1757.04 (calculated molecular mass: 1654.930 Da), corresponding to the **K3** species, is the first glycoform presenting the Gro residue (Figure 4.5)

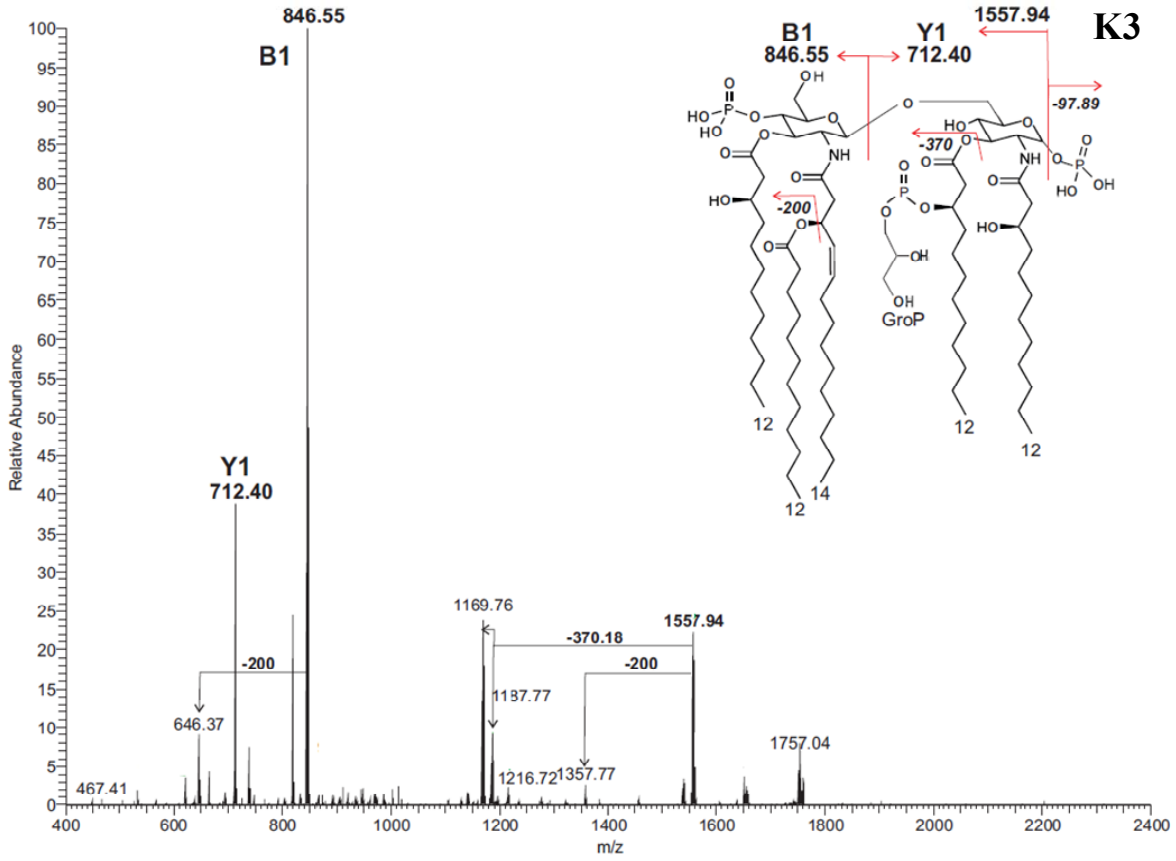

Figure 4.5: MS/MS positive ion mass spectrum of the selected parent ion at *m/z* 1757.04.

Again this species showed the **B**1 fragment at *m/z* 846.55, thus indicating that the Gro was linked to the GlcNI. Instead, **Y1** fragment at 712.40 *m/z* corresponded to the following composition: GlcN[C12:0(3OH)]$_2$GroP. The neutral loss of 370 u indicated that the GroP was phosphodiester linked to the hydroxyl of fatty acid at position 3 of GlcNI. Finally, the tandem mass spectra indicated that the additional fatty acids of the hexa- and hepta-acylated species are linked to the GroP.

4.1.3 Discussion

In this study, it has been shown that the lipopolysaccharude or free lipid A can trigger morphological changes that could be responsible of cold adaptation. To investigate the structural features that might be involved in this phenomon, the lipid A from *Colwellia psychrerythraea* 34H was isolated and characterized by mass spectrometry. The high heterogeneity of this structure, already indicated by the fatty acids analysis, was confirmed by the complexity of MS and MS/MS

spectra. These last experiments, performed in positive ion mode on a Q Exactive Hybrid Quadrupol Orbitrap mass spectrometer, indicated a variable state of acylation ranging from tetra- to hepta-acylated glycoforms.

All lipid A species contained a set of conserved primary acyl chains consisting of a *N*-linked [C12:0(3-OH)] at the 2 position, an unusual *N*-linked [C14:1(3-OH)] at the 2'-position, and two *O*-linked [C12:0(3-OH)] at the 3 and 3' positions, respectively. The secondary C12:0 fatty acid was present in all the glycoforms at the position 2'. Most surprising was the unusual set of modification at the secondary acylation site of the 3 position consisting of phosphoglycerl (GroP) differently substituted. The lipid A from *C. psychrerythraea* 34H moiety displayed a structure that is quite new among the LPSs. In fact, it shows the presence of unsaturated 3-hydroxy fatty acids, a feature that up to now is reported only for *Agrobacterium tumefaciens* (*Silipo et al., 2004*) and *Vibrio fischeri* (*Philips et al., 2011*). In particular, the structure of lipid A from *Colwellia psychrerythraea* 34H is very similar to that of *Vibrio fischeri*, for the presence of phosphoglycerol (GroP) differently substituted.

4.2 Capsular polysaccharide (CPS)

4.2.1Isolation and purification of CPS

The presence of capsular structure around the cells of *Colwellia psychrerythraea* 34H grown at 4 °C was first highlighted by classic Indian ink staining (data not shown) and then confirmed by TEM analysis. TEM images (Figure 4.6) revealed details of the cell envelope, including the presence of a capsular structure surrounding most of the observed cells.

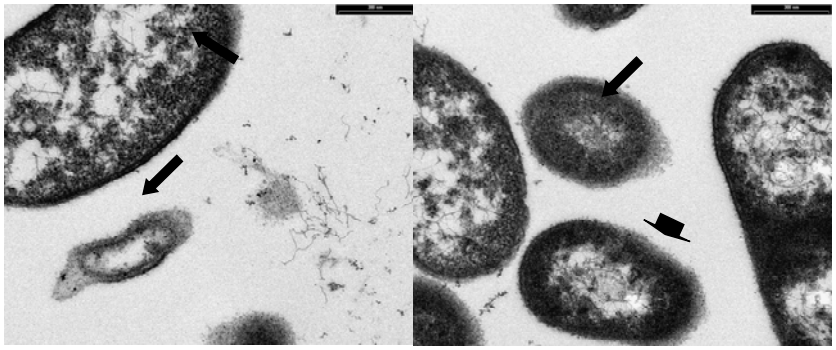

Figure 4.6: Transmission electron microscopy (TEM) images of thin sections of *Colwellia psychrerythraea* 34H. The black arrows indicate the bacterial capsule.

Colwellia psychrerythraea strain 34H was grown aerobically at 4°C in Marine Broth medium until late exponential phase, then cells were separated from spent medium by gentle centrifugation. Both resulting fractions (i.e. cell pellet and culture supernatant) were kept and stored at -20°C. The lipooligosaccharide (LOS), which is the major component of the outer leaflet of bacterial external membrane (*Carillo et al., 2013*), and CPS molecules (*Carillo et al., 2015*) were extracted and from the cells by using PCP and water/phenol method, respectively. The water extract was extensively dialyzed against water, and the dyalizate was lyophilized and depleted of nucleic acid proteins through enzymatic digestion. The purified sample was visualized by 14% DOC-PAGE using either silver nitrate or Alcian blue staining methods (Figure 4.7). The silver nitrate showed the presence of only one band at low molecular masses, corresponding to LOS, which has been characterized elsewhere (*Carillo et al., 2013*). Instead, the Alcian blue staining method, which is sensitive to polyanionic substances, allowed us to visualize bands at higher molecular masses too.

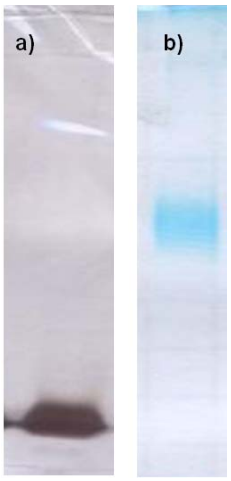

Figure 4.7: Analysis of the CPS fraction from *C. psychrerythraea* 34H by 14% DOC-PAGE. The gel was stained with silver nitrate (a) and Alcian blue dye (b).

Sugar and fatty acid analysis of the sample showed the presence mainly of galacturonic acid (GalA), glucuronic acid (GlcA), 2-amino-2-deoxy-glucose (GlcN) and 2-amino-2-deoxy-galactose (GalN), together with 3,6-dideoxyhexose, mannose and 3-hydroxylated dodecanoic acid, which belong to the LOS, confirming its presence in the aqueous extract. The molecular masses of CPS and LOS species were expected to be very different on the basis of the DOC-PAGE analysis. Nevertheless, the well-known ability of the LOS to form micellar aggregates in aqueous solution did not allow the separation of the two molecular species by size exclusion chromatography. As an alternative, the sample was hydrolyzed under mild acidic conditions to cleave the glycosidic linkage between the lipid A and the saccharidic region of the LOS. After centrifugation, the supernatant containing the CPS and the core oligosaccharidic portion of the LOS was separated from a precipitate constituted by the lipid A. The supernatant mixture was separated on a Biogel P-10 chromatography column, using pyridinium acetate buffer as eluent. Two fractions were obtained: the first one, eluted in the void volume, contained the higher molecular mass material; the second one (OS) contained species with lower molecular mass, corresponding to the core oligosaccharide of the LOS. A further purification of the higher molecular mass material on a Sephacryl S-400HR chromatography column, using ammonium hydrogen carbonate as eluent, resulted in obtaining a major fraction containing the capsular polysaccharide under study (CPS).

In collaboration with Prof. Luigi Paduano, the molecular mass of CPS was evaluated through the static light scattering technique. The analysis indicated an average molecular weight of 1500 KDa, and revealed the presence of a single distribution around 100 nm. The large size of the scattering object suggests that probably the CPS self-assemble in a single aggregate.

To determine monosaccharides composition a methanolysis reaction followed by an acetylation was performed on the CPS, and the obtained acetylated methyl glycosides were injected into the GC-MS. This analysis revealed the presence of GalA, GlcA, GlcN and GalN, besides to a signal attributed to a threonine residue on the basis of the comparison with an authentic standard. The absence of fatty acids in the GC-MS chromatogram indicated that the LOS was definitively removed. A D configuration was identified for all the monosaccharides, whereas L was found for threonine. Finally, the methylation analysis revealed the presence of 4-substituted GlcA, 3-substituted GlcN and 3-substituted GalN. No indications about the GalA substitution were found out.

4.2.2 NMR analysis of purified CPS

CPS polysaccharide was then analyzed by mono- and two-dimensional NMR (DQF-COSY, TOCSY, ROESY, NOESY, ^{1}H-^{13}C DEPT-HSQC, ^{1}H-^{13}C HMBC, 2D *F2*-coupled HSQC). The 2D-NMR analyses allowed the complete characterization of all of the spin systems. The anomeric configurations have been deduced from the $^{1}J_{C1,H1}$ coupling constants and, *inter alia*, by $^{3}J_{H1,H2}$ and chemical shifts values.

The ^{1}H-^{13}C DEPT-HSQC NMR spectrum (Figure 4.8, Table 4.3) displayed the presence of four anomeric cross-peaks at δ 5.31/98.3 (**A**), 4.50/104.7 (**B**), 4.35/104.5 (**C**) and 4.36/102.3 ppm (**D**). The correlations present in the COSY, TOCSY spectra (Table 4.3) indicated a *gluco*-configuration to residues **B** and **C** and a *galacto*-configuration to residues **A** and **D**. In particular, for residue B, starting from H1 signal in the COSY and TOCSY experiments, H2 up to H5 signals were rapidly identified, due to large $^{3}J_{H,H}$ ring coupling constants. Then, the identification of H6 protons was obtained from HMBC spectrum, based on the correlations between C4 carbon atom at δ 69.8 ppm and the two H6 protons at δ 3.78/3.61 ppm. As for residue **C**, we observed a coincidence of the chemical shift value of its proton anomeric signal with that of **D**. Therefore, after identification of H2 of C at δ 3.23 ppm in the COSY spectrum, the glucuronic acid was recognized, due to the cross-peaks from this proton up to H5 in the TOCSY experiment. This last was in turn connected in the HMBC spectrum with a carboxyl signal at δ 175.4 ppm. The H5 was therefore identified in the NOESY and ROESY spectra by NOE contacts between H5 and H1/H3.

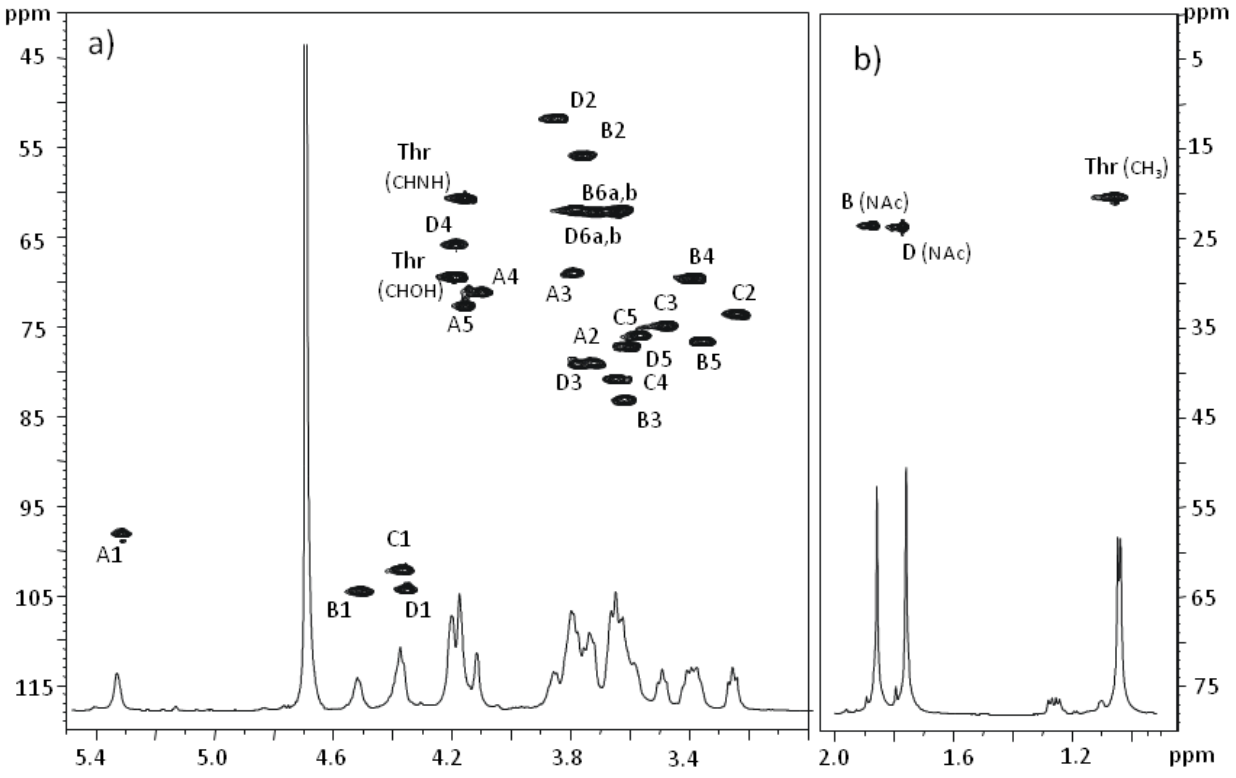

Figure 4.8: Carbinolic anomeric (a) and aliphatic (b) regions of $^{1}H,^{13}C$ DEPT-HSQC spectrum of CPS from *C. psychrerythraea* 34 H. The spectrum was recorded in D_2O at 298 K at 600 MHz.
The letters refer to residues as described in Table 1.

An additional spin system of a threonine residue was present. In fact, three resonances at 1.05/20.5, 4.18/69.8 and 4.15/60.8 ppm, attributed to CH_3, CHOH and CHNH groups respectively were found. Finally, threonine carboxyl group (δ 177.2 ppm) was revealed by the long-range scalar coupling present in the HMBC experiment (Table 4.1, Figure 4.9).

Table 4.3: ^{1}H and ^{13}C NMR assignments of CPS. Spectra were recorded in D_2O at 298 K. Signals at δ 5.31/98.3 ppm, previously assigned respect to acetone as internal standard (δ H 2.225 ppm and δ C 31.45 ppm), were used as reference.

Residue	H1 C1	H2 C2	H3 C3	H4 C4	H5 C5	H6a,b C6
A 2-α-D-Galp*A*6LThr	5.31	3.72	3.79	4.09	4.16	-
	98.3	79.2	69.2	71.2	72.9	171.5
B 3-β-D-Glc*p*NAc	4.50	3.75	3.62	3.38	3.35	3.78-3.61
	104.7	56.0	83.3	69.8	76.8	62.1
C 4-β-D-Glc*p*A	4.35	3.23	3.48	3.65	3.59	-
	104.5	73.9	74.9	81.0	77.3	175.4
D 3-β-D-Gal*p*NAc	4.36	3.84	3.76	4.19	3.56	3.71-3.64
	102.3	52.0	79.3	66.1	76.1	62.3

Additional chemical shifts:

NAc at δ 1.86/23.7 ppm (CH_3), 176.4 ppm (CO); δ 1.77/23.8 ppm (CH_3), 176.0 ppm (CO)

Thr at δ 1.05/20.5 ppm (CH_3), 4.18/69.8 ppm (CHOH), 4.15/60.8 ppm (CHNH), 177.2 ppm (COOH)

Residue **A** was assigned to a 2-substituted galactopyranuronic acid as its C2 resonance was shifted downfield (δ 79.2 ppm) with respect to that of an unsubstituted galacturonic acid unit (Ramos et al., 1996), and its α configuration was deduced from the $^1J_{C1,H1}$ coupling constant value (181 Hz). Moreover its H5 proton showed a long range scalar connectivity with its C6 carbon atom at 171.5 ppm. This last value was shifted up-field respect to the reference value (Ramos et al., 1996), thus indicating that the carboxyl group is involved in an amide linkage (Sidorczyk et al., 1995). This fact indicated that threonine substitutes the position C6 of residue **A**, according to NOESY spectrum in H_2O/D_2O. Residue **C** was assigned to a 4-substituted glucuronic acid, as its C4 resonance was shifted downfield (δ 81.0 ppm) with respect to the reference value (*Bock et al., 1983*), and its β configuration was inferred from the $^1J_{C1,H1}$ (169 Hz). In addition, both its H4 and H5 protons showed a correlation in the HMBC spectrum with a carboxyl signal at δ 175.4 ppm (Figure 4.4).

Residue **B** and **D** were identified as a 3-substituted β-glucosamine and β-galactosamine, respectively, on the basis of $^1J_{C1,H1}$ values (169 Hz for both) and the correlations of their H2 protons at δ 3.75 and δ 3.84 ppm, with the nitrogen-bearing carbons at δ 56.0 and 52.0 ppm, respectively. Moreover, both residues showed downfield chemical shifts for their C3 carbons (δ 83.3 and 79.3 ppm, respectively). Both H2 protons were also shifted downfield indicating the presence of acyl substituents on the amino groups, which are acetyl groups. In fact, both methyl signals at δ 1.86 and 1.77 ppm displayed in the HMBC experiment long-range scalar couplings with signals at δ 56.0/176.4 and 52.0/176.0 ppm, respectively (Figure 4.9).

The sequence of residues and the confirmation of the attachment points of glycosidic linkages were obtained by an in depth analysis of the HMBC, NOESY and ROESY spectra. Long range scalar

correlations were observed in the HMBC spectrum for C1 of **D** (C1**D**) and H4 of **C** (H4**C**), H1**C** and C3**B** and H1**B** and C2**A**. The substitution of residue **D** by the residue **A** was deduced from the ROESY and NOESY experiments, as both spectra showed inter-residue dipolar couplings between H1**A** and H3**D** and H4**D**. Inter-residue dipolar couplings were also observed between H1**D** and H4**C**, H1**C** and H3**B** and H1**B** and H2**A**.

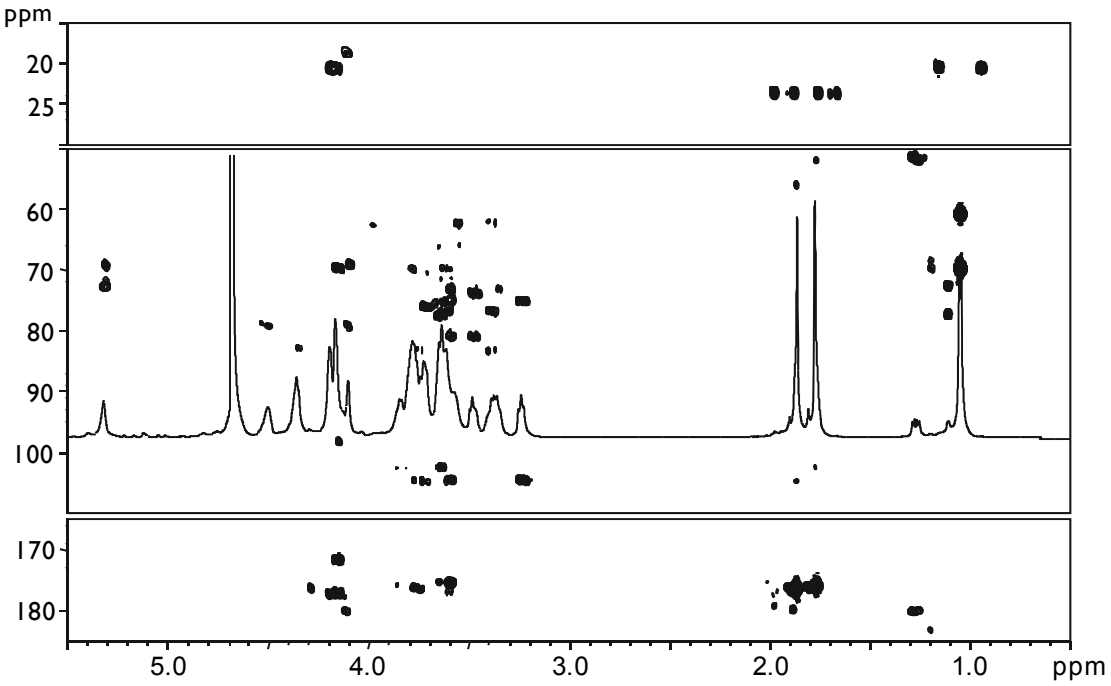

Figure 4.9: HMBC experiment of CPS from C.psychrerythraea 34H.
Spectrum was recorded at 298K in D_2O.

Finally, the amide linkage between threonine and C6 of galacturonic acid was confirmed by a NOE contact between the amino acid NH (δ 7.60 ppm), identified in the TOCSY experiment , and H5 of residue **A** (δ 4.16 ppm), measured in a NOESY experiment in H_2O/D_2O.

All the above data allowed us to attribute a linear structure to the repeating unit of the capsular polysaccharide from *C. psychrerythraea* 34H, as illustrated in Figure 4.10.

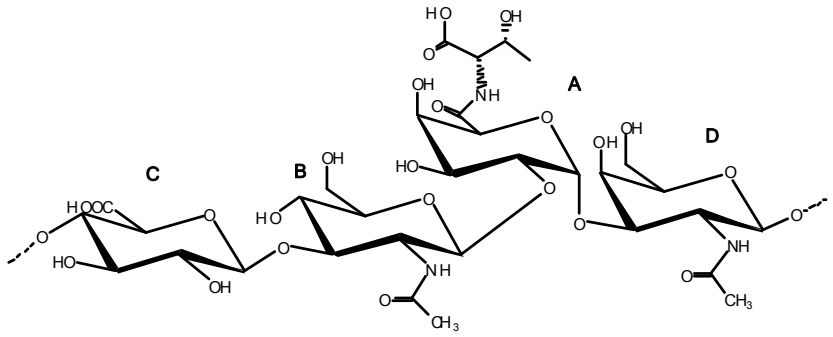

Figure 4.10: Primary repeating tetrasaccharide structure of the capsular polysaccharide isolated from *C. psychrerythraea* 34 H

4.2.3 Three-dimensional structure characterization

Three-dimensional structure characterization was performed by Prof. Antonio Randazzo, Departement of Pharmacy. In order to determine the three-dimensional structure of the capsular polysaccharide, an in-depth analysis of all NMR experiments was performed. The large proton-proton coupling constants observed in residues **B** and **C** suggested that all the protons are in axial positions. Then, also the large coupling between H2 and H3 in residues **A** and **D** suggested a trans-diaxial arrangement of these hydrogens. These data, along NOE connectivities in the NOESY spectra between 1,3-diaxial protons unambiguously indicated the all four sugar moieties assume the classical $^4C_1$ chair conformation. Therefore, dihedral angle constraints were used to keep the sugar in this conformation during structure calculations. NOESY spectra also showed NOEs between H2**A** and H1**B**, and between H1**A**/H1**B**-H5**B**-H3**D**-H4**D**, H3**B**/H1**C**, H4**B**/H1**C**-H2**C** and H5**B**/H1**C** indicating the relative spatial orientation of the sugars. Interestingly, NOEs between H1**B**/H4**D** and H4**B**/H1**D** clearly indicated that the sugar moieties **B** and **D** were spatially close to each other. In order to build a three-dimensional model taking into account all of the experimental data, restrained molecular mechanic and dynamic calculations were performed. Considering that the molecular weight of the polysaccharide is approximately 1500 kDa, and that performing reliable structure calculations at atomic level on a such high molecular mass structure is not possible (especially considering the lack of long-range distance restraints), we opted to create a simplified model (**M1,** Figure 4.11), taking into account about five repetitions of the tetramer A-B-C-D. Using the approach described in Methods, a total of 200 structures were generated. The calculations provided a mixture of isoenergetic conformers characterized by no NOE violations > 0.4 Å.

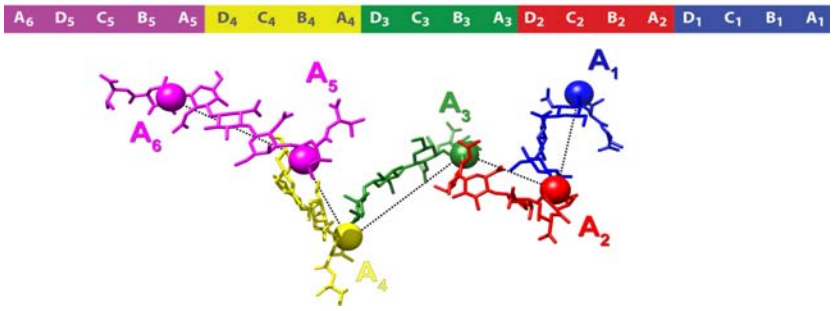

Figure 4.11: Front view of the average **M1** structure deriving from the 20 ns MD production run together with a pictorial representation of its sugar residue sequence.

However, the central repeat, having a more realistic environment, could be clustered in a well-defined family having a good superimposition with root mean squared difference (RMSD) values of 0.77 Å calculated on all heavy atoms of the sugar rings (Figure 4.12 and 4.13). Thus, the representative structure (i.e. the closest to the centroid of the cluster) of this cluster was subjected to molecular dynamics (MD) simulations to probe its thermodynamic stability and to further refine this model in explicit solvent.

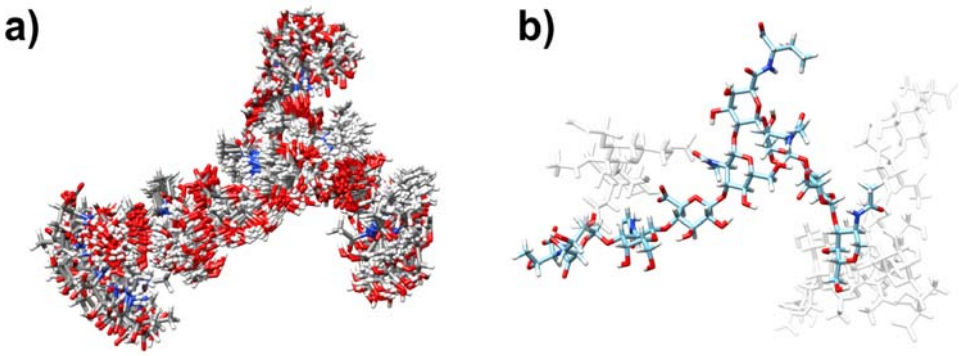

Figure 4.12: (a) Superimposition of the 51 conformations of **M1** belonging to the most populated cluster as calculated through annealing sim-ulations. For clarity reasons, only the central 2 repetitions of the tetramer A-B-C-D, on which the clustering was attained, are represented. (b) Representative **M1** conformation of the most populated cluster. The central 2 repetitions of the tetramer A-B-C-D are represented as cyan sticks while the remaining repetitions are displayed as transparent white sticks.

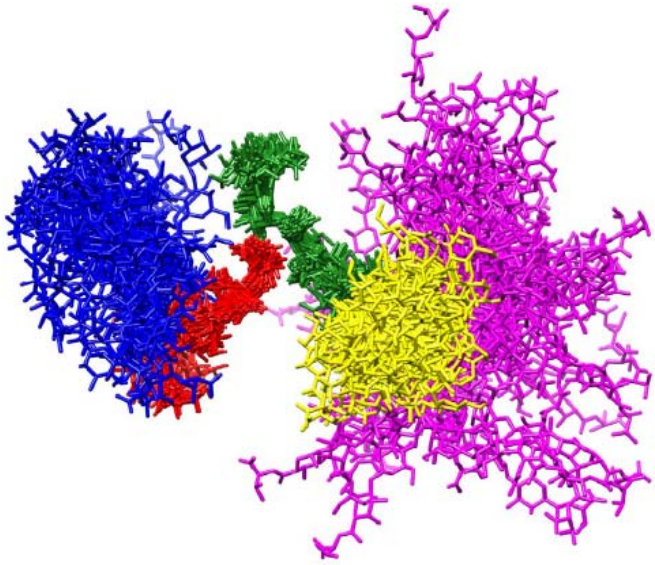

Figure 4.13: Superimposition of the 51 conformations of M1 belonging to the most populated cluster as calculated through annealing simulations. The central 2 repetitions of the tetramer A-B-C-D were used for clustering and superimposition. Repetitions 1 (A1-B1-C1-D1), 2 (A2-B2-C2-D2), 3 (A3-B3-C3-D3), 4 (A4-B4-C4-D4) and 5 (A5-B5-C5-D5-A6) are represented as blue, red, green, yellow and magenta sticks, respectively.

4.2.4 Ice recrystallization inhibition assay

In order to test if CPS actively interacts with ice, Dott. Maddalena Bayer Giraldi (Alfred Wegener Institut, Helmholtz Centre for Polar and Marine Research), tested its effect as ice recrystallization inhibitor. Ice grains recrystallize over time, as large crystals develop at the expenses of smaller ones. Some molecules able to attach to ice, like for example AFPs, inhibit recrystallization (*Bayer-Giraldi et al., 2011; Knight et al., 1986*). Due to light refraction at ice grain boundaries, light transmittance through ice is directly proportional to the size of crystals in the sample. Large ice crystals result in high light transmittance, while small crystals result in low transmittance. Therefore, the recrystallization of ice crystals can be followed recording the change of light intensity over the time. Chondroitin, that is an anionic polysaccharide constituted by an alternating of *N*-acetyl galactosamine and glucuronic acid residues, was used as negative control, due to the similarity of its structure with that of CPS.

Ice recrystallization assay (Figure 4.14) showed that the presence of CPS inhibits recrystallization. Indeed, the light intensity change of the CPS-sample was smaller than the increase recorded for both negative controls. The chondroitin had no statistically relevant effect on ice recrystallization.

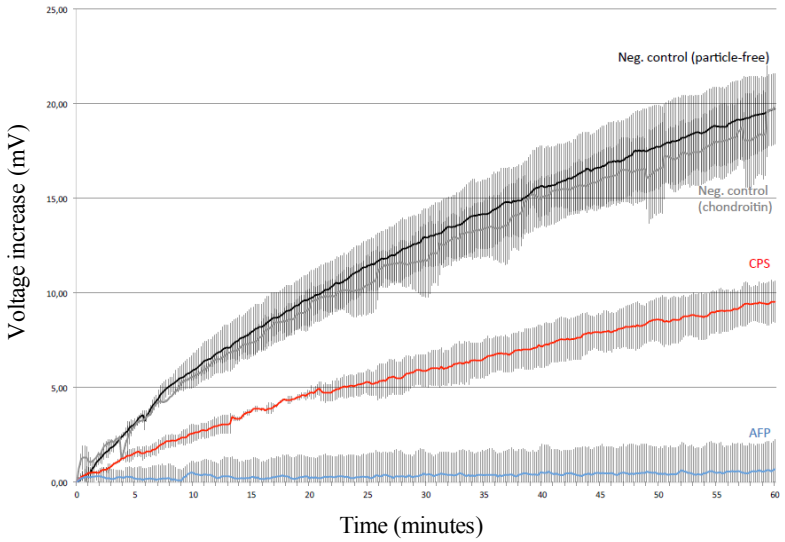

Figure 4.14: Recrystallization of frozen samples as assayed in the Optical Recrystallometer. The light intensity increases as a function of time is indicative for recrystallization processes of ice crystals. Measurements were performed for 1 hour at 4°C. We measured a solution with CPS (red), a positive control with AFP from *F. cylindrus* (blue), a negative control with chondroitin (grey) and a particle-free positive control (black). The solutions were prepared in ultrapure MilliQ water with 9 ‰ NaCl, particle concentration was adjusted to 6.6 µM. The curves are an average of three samples, error bars show standard deviation.

4.2.5 Discussion

The results of chemical and spectroscopic analyses of the purified capsular material revealed a structure new among bacterial polysaccharides: a linear tetrasaccharide repeating unit containing two amino sugars and two uronic acids, of which one is amidated by a threonine. Even though the glycosyl composition may be comparable to that of EPS produced by many marine bacteria, the presence of amino acids is quite uncommon (*Bock et al., 1983; Komandrova et al., 2010; Palusiak et al., 2013*). The decoration of the polysaccharide with Thr is particularly intriguing to consider. In fact, amino acid motifs are common, and crucial for the interaction with ice, in several different kinds of antifreeze proteins (AFPs) (*Nichols et al., 2005a; Nichols et al., 2005b; Daley et al., 2003*). For example, antifreeze glycoproteins (AFGPs) isolated from fish blood plasma consist of a regular tripeptide sequence of Ala-Ala-Thr with a disaccharide fragment (β-D-galactosyl-(1-3)-α-D-galactosamine) linked to the threonine residue (*Ben at al., 2001*). Antifreeze proteins are known to control ice growth by attaching to ice crystals by their ice-binding-site. The spacing between relevant amino acids on the ice-binding sites often resembles the atomic distances typical for the ice

lattice. Several times, the amino acids show a repetitive pattern or periodic folding, thus showing regularly spaced OH groups (*Jay et al., 2002; Scotter et al., 2006; Pertaya et al., 2008*). The periodic folding of this kind of structures is of a particular interest, and the composition of the polysaccharide, that is composed by repetitive tetrasaccharide units, would suggest a periodic folding as well. In order to determine a possible spatial arrangement of the capsular polysaccharide, all the NMR experiments were analyzed and molecular mechanic and dynamic calculations were performed. We focused our attention on a simplified model (**M1**) of the capsule comprising basically five repeats of the tetrasaccharide base unit. A number of isoenergetic conformations were obtained and only information about the local conformation adopted by the polysaccharide could be retrieved. Interesting structural features characterized the obtained models. First of all, the chains of the sugars A-B-C-D were fairly linear. Furthermore, the orientation of sugars B and D, linked to equatorial position O2 and axial position O1 of sugar A, conferred a "hairpin- like" disposition to the chains. This portion of the polysaccharide seems to be repeated in the space forming an overall "zig-zag" structure, where threonines of sugars A are placed at the very corner of the polysaccharide and are available to interact with the ice. These results, the resemblance of our CPS structure to that of AFGPs, and the lack of sequence coding for a known AFP in the genome of *C. psychrerythraea* 34 H (*Raymond et al., 2007*) prompted us to assay for ice recrystallization inhibition activity of the *Colwellia* capsular polysaccharide purified extract. Our analyses of ice recrystallization activity suggested that CPS interacts with ice in a way resembling AFPs, further supporting structural CPS observations. Results showed that CPS has an effect on recrystallization, whereas other particles like the negative control chondroitin have no statistically relevant effect. It is therefore conceivable that CPS binds to ice, pinning and immobilizing ice grain boundaries with a similar effect as that reported for AFPs. The results showed an effect less marked with respect to that displayed by a recombinant AFP from the sea-ice diatom, which is a strong inhibitor of recrystallization also compared to other AFPs (*Bayer-Giraldi et al., 2011*). However, the comparison between two very different molecules, such as a polysaccharide and a protein, could be not rigorous. Besides the ice-binding patterns, also the size of the molecules, composition and conformation play a role in modulating the effect on ice. Furthermore, it should be considered that the natural concentration of both CPS and AFP, and therefore the effective magnitude of ice activity relevant under physiological conditions, is yet unknown. The only other example of a polysaccharide reported to have properties resembling AFPs activity was extracted from a freeze-tolerant beetle, *Upis ceramboides* (*Walters et al., 2009*). The fact that the polysaccharide examined also contained lipid leaves unresolved whether the polysaccharide or the lipid component was responsible for the activity (*Walters et al., 2009*). This study has demonstrated for the first time the

existence of a purified capsular polysaccharide endowed with ice recrystallization inhibition activity. Its unique structure, in contrast to that isolated from the beetle *U. ceramboides*, is strongly related to that of AFGPs, both for the presence of a Thr residue and for the Gal-Gal disaccharide motif.

4.3 Extracellular polysaccharide (EPS)

4.3.1 Isolation and purification of EPS

The culture supernatant was extensively dialyzed against water, and the dyalizate was lyophilized; a defined amount was loaded on 14% DOC-PAGE (Figure 4.15, line a), together with a pure CPS sample (Figure 4.15, lane c), and the polysaccharidic components visualized by Alcian blue staining. Bands at low molecular masses attributable to LOS molecules were clearly visible, together with CPS bands at higher molecular masses (Figure 4.15, lanes a and c). In addition, the alcian blue visualized another group of bands not visible in the cells extraction (Figure 4.15, lane a).

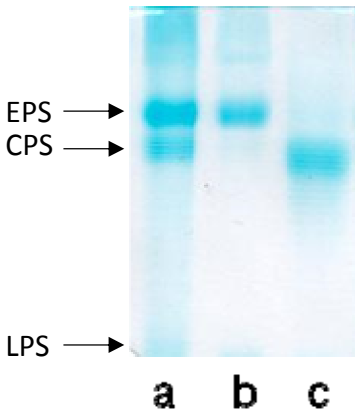

Figure 4.15: Biochemical analysis shows the presence of different polysaccharides in *Colwellia psychrerythraea* 34H growth broth. The broth was dialysed (cut-off 10-12 KDa) and the retained fraction was analysed by gel-electrophoresis DOC-PAGE 14%. The gel was stained with alcian blue. (a) dialysate broth, (b) purified EPS from growth broth, and (c) purified CPS from cells.

The GC-MS analysis of the monosaccharides derivatized as acetylated methyl glycosides (MGA), revealed that all the components of LOS and the CPS were present (*Carillo et al., 2013; Carillo et al., 2015*). In particular, glucuronic acid (GlcA) and 2-amino-2-deoxy-galactose (GalN) together with galacturonic acid (GalA) and 2-amino-2-deoxy-glucose (GlcN) belonged to CPS, while colitose (Col) and was assigned to LOS molecules. In addition, a fairly intense signal of mannose (Man) suggested the presence of a mannan polysaccharide (see below) Finally, the analysis showed the presence of 2-amino-2,6-dideoxyglucose (quinovosamine, QuiN) that was never been identified in the cells extracts.

In order to purify the EPS, the dialysate cells supernatant was treated with acetic acid to dissociate micellar aggregates of LOS, CPS and EPS. This procedure allows the separation of the saccharidic

piece of LOS from the lipid A, the glicolipid moiety of the LPS, the phosphate groups of which could be responsible of saline bridges with the anionic polysaccharides through divalent cations (Mg^{2+} and/or Ca^{2+}).

Hence, the sample was hydrolyzed under mild acidic conditions and after centrifugation, the supernatant containing the saccharidic portion was separated from a precipitate containing the lipid A. The supernatant mixture was then ran on a Sephacryl S-400 HR chromatography column, using ammonium hydrogen carbonate as eluent. Two main peaks were obtained: the first, eluted in the void volume, contained the higher molecular weight compounds, corresponding to CPS and EPS, while the second one contained the core oligosaccharide of LOS, and growth medium components not excluded from the dialysis tubes (data not shown). The polysaccharides mixture was then chromatographed on a Q-Sepharose fast flow ion exchange chromatography column, and eluted with a gradient of NaCl (data not shown). The fraction containing the EPS, visualized by 14% DOC-PAGE 14% (Figure 4.15, lane b), was eluted in the range of 500-600 mM NaCl. The gel also indicated for the EPS a molecular weight higher than CPS (*Carillo et al., 2015*), due to the higher migration distance of EPS respect to the dye front of the gel (Figure 4.15, lanes b and c).

To determine monosaccharides composition, a methanolysis reaction followed by an acetylation was performed, obtaining MGA injected to the GC-MS. This time the analysis showed the presence of GalA and QuiN as the main components, together with a signal assignable to an alanine residue, on the basis of the comparison with a pure standard. A D configuration was determined for both monosaccharides, whereas the alanine residue showed a L-configuration.

4.3.2 NMR analysis of purified EPS

EPS polysaccharide was then analyzed by mono and two-dimensional NMR spectroscopy. In particular, ^{1}H-^{1}H DQF-COSY, ^{1}H-^{1}H TOCSY, ^{1}H-^{1}H NOESY, ^{1}H-^{13}C DEPT-HSQC, ^{1}H-^{13}C HMBC and 2D F2-coupled HSQC experiments were performed. The 2D-NMR analysis allowed the complete characterization of all of spin systems.

The ^{1}H-^{13}C DEPT-HSQC spectrum (Figure 4.16, Table 4.4) displayed the presence of three anomeric cross-peaks at δ 5.54/100.9 (**A**), 4.98/100.8 (**B**), and 4.56/103.5 ppm (**C**).

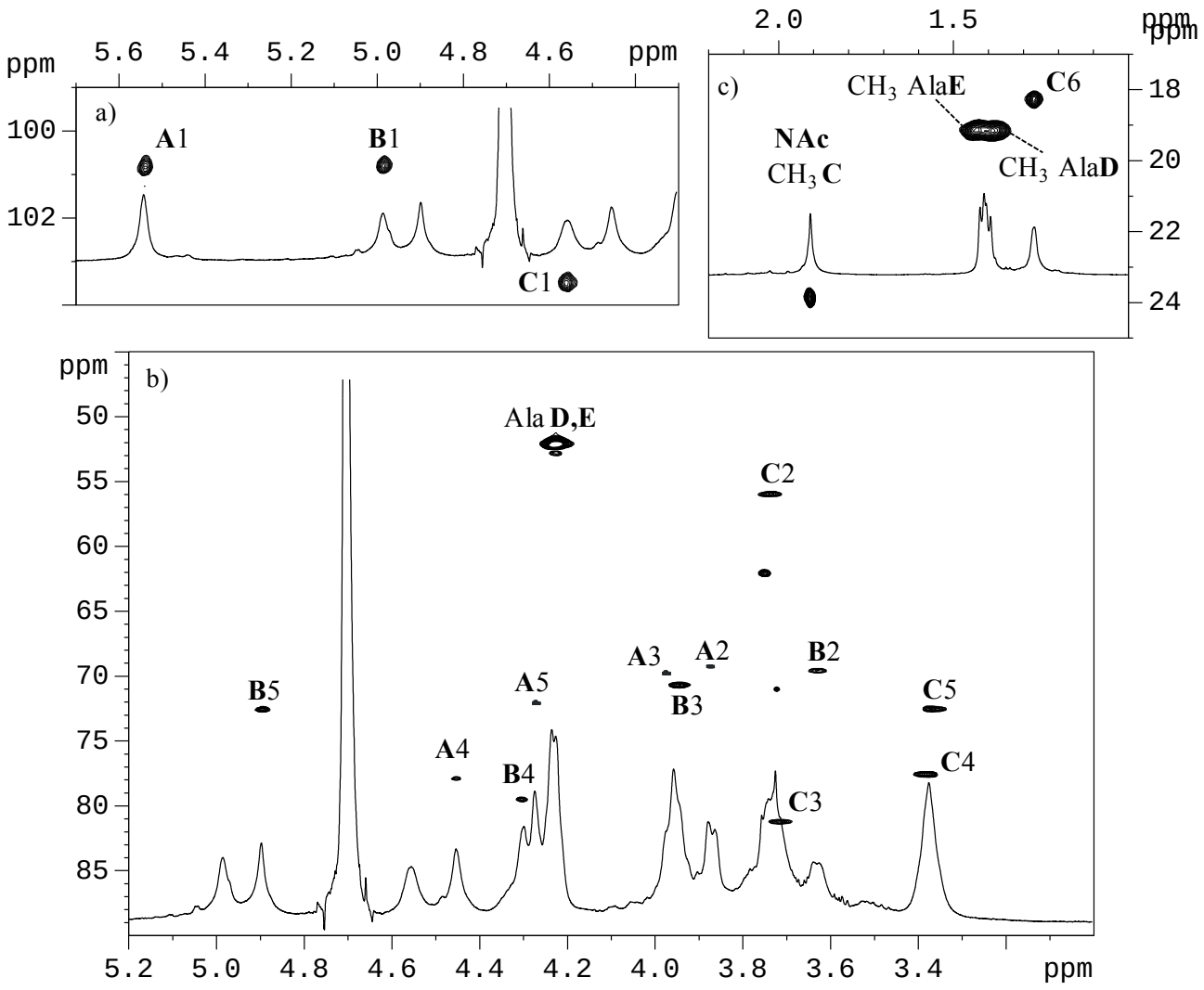

Figure 4.16: Expansions of the ^{1}H-^{13}C heterocorrelated HSQC spectrum together with the corresponding ^{1}H spectrum of EPS from *C. psychrerythraea* 34 H. Anomeric (a), carbinolic (b) and aliphatic (c) regions of ^{1}H-^{13}C HSQC spectrum was recorded in D_2O at 310 K at 600 MHz. The letters refer to residues as described in Table 4.4.

The anomeric configuration of the residues was established by the one bond ^{13}C-^{1}H couplings constants ($^{1}J_{C1\text{-}H1}$) measured in a 2D F*2*-coupled HSQC experiment (Figure 4.16), that suggested an α-configuration for residues **A** and **B** (185 Hz and 177 Hz, respectively), and a β-configuration for residue C (164 Hz).These configurations were further supported by a NOESY experiment (Figure 4.17). Indeed, intra-residue NOE connectivities between H-1 and both H-3 and H-5 for β anomer **C**, and between H-1 and H-2 for α-anomers **A** and **B** were founded.

Table 4.4 .^{1}H and ^{13}C NMR assignments of EPS from *C. psychrerythraea* 34 H. Spectra were recorded in D_2O at 310K at 600 MHz using acetone as external standard (δ_H/δ_C 2.25/ 31.45 ppm).

Residue	H1/ C1	H2/ C2	H3/ C3	H4/ C4	H5/ C5	H6/ C6
A	5.54	3.87	3.97	4.46	4.28	-
4-α-D-Gal*p*A6LAla(D)	100.9	69.0	69.8	77.9	72.0	170.2
B	4.98	3.63	3.95	4.30	4.90	-
4-α-D-Gal*p*A6LAla(E)	100.8	69.6	70.7	79.4	73.0	171.0
C	4.56	3.74	3.72	3.39	3.37	1.27
3-β-D-Qui*p*NAc	103.5	56.0	81.2	77.7	72.5	18.4

Additional chemical shifts:

NAc: at δ 1.91/24.0 (CH_3), 175.9 (CO)

Ala (D): at δ 4.23/52.0 (CH), 1.39/19.2 (CH_3), 180.3 (COOH), 7.91 (NH, H_2O/D_2O)

Ala (E): at δ 4.22/52.2 (CH), 1.42/19.2 (CH_3), 181.2 (COOH), 7.70 (NH, H_2O/D_2O)

Residues **A** and **B** were recognized as *galacto*-configured residues based on the presence of cross-peaks from H-1 up to H-4 in the TOCSY spectrum. Then, in the NOESY spectrum, starting from H-4, the H-5 resonance was identified. Both these residues were assigned to 4-substituted galactopyranuronic acids since their C-4 signals were shifted downfield (δ 77.9 ppm for **A** and δ 79.4 ppm for **B**, respectively) with respect to that of an unsubstituted galacturonic acid (*Bock et al., 1983*). In both residues, H-5 proton signals showed in the HMBC experiment a long-range scalar connectivity with the C6 carboxyl signals at δ 170.2 ppm and δ 171.0 ppm, for residues **A** and **B** respectively. These last values were upfield shifted with respect to the reference value (*Bock et al., 1983*), thus indicating that these carboxyl groups were involved in amide linkages. Indeed, two additional spin systems of alanine residues were present. In particular, resonances at δ 4.23/52.0 and δ 1.39/19.2 ppm for the spin system Ala (**D**) and 4.22/52.2 and 1.42/19.2 ppm for the spin system Ala (**E**), attributable to CH and CH_3 groups, respectively, were found (Figure 4.16). Finally,carboxyl groups at δ 180.3 ppm and 181.2 ppm, for **D** and **E** respectively, were revealed by the long range scalar couplings in the HMBC experiment.

Residue **B** was linked to C-4 position of residue **A,** as deduced from the HMBC experiment which displayed a long range scalar correlation between H-1 of **B** at δ 4.98 ppm and C-4 of **A** at δ 77.9 ppm. The substitution was also confirmed by the NOESY spectrum, that showed inter-residue contact between H-1 of **B** and H-4 of **A** (Figure 4.17).

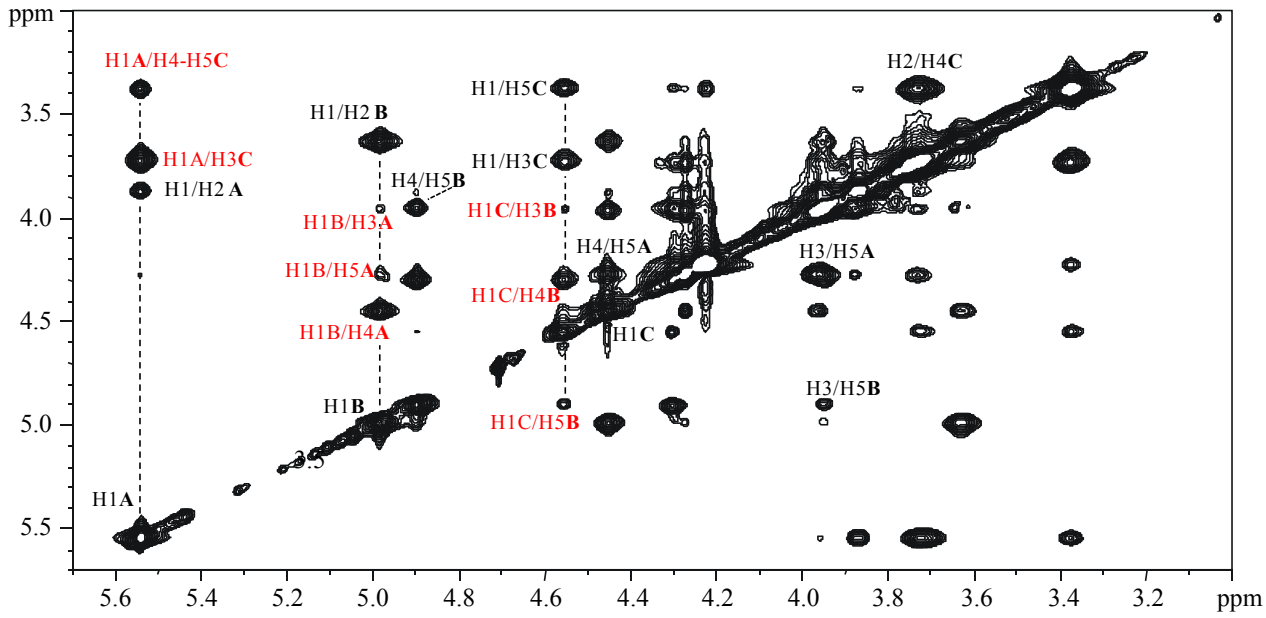

Figure 4.17: Expansion of the NOESY spectrum measured at 310K in D_2O (50 ms as mixing time). Correlations' attribution follows the letters system of Table 4.4; in black and red are reported intra-residues and inter-residues correlations, respectively.

The correlations present in COSY and TOCSY spectra indicated a *gluco*-configuration for residue **C**. In the TOCSY spectrum, starting from H-1 proton signal at δ 4.56 ppm up to the methyl protons signal at δ 1.27 ppm, all ring protons chemical shifts could be identified. Residue **C** was then identified as a β-quinovosamine, since in the ^{1}H-^{13}C DEPT-HSQC experiment its H-2 correlated with a nitrogen bearing carbon at δ 56.0 ppm (Figure 4.16). The H-2 signal (δ 3.74 ppm) was found to be downfield shifted, due to the presence of an acyl substituent on the amino group, that was identified as an acetyl. In particular, NOESY experiment measured in H_2O/D_2O (Figure 4.18) revealed a NOE contact between the N-H at δ 8.39 ppm and H-2 of **C**, that in turn correlated with the methyl group at δ 1.91 ppm.

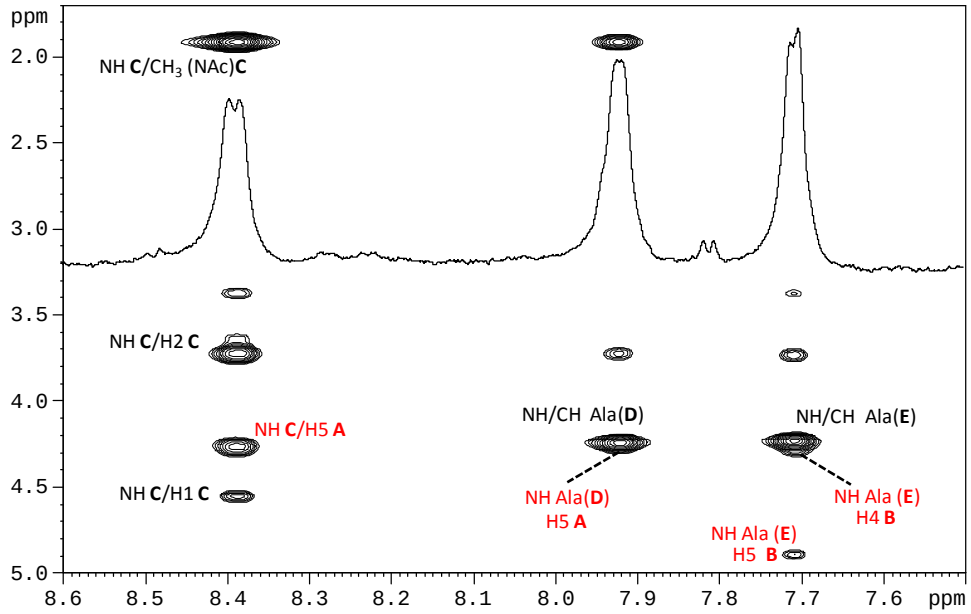

Figure 4.18: Expansion of the ^{1}H-^{1}H NOESY spectrum together with the corresponding ^{1}H spectrum of EPS from *C. psychrerythraea* 34 H. The spectrum was performed in H_2O/D_2O 9:1 at 310 K. NH relevant cross-peaks for alanines **D** and **E**, and quinovosamine **C**. Correlations' attribution follows the letters system of Table 4.4; in black and red are reported intra-residues and inter-residues correlations, respectively.

Finally, this last signal showed a long range scalar connectivity with the carbonyl signal at δ 175. 9 ppm in the HMBC experiment (Figure 4.19) . Furthermore, C-3 resonance of the same residue, was shifted downfield (δ 81.2 ppm, Table 4.4) with respect to that of an unsubstituted quinovosamine residue (*Knirel et al.,1987; Corsaro et al., 2006*), suggesting a glycosidic linkage at this position. In fact, this carbon signal displayed a weak long range scalar connectivity in the HMBC spectrum with H-1 of residue **A** (δ 5.54 ppm). The NOE contact between H-1 of A and H-3 of C confirmed the linkage between **A** and **C** (Figure 4.17).

Residue **C,** in turn, was linked to C-4 position of **B**, in agreement with a long range scalar connectivity between H-1 of **C** at δ 4.56 ppm and C-4 of **B** at δ 79.4 ppm. This substitution was also confirmed by a strong NOE contact between H-1 of **C** and H-4 of **B**.

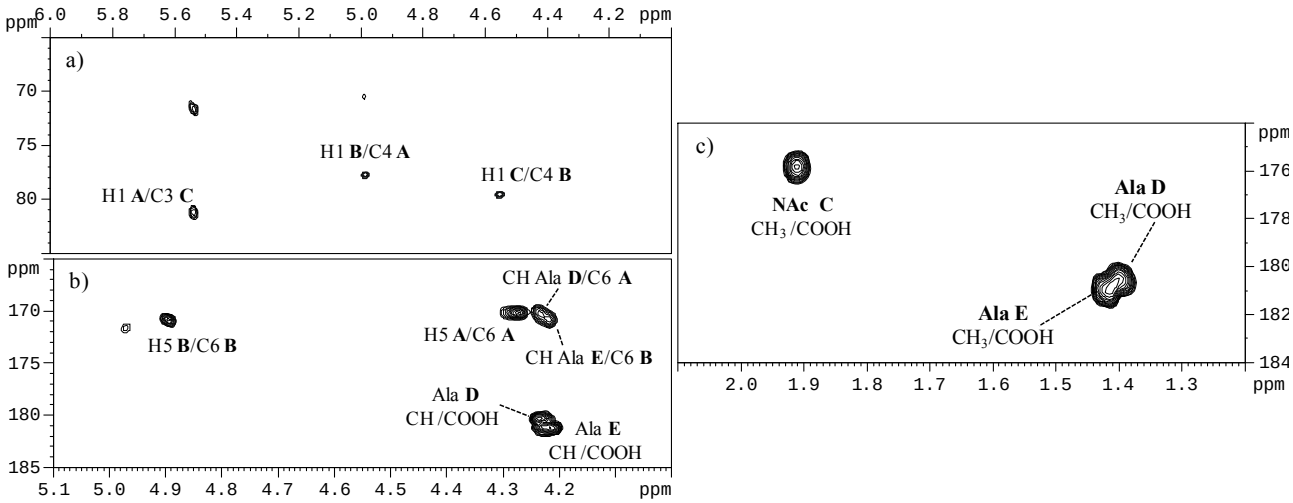

Figure 4.19: Expansiona of the HMBC spectrum measured at 310K in D_2O. Correlations' attribution follows the letters system of Table 4.4

Finally, the substitution of the two carboxyl groups of **A** and **B** by alanine aminoacids **D** and **E**, respectively, was deduced by NOESY (Figure 4.17) and TOCSY data measured in H_2O/D_2O. In particular, the amide linkage between C-6 of residue **B** and alanine **E** was revealed from a NOE contact between the amino acid N-H (δ 7.70 ppm), identified in the TOCSY experiment, and both H-5 and H-4 signals of residue **B** (δ 4.90 and 4.30 ppm, respectively). In the same way, the NOE contact between N-H of **D** (δ 7.91 ppm) and H-5 of **A** (δ 4.28 ppm) confirmed the substitution of **A**. All the above data indicated for EPS from *Colwellia psychrerythraea* 34H a trisaccharidic repeating unit, as illustrated in Figure 4.20.

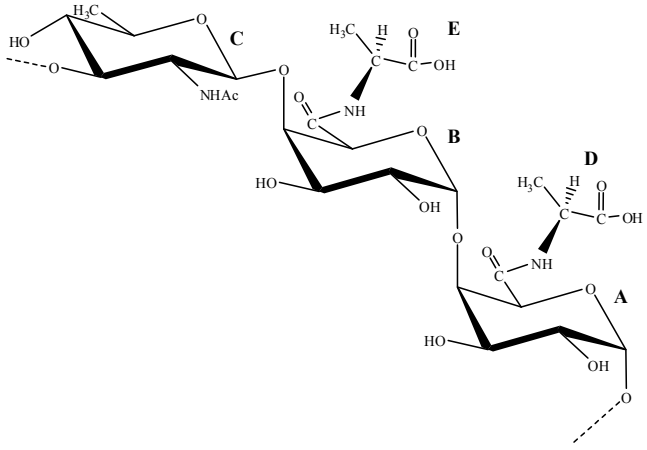

Figure 4.20: Primary repeating trisaccharide structure of the EPS produced by *C. psychrerythraea* 34 H.

4.3.3 Three-Dimensional Structure Characterization

In order to determine the three-dimensional structure of the EPS, an in-depth analysis of all NMR experiments was performed, and the 3D structure was obtained thanks to the collaboration with Prof. Antonio Randazzo. The NOE connectivity in the NOESY spectra between 1,3-diaxial protons (H-3 and H5 of **A** and **B**, and H-1/H-3/H-5 and H-2/H-4 of **C**), unambiguously indicated that all three sugar moieties assume the classical $^4C_1$ chair conformation. Therefore, dihedral angle constraints were used to keep the sugar in this conformation during structure calculations. NOESY spectra also showed interesting inter-residue NOEs that are diagnostic for the determination of the general conformation of the polysaccharide. Particularly, strong NOEs between H-1 of **A**, **B** and **C** and H-4 of **C**, **A** and **B**, respectively, along with strong NOEs between H-1 of **A** and H-3/H-5 of **C**, weak NOEs between H-1 of **B** and H-3/H-5 of **A**, and between H-1 of **C** and H-3/H-5 of **B** indicate the relative spatial orientation of the sugars. The lack of long-range NOEs indicates that the overall structure of the polysaccharide is fairly linear. These structural information were employed to construct a reliable model of the EPS polysaccharide through restrained molecular dynamics simulations. In this respect, it should be outlined that the molecular weight of the purified EPS is higher than CPS molecules, which was found to be 1500 KDa (*Carillo et al., 2015*), thereby hampering the simulation of the entire system. Therefore, following the strategy already applied in a previous study on CPS (*Carillo et al., 2015*), also in this case we decided to construct and simulate a simplified model of the EPS structure. Most precisely, a polysaccharide made up by five repetition of the trimer A-B-C was constructed resulting in a 15-mer structure. By employing the computational protocol described in the computational methods, an ensemble of 200 isoenergetic structures was calculated featuring for all the considered distances a maximum violation of 0.4 Å. Subsequently, these different conformations were clustered considering the sugar ring atoms of the three central repeats with rmsd value of 1.5 Å. This choice to disregard the terminal repeats from the clustering was dictated by the fact that these are less representative of the whole conformational behavior of the polysaccharide. By clustering the 200 conformations of our model system, 14 different clusters were obtained in which cluster number 1 represented the 83% of the total ensemble demonstrating a good convergence of our calculations toward a well-defined structure. For this cluster the representative conformation was considered (i.e. the one closest to the centroid of the cluster) for further 310 K MD simulations aimed at probing the thermodynamic stability in explicit solvent and assessing the behavior of water molecules around the considered structure.

From this analysis, it was clear that the three central repeats adopt a fairly linear conformation that roughly resembles a left-handed helix (Figure 4.21).

This conformation seems to be stabilized by a series of inter residue H-bond interactions. Of particular interest is the formation of a H-bond between the amide nitrogen of the N-acetyl quinovosamine (residue **C**) and the carbonyl oxygen of the adjacent galacturonic acid (residue **B**). Indeed the β-glycosidic linkage of residue **C** forces the aforementioned atoms in closed vicinity so as to make this interaction possible (Figure 4.21).

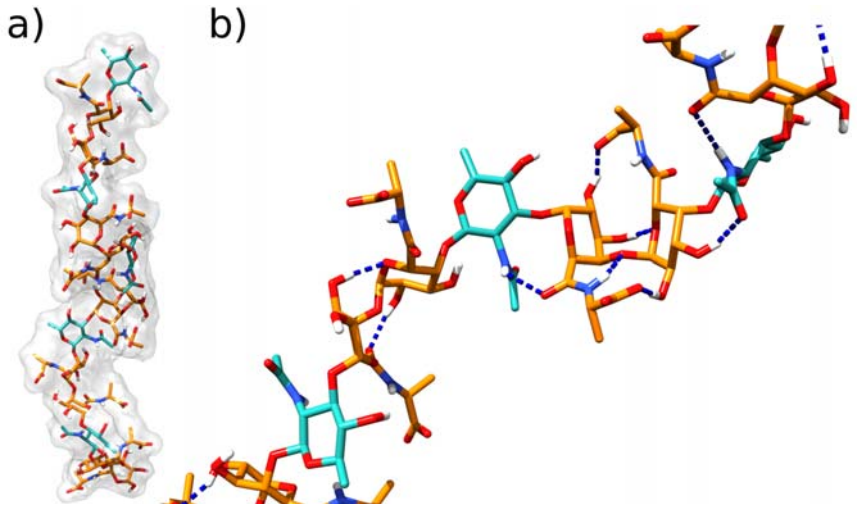

Figure 4.21: Front (a) and zoomed (b) view of the representative structure of EPS as calculated by restrained SA calculations. Residue **A** and **B** are represented as orange sticks while residue **C** as cyan sticks. H-bonds are represented as dashed blue lines.

Additional polar interactions are further established by the alanine attached to residue B and the C2 hydroxy group of residue A. These interactions seem to play a prominent role in the induction of a pseudo helicoidal structure and would lock the conformation of the amino acid with respect to the sugar skeleton. Thus, these studies would outline the importance of three structural features: i) the amide nitrogen of quinovosamine, ii) the specific β-glycosidic linkage of this residue, and ii) the presence of the alanine attached to the galacturonic acid.

In particular, MD data were analyzed to estimate the thermodynamic values for the water molecules interacting with our polysaccharide through the Grid Inhomogeneous Solvation Theory Method (GIST) developed by Nguyen et al. (*Nguyen et al., 2012*). This method enables the characterization of each region around the solute with respect to its water occupancy, the energetic interaction with other water molecules and the solute, and its entropic contribution. Herein, these data allowed us to visualize the regions of the modeled polysaccharide that are more positively contacted by water molecules. In particular, by calculating the density weighted solute-water interaction energy

(kcal/mol/A^3) it was possible to visualize the regions where water molecules are found to have more favorable interactions with the polysaccharide (Figure 4.22a). These calculations suggest that the specific conformation induced by the polar interactions described would allow for the energetically favored presence of a water molecule in the cage formed by residue C and its adjacent residues A and B (before and after, respectively); as expected additional favorable solute-water interactions areas are placed around the alanine carboxylate groups (Figure 4.22a).

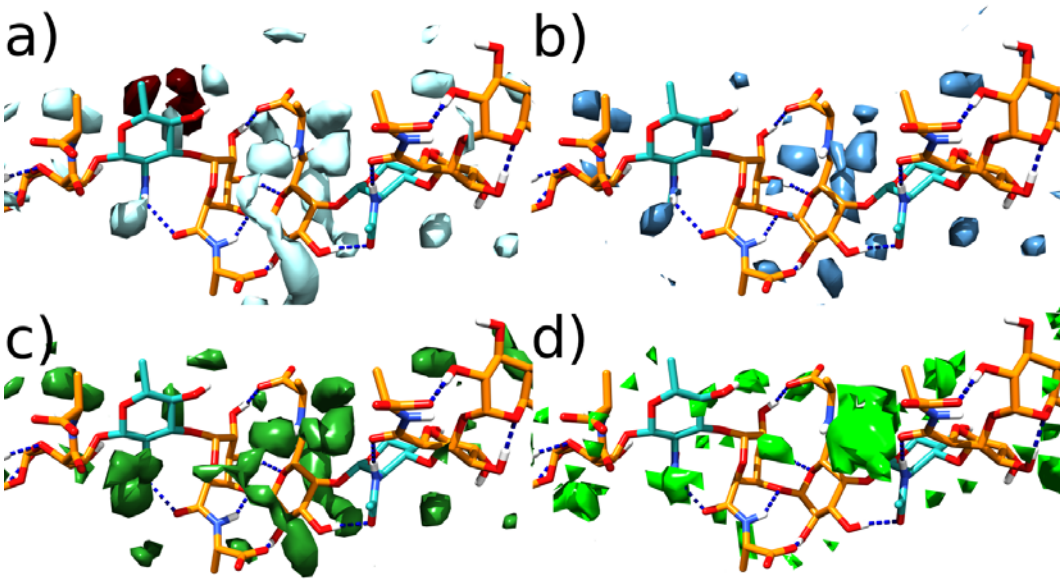

Figure 4.22a: Average structure of EPS polysaccharide deriving from the 20 ns MD production run (a-d). Residue **A** and **B** are represented as orange sticks while residue **C** as cyan sticks. Cyan and brown surfaces in a) represent the regions of the density weighted solute-water interaction energy for an isovalue of 0.67 kcal/mol/A^3. Panels b and c report the density weighted translational (blue surfaces) and orientational entropy (dark green surfaces) maps at an isovalue -0.06 kcal/mol/A^3, respectively. Panel d reports the regions around the solute were a Tetrahedral Order Parameter (Q_k) for surrounding waters has a value of -0.02, meaning no tetrahedral arrangement of water molecules.

Moreover, in this conformation residue **C** exposes its hydrophobic face to the solvent resulting in unfavorable interactions. The trapping of water molecules in the aforementioned cage is further outlined by visualizing the density weighted translational and orientational entropy maps (Figure 4.22 b and c). On the basis of these observations, the effect of the polysaccharide on the structural order of waters in the vicinity was also evaluated. To this end, the tetrahedral order parameter Q_k

was also calculated (*Errington et al., 2001*); this is a measure of the propensity of a particular water molecule and its four neighboring molecules to adopt a tetrahedral arrangement. In this case, negative Q_k values were detected in the sugar cage described above indicating no tetrahedral geometry of water molecules in this area (Figure 4.22d).

4.3.4 Ice Recrystallization Inhibition assay

To assess any cryoprotective effect of this polysaccharide, ice recrystalization inhibition (IRI) activity was measured in collaboration with Prof. Matthew Gibson, University of Warwick. To test this, a modified 'splat' assay was used. Briefly, 10 μL droplets of the polysaccharide in PBS was dropped down a tube into a cooled (~ -70 ºC) glass cover slip, and then transferred to a microscope set at – 6 ºC. After 30 minutes the mean largest grain size (MLGS) was measured and reported relative to a PBS control. It is worth considering that in this assay, MLGS values below ~ 20 % indicate zero growth (as the initial crystals cannot have zero size). The activity of the EPS is reported in Figure 4.23.

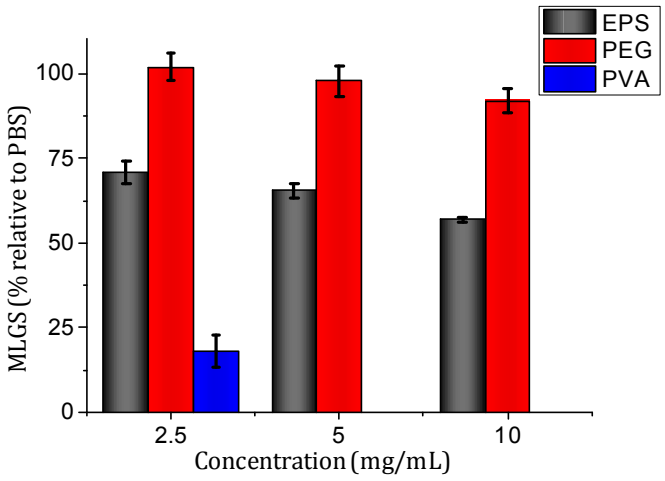

Figure 4.23: Ice Recrystallization Inhibition activity of EPS from *C. psychrerythraea* 34 H was compared with PEG, used as a negative control, and PVA as a positive. Mean largest grain size is expressed as a percentage of PBS buffer, and small MLGS value indicate increased IRI activity.

A positive control poly(vinyl alcohol) and negative control were also used. In the concentration range reported, there was a clear inhibition of ice growth which is rather unique to this polysaccharide. For example, dextran cyclodextrins and other saccharides have little or no IRI (*Deller et al., 2013*). Interestingly, EPS was found to have moderate IRI activity in the concentration range of 2.5 – 10 mg.mL-1.

4.3.5 Discussion

Generally, capsular structure can be found both as cell-membrane associated and released in the culture medium. We demonstrated with this study that the released polymeric carbohydrates were constituted by another polysaccharide too.The repeating unit of the EPS is constituted by a N-acetyl quinovosamine unit and two residues of galacturonic acid both decorated with alanine amino acids.

MD simulations revealed that the local conformation adopted, resembles a left-handed helix. Furthermore, the capacity of the EPS to alter the water ability to adopt such an arrangement could be at the basis for the antifreeze properties of EPS. Interestingly, similar results were also achieved for some antifreeze glycoproteins by Mallajosyula et al. (*Mallajosyulaet al., 2014*) that demonstrated how these perturbation effects are propagated distant hydration layers.

Quantitative ice recrystallization inhibition (IRI) assays were employed to link the structural characterization of the poly(saccharide), its influence on local water structure and ice growth interactions. Interestingly, EPS was found to have moderate IRI activity comparable to the activity of synthetic polymer mimics of antifreeze proteins, which have been found to confer cryoprotective effects (*Mitchell et al., 2015*) suggesting that EPS plays a role in cold-survival. Interestingly, the NMR studies suggested a helical structure, which is similar to that observed in antifreeze glycoproteins (AFGP) – it should be noted that there is no crystal structure of AFGP but a polyproline-type helix is observed in circular dichroism spectrscopy and NMR (*Tachibana et al., 2004*). A second feature of AFP and AFGP is the presence of distinct hydrophobic and hydrophilic regions which are crucial for IRI activity. The hydrophobic face of residue **C** (Figure 4.23) could contribute to this activity alongside potential water ordering, as as seen in AFPs (*Sun et al., 2014*). In consideration that very few macromolecules have been reported to have IRI activity, the observations reported in this paper are rather significant.

The full characterization of the EPS primary structure and molecular dynamics simulations have revealed a unique strategy for cold adaptation of *Colwellia psychrerythraea* 34H.

4.4 Mannan polysaccharide

4.4.1 Isolation and purification of Mannan polysaccharide

During the purification of the EPS from the culture supernatant of *Colwellia psychrerythraea* 34H, the sugar analysis suggested the presence of another polysaccharide, constituted by only mannose residues. Actually, gel filtration chromatography column revealed the presence of a much less noticeable peak, together with that corresponding to EPS fraction and medium compounds. Sugar analysis of this peak, showed the presence of mannose with traces of glucose; a defined amount was also loaded on a 14% DOC-PAGE and visualized by Alcian blue staining. Bands at high molecular mass attributable to a mannan polysaccharide were clear visible (Figure 4.24).

Figure 4.24: DOC-PAGE 14% of the mannan polysaccharide sample from *C.psychrerythraea* stained with Alcian blue

4.4.2 NMR analysis

The mannan polysaccharide was then analyzed by mono and two-dimensional NMR spectroscopy. In particular, all the 2D NMR experiments were performed. The NMR analysis allowed the complete characterization of all of spin systems. The ^{1}H showed the presence of several signal in the anomeric region (Figure 4.25). The ^{1}H-^{13}C DEPT-HSQC spectrum (Figures 4.26 and 4.27; Table 4.5) confirmed the presence of different anomeric cross peaks at δ 5.19/101.8 (**A**), 5.04/103.5 (**B**), 5.01/99.4 (**C**), 4.99/99.4 (**D**), 4.95/103.5 (**E**), 4.94/103.5 (**F**), 4.79/100.6 (**G**), 5.36/97.3 (**H**) ppm, all ascribable to mannose units, and the signal at δ 4.37/105.1 (**I**) attributable to a glucose residue.

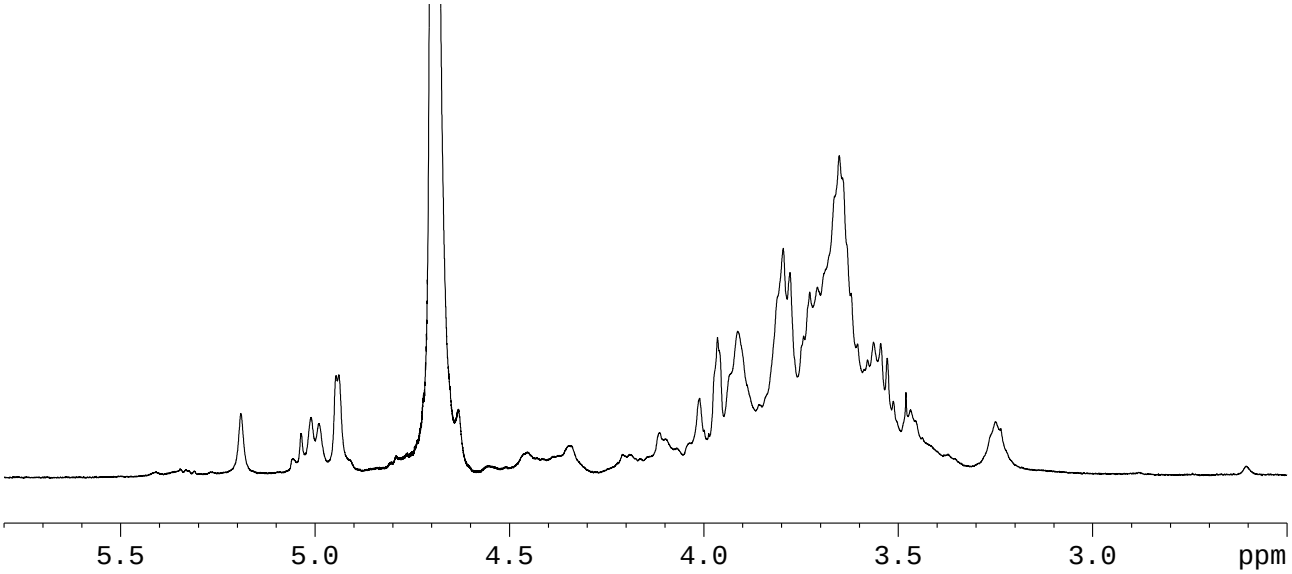

Figure 4.25: ^{1}H NMR spectrum of mannan polysaccharide from *Colwellia psychrerythraea* 34 H. The spectrum was recorded in D_2O at 298 K.

The anomeric proton chemical shift together with the $^{1}J_{C\text{-}H}$ values, indicated α and β configurations for mannose and glucose units, respectively. The chemical data and the close similarity of chemical shifts with those reported in literature, (*Leontein et al., 1978; Vinogradov et al., 1998*) supported a sugar backbone consisting of α-(1→6)-linked mannopyranose units branched at C-2. The arms are made up of 2- and/or 3-linked mannose units ending with mannose or glucose as deduced from NMR data. Usually the punctual structure of a mannan is deduced from the structure of the oligosaccharidic products, obtained after a treatment with sulphuric acid and acetic acid (acetolysis), that cleaves selectively 1→6- linkages, determining several oligosaccharides that differ for the length of the arms. In this study, due to the very low amount of sample, the detailed structure of the polysaccharide was hampered.

The presence of an α-(1→6) backbone was suggested by long range scalar connectivity between anomeric proton signal at δ 4.99/5.02 of residues **C** and **D** with carbon signal at δ 66.9 of **C**. NOE contacts between both H1-**C** and H1-**D** with H6-**C** confirmed this hypothesis. The downfield shifted signals of C-2 of residue **C** (δ 80.6 ppm) and **D** (δ 80.0 ppm) indicated their substitution. Residue **A** was linked to residues **C** and **D**, as revealed by the long range scalar correlation of H1-**A** and C2-**C**/C2-**D**. In addition, the C-2 resonance of **A** was downfield shifted at δ 79.7 ppm, thus indicating its substitution. The different length of branching is suggested by the different substitution of residue **A**; in fact, in some arms residue **A** is substituted by terminal mannose residue **E**, as

indicated by a strong NOE contact between H1-**E** and H2-**A**, whereas in others, the length of arm is longer, as suggested by the linkage of the 3-substituted mannose residue **F** to residue **A**. This is confirmed by a long range correlation between H1-**F** and C2-**A**. Residue **F**, in turn, is substituted by a terminal mannose **B,** as suggested by a long range scalar connectivity between H1-**B** and C3-**F**. Finally, some arms end with a terminal residue of glucose **I**, as suggested by a NOE contact between H1-**I** and H2**A**.

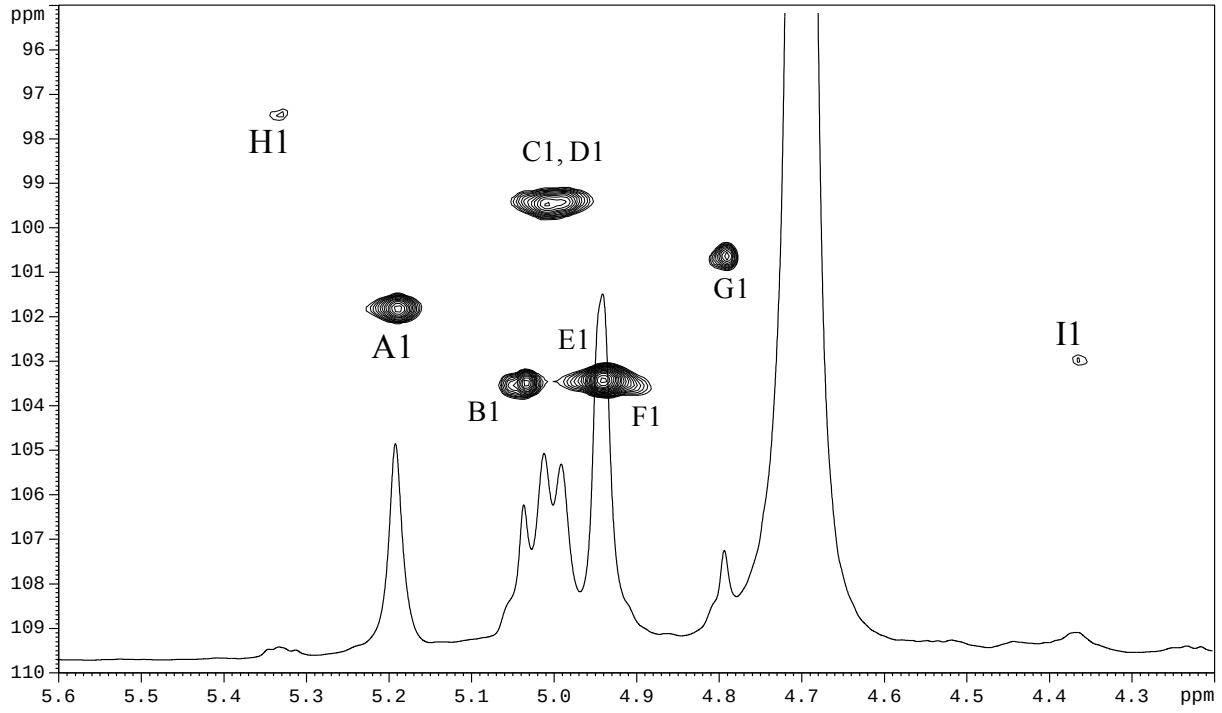

Figure 4.26 : Expansion of the ^{1}H-^{13}C heterocorrelated HSQC spectrum of mannan from *C. psychrerythraea* 34 H. The spectrum was recorded in D_2O at 310 K at 600 MHz. The letters refer to residues as described in Table 4.5.

Furthermore, in the HSQC experiment, the correlation founded for anomeric proton signal at δ 5.36 with a carbon signal at δ 97.3 ppm was in agreement with a phosphorylated mannose unit (*Leontein et al., 1978*). The presence of a phsphodiester linkage is confirmed by ^{1}H-^{31}P HSQC, thanks to the correlation between H1 of residue **H** at δ 5.36 ppm and the phosphate signal at δ -1.93 ppm (Figure 4.28). This last was in turn correlated with a proton signal at δ 4.06 ppm, that is correlated in the HSCQ experiment with a C6 downfield shifted carbon at δ 62.7 ppm. These correlations suggested a phosphodiester linkage between residue **H** and another residue of the arm.

Table 4.5: ^{1}H and ^{13}C NMR assignments of mannan polysaccharide from *C. psychrerythraea* 34 H. Spectra were recorded in D_2O at 298K at 600 MHz using acetone as external standard (δ_H/δ_C 2.25/ 31.45 ppm).

Residue	H1/C1	H2/C2	H3/C3	H4/C4	H5/C5	H6/C6
A	5.19	4.01	3.81	3.64	3.66	3.65/3.80
2- Man*p*	101.8	79.7	71.5	67.6	74.3	62.4
B	5.04	3.98	3.75	3.54		
t- Man*p*	103.4	71.3	71.7	68.1		
C	5.02	3.94	3.83	3.72	3.73	3.75/3.91
2,6- Man*p*	99.4	80.0	71.5	67.6	72.1	66.9
D	4.99	3.92				
2,6- Man*p*	99.4	80.6				
E	4.95	3.97	3.72	3.69	3.75	
t- Man*p* E	103.4	71.3	72.1	67.9	74.3	
F	4.94	4.12	3.85	3.64	3.70	
3- Man*p*	103.5	70.9	79.2	67.6	72.5	
G	4.79	3.88	3.72	3.59	3.67	
6- Man*p*	100.6	71.3	72.1	68.1	66.7	
H	5.35	4.04	3.32			
1-*P* Man*p*	97.3	71.4	70.9			
I	4.37	3.26	3.48	3.65	3.67	
t- Glc*p*	105.1	73.5	74.9	72.5	77.0	

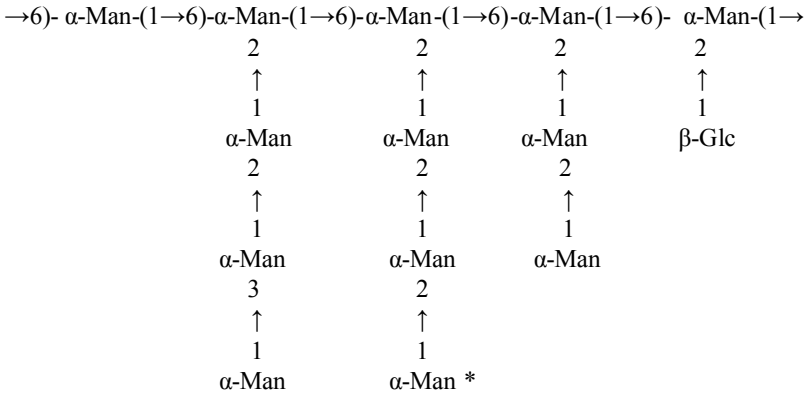

Figure 4.27: Mannan from *C.psycherythraea* 34H

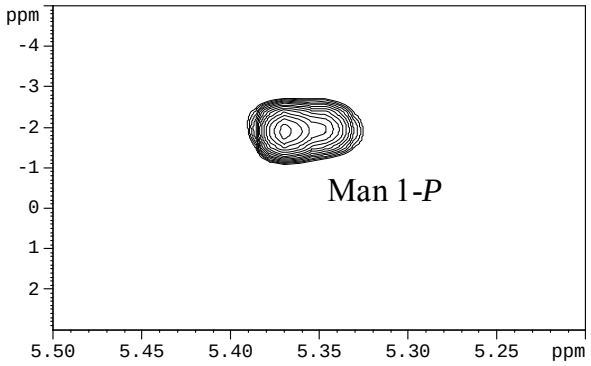

Figure 4.28: expansion of ^{1}H-^{31}P HSQC of mannan polysaccharide from *Colwellia psychrerythraea* 34H. The spectrum was recorded in D_2O at 298K at 400 MHz.

4.4.3 Ice Recrystallization Inhibition assay

To assess cryoprotective activity of the mannan polysaccharide, ice recrystallization inhibition (IRI) activity, in collaboration with Prof. Matthew Gibson was performed. The assay was carried out at different concentration; results highlights a significant ice recrystallization inhibition activity (Figure 4.29).

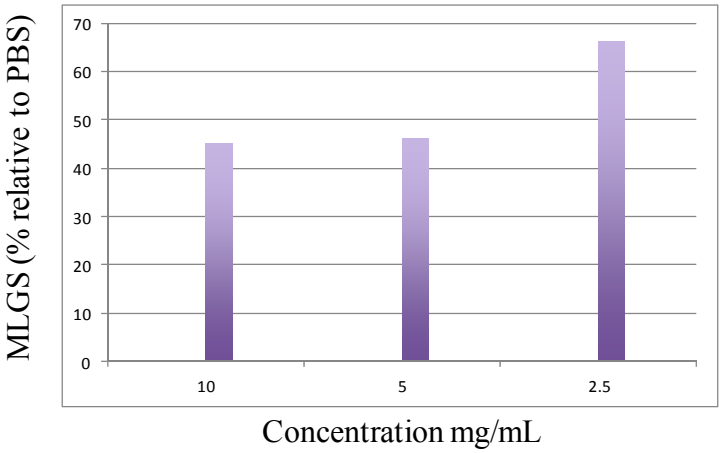

Figure 4.29: Ice Recrystallization Inhibition activity of mannan polysaccharide from *C. psychrerythraea* 34 H. Mean largest grain size is expressed as a percentage of PBS buffer, and small MLGS value indicate increased IRI activity.

4.4.4 Discussion

Colwellia psychrerythraea 34H is involved in the production of a mannan polysaccharide, completely released in the surrounding medium. Usually, mannan polysaccharides do not show a

repeating unit, due to the presence of random side chains; therefore, it is only possible to give information about the length and frequence of such arms. Unfortunately, the very low amount of *Colwellia* mannan did not allow the obtainment of a detailed structure. Neverthless, the chemical and NMR analyses suggested the presence of a sugar backbone consisting of α-(1→6)-linked mannopyranose units, most of which branched at C-2. The arms are made up of 2- and/or 3-linked mannose units ending with mannose or glucose, and some arms are cross-linked through phosphodiester bridges. This arrangement is commonly founded in mannan polysaccharides isolated from fungi and yeasts. Mannan from *C. psychrerythraea* was compared with that of commercial product of mannan from *S. cerevisiae.* Chemical and NMR data revealed the absence of glucose residue at the end of side chains, and the lack of phosphodiester bridges. The ice recrystallization inhibition assay showed that it is as active as the CPS produced by the same bacterium. These differences in structural features could be related to the absence of ice recrystallization activity founded for mannan from *S. cerevisiae.* Most of the functions ascribed to exopolysaccharide concern their protective nature. The ability of a microorganism to surround itself with a highly hydrated exopolysaccharide layer may provide it with protection against desiccation and predation by protozoans. In addition, the presence of a gelled polysaccharide layer around the cell may have paramount effects on the diffusion properties, both into and out of the cell (*Dudman 1977*). At the best of our knowledge, only another example of mannan with cryoprotectant activity is reported. In particular, this polysaccharide, isolated from *Pseudoalteromonas* sp. Strain SM20310, has been demonstrated its action to enhance the high-salinity tolerance and to improve the survival of the bacteria after freeze-thaw cycles (*Liu et al., 2013*).

4.5 Polyhydroxyalkanoates (PHA)

The presence of polyhydroxyalkanoates in the cells of *Colwellia psychrerythraea* 34H grown at 4 °C was first highlighted by TEM images (Figure 4.30) that revealed clearly lipophilic cytoplasmatic inclusions.

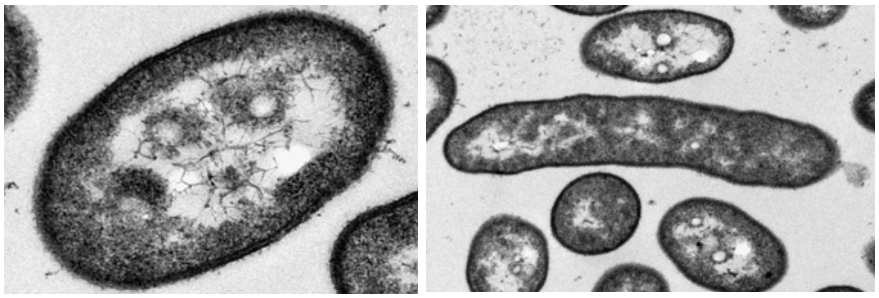

Figure 4.30: Transmission electron microscopy (TEM) images of thin sections of *Colwellia psychrerythraea* 34H.

For PHAs analysis, *C. psychrerythraea* cells were treated in order to convert intracellular biopolymer into the corresponding monomer-methylesters, and analyzed by GC-MS. The production of PHA from *C. psychrerythraea* was tested by considering two different growth conditions. The % of PHAs were expressed as the ratio between produced PHAs (mg) and cell dry weight CDW (mg) of lyophilized cell material. The identification of compounds was performed by comparison with mass spectra of standards. PHA contents (mg/l) was calculated by using calibration curves.

In the first analysis, *C. psychrerythraea* was grown in CONDA medium at 4°C, and the production was evaluated at different times of growth, from 24 to 96 hours. The results revealed that the best condition was found to be 72 hours (Table 4.6) with 0.009% of PHAs corresponding to 100% of 3-hybroxybutyrate (3HB).

Table 4.6: %PHAs was expressed as the ratio between produced PHAs (mg) and CDW (mg) of lyophilized cell material.

4°C CONDA	24 h	48 h	72 h	96 h
% PHA	0.003	0.004	0.009	0.00

Starting from the previous results, with the aim to verify in which condition is enhanced the production of PHAs, two different media, CONDA and MB media have been tested. In these two different conditions, the monomeric composition of PHAs changes: when *C. psychrerythraea* grows in MB medium, the production of a heteropolymer consisting of 10% of 3HB and 90% of 3-hydroxyhexanoic acid (3HHx), is observed. Instead, in CONDA medium is confirmed the presence of 3HB as unique component (Table 4.7) .

Table 4.7: %PHAs was expressed as the ratio between produced PHAs (mg) and CDW (mg) of lyophilized cell material.

MB medium	10% 3HB, 90% 3HH
CONDA medium	100% 3HB

Discussion

Polyhydroxyalkanoates have a wide range of applications from bioplastics, fine chemicals, medicine to biofuels. Recently, bacteria PHAs synthesis has been found to be useful for improving robustness of industrial microorganisms and regulating bacterial metabolism, leading to yield improvement on some fermentation products (*Guo 2009*). A novel perspective of bio-production of PHAs is represented by psychrophilic bacteria, as *Colwellia psychrerythraea* 34H.

TEM images of *C. psychrerythraea* cells, revealed the presence of intracellular granules, in identified as PHAs. The tested conditions suggested that *C. psychrerythraea* could be implicated in the production consisting of different monomer composition. This bacterium could be is therefore

an innovative source for PHAs production and the polymer accumulated could expand the biotechnological application.

Conclusion

Colwellia psychrerythraea 34 H grown at 4°C

Cold-adapted microorganisms have developed several strategies to live and proliferate in extreme habitats, such as glacial and sub-glacial environments. Their ability to live under subfreezing temperatures implies the production of compounds conferring cryotolerance. For this reason they have been extensively studied due to their relevant ecologic role and biotechnological applications. These bacteria have evolved different mechanisms to resist the inhospitable conditions, including the production of lipids and enzymes that retain sufficient physical flexibility below the freezing point to support cellular membrane homeostasis and biochemical catalysis (*Feller et al., 2003*). Other important means of adaptation include the production of anti-freeze proteins and carbohydrate-based extracellular polymeric substances (EPS), which serve as cryo- and osmo-protectants (*Kremb et al., 2011; Stibal et al., 2012*). A model to study cold-adapted life-style, is *Colwellia psychrerythraea* 34 H, a psychrophile isolated from the arctic marine sediments.

Cellular membrane plays a key role in the interaction with the external environment; hence it is reasonable to think that cellular structures associated with it, are involved in the forefront in the adaptation. Among these, the lipopolysaccharides (LPSs) and the capsular polysaccharides are essential for Gram-negative bacteria.

The structure of core region of LPS from *Colwellia*, completely characterized during my master degree (*Carillo et al., 2013*), is part of the few examples of LPSs from psychrophilic microorganisms.

By comparing the *C. psychrerythraea* 34H LOS structure with those obtained from *P. haloplanktis* TAC125 (*Corsaro et al., 2001*; *Corsaro et al., 2002*) and *P.haloplanktis* TAB 23, (*Carillo et al., 2011*) and from *P. arctica* , (*Corsaro et al., 2008*) it turned out that they have in common the lack of an O-chain and the presence of a high charge density in the core region due to the presence of acidic monosaccharides and phosphate groups. In addition, the core regions have been found to be made up of only a few sugar units. These structural features seem to be common to cold-adapted microorganisms.

Molecular adaptation also involved the lipid A portion of LPS, the. The lipid A moiety displayed a structure that is quite new among the LPSs. In fact, it shows the presence of unsaturated 3-hydroxy fatty acids, a feature that up to now is reported only for *Agrobacterium tumefaciens* and *Vibrio fischeri*. In particular, the structure of lipid A from *Colwellia psychrerythraea* 34H is very similar to that of *Vibrio fischeri*; in both structures, very intriguing is the presence of an unusual set of modifications at the secondary acylation site of the 3-position consisting of phosphoglycerol (GroP) differently substituted. The high heterogeneity of this structure, showed by the fatty acids analysis, was confirmed by the complexity of MS and MS/MS spectra. These experiments indicated a variable state of acylation ranging from tetra- to hepta-acylated glycoforms. The presence of 3-hydroxy unsatutared fatty acids, compared to that of fatty acids of LPS from higher temperature grown cells (*Kumar et al., 2002*), is related to cold shock response, by inducing homeoviscous adaptation of phosholipid acyl structure in order to preserve membrane integrity (*Sweet et al., 2014*). Another important way to adaptation in cold-adapted bacteria is related to the production of exopolysaccharides. In this context, *Colwellia psychrerythraea* 34H produces a pool of polysaccharidic structures.

The first exopolysaccharide (CPS) from *Colwellia* is composed of a tetrasaccharidic repeating unit containing two amino sugars and two uronic acids. The unique characteristic of the capsular polysaccharide is the presence of the α-aminoacid threonine as a substituent (*Carillo et al., 2015*).The decoration of the polysaccharide with threonines is partıcularly intriguing to consider. In fact, amino acid motifs are common and crucial for the interaction with ice in several different kinds of antifreeze proteins (AFPs) and antifreeze glycoproteins (AFGPs) (*Graether 2000*). The molecular mechanic and dynamic calculations show that the CPS seems to assume in the space a "zig-zag" flexible arrangement, where the threonines are placed externally and available to interact with the ice. The analyses of ice recrystallization inhibition activity, suggest that CPS interacts with ice and that CPS has an effect on recrystallization (*Carillo et al., 2015*).

Further, *Colwellia* produces another two different exopolysaccharides, named EPS and mannan, released in the surrounding medium.

The repeating unit of EPS is constituted by a N-acetyl quinovosamine unit and two residues of galacturonic acid both decorated with alanine amino acids. This structure is decorated with amino acids, represented by an alanine linked to the galacturonic acid residues, and recalls that of AFGP. Ice recrystallization inhibition activity show that also EPS has an effect on recrystallization, even if less marked with respect to the CPS. Three-dimensional arrangement of the polymer was obtained through MD simulations and suggests a pseudohelicoidal structure which prevent the local tetrahedral order of the water molecules in the first hydration shell, by expounding its antifreeze

activity. In summary, our investigations reveal a close interplay between the polysaccharidic structures, very similar to the AFGP, and the antifreeze properties. The peculiar presence of this type of structures should not be underestimated, but related to the lack in the genome of *C. psychrerythraea* 34H of sequence coding for a known AFP.

In a previous paper a cryoprotectant activity, meant the survival of the bacteria after freeze-thaw cycles, was attributed to an exopolysaccharide from *C. psychrerythraea*, probably attributable to the mannan. Also the mannan displays an high ice recrystallization activity, comparable to that of CPS. Unlike the EPS, that remains in part immobilized onto the cells , the mannan polysaccharide is completely released in the surrounding medium. This polysaccharide is built up of a backbone of mannose α-(1→6) units branched at C-2 with oligosaccharidic side chains, a common arrangement of mannans isolated from fungi and yeasts. The peculiarity of these structures is that some of these arms end with a β-glucose residue, and that some arms are cross-linked through phosphodiester bridges. It is important to underline the combined action of these molecules, as reported in the final ice recrystallization inhibition assay (Figure 4.31). This suggests as expected, that the polysaccharide display an higher activity than the single molecule, as it really mimics the *Colwellia*'s response in its natural environment.

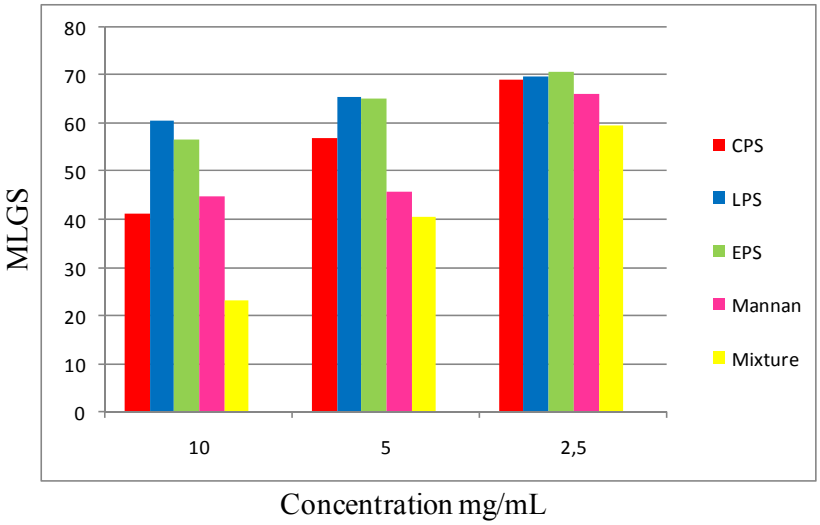

Figure 4.31: : Ice Recrystallization Inhibition activity of all the molecules from *C. psychrerythraea* 34 H. Mean largest grain size is expressed as a percentage of PBS buffer, and small MLGS value indicate increased IRI activity.

Thus, this microorganism living in the brine channels must have evolved adaptations to tolerate high salinity and repeated freezing and thawing. Therefore, the approach involving the production of extracellular polysaccharides is confirmed to be a successful evolutionary strategy for bacteria inhabiting extreme sea ice environment.

Chapter V

Colwellia psychrerythraea 34H grown at 8°C and -2 °C

Reproducing the natural environment where bacteria live is complicated, especially when the environment itself constantly changes. An example is given by the Arctic and Antarctic regions that are subjected to the seasonal fluctuations in temperatures, due to the cycle of formation-melting of glaciers. Therefore, these changes force the microbial population to adapt continuously.

C. psychrerythraea in its natural habitat must adapt to these changes, by showing off its capacity to response to environmental variations. For this reason, in order to mimic the adaptation to these seasonal changes, *C. psychrerythraea* has been grown at two temperatures other than 4°C. In particular, 8°C and -2°C have been chosen, to verify, if present, any differences respect to the molecular structures produced at 4°C.

5.1 Lipopolysaccharide structure

5.1.1 LPS purification and characterization

C. psychrerythraea cells grown at 8 and -2°C were extracted using PCP method; the extracted samples, analyzed by DOC-PAGE electrophoresis (Figure 5.1), suggested the presence of a LOS, as already founded for *Colwellia* grown at 4°C (*Carillo et al., 2013*).

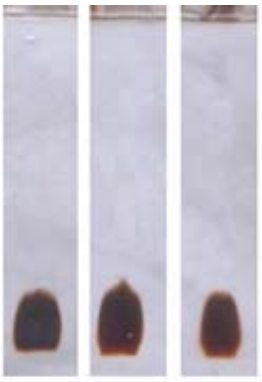

a b c

Figure 5.1: 14% DOC-PAGE analysis of PCP extracts from *Colwellia* at 4 (a), 8 (b) and -2°C (c), visualized by silver staining.

Again, the sugar composition of the LOS obtained by GC–MS analysis of the MGA, confirmed the occurrence of GalA, GlcN, Man, Col, and Kdo. The latter residue was revealed only after dephosphorylation of the LOS, which was achieved by HF treatment (*Corsaro et al., 2008*). In contrast, fatty acid analysis shows, in addition to the fatty acids reported for the lipid A at 4°C, a different composition of 3-hydroxy fatty acids, thus suggesting some differences in the lipid A structure. In particular, the occurrence of 3-hydroxy-decenoic acid, 3-hydroxy-undecenoic acid and 3-hydroxy-tridecenoic acid was observed.

5.1.2 Mass Spectrometric Analysis of the O-Deacylated LOS$_{PCP}$

The LOS PCP was O-deacylated with anhydrous hydrazine, (*Holst et al., 2000*) and the product obtained (LOS-OH) was analysed by MALDI MS. The spectrum (Figure 5.2) showed the presence of mainly one species at 1843.74 Da, attributable to the following composition:

GroPColGalAManKdoPGlcN$_2$P$_2$[C12:0(3OH)] [C14:1(3OH)]H$_2$O

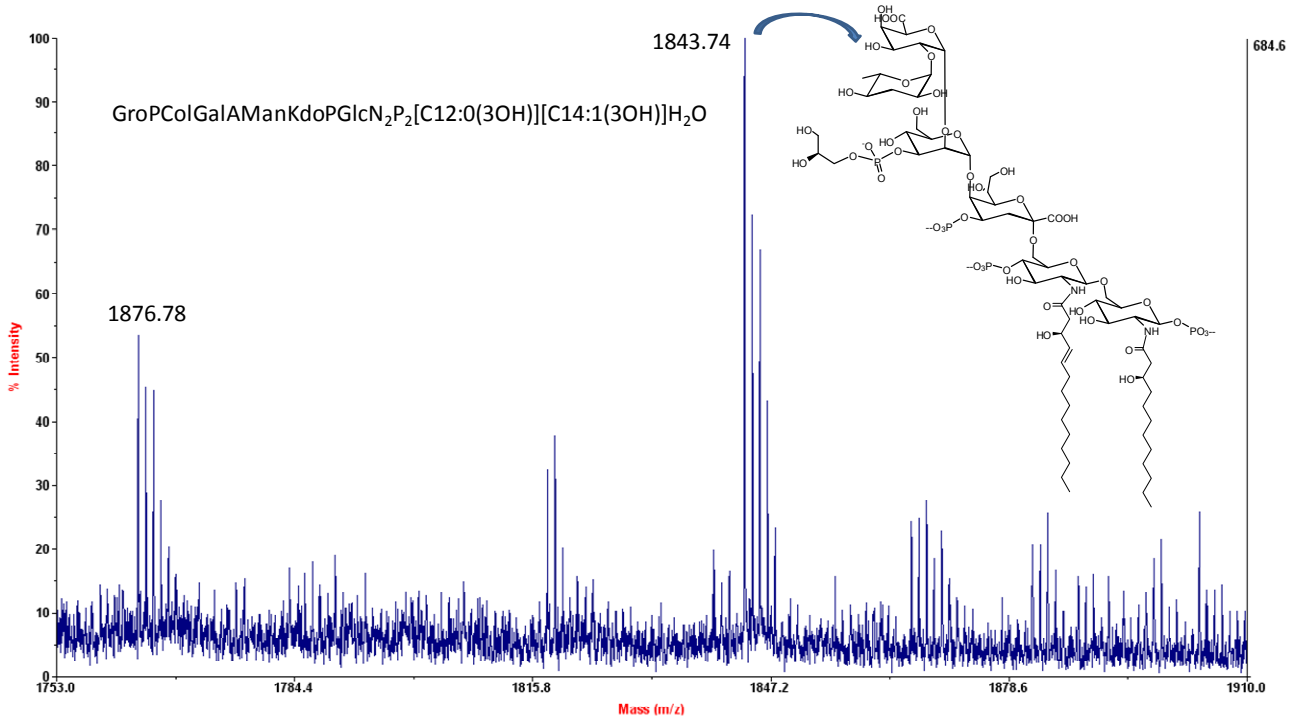

Figure 5.2: MALDI MS spectrum of the partially deacylated LOS (LOS-OH) from *C.psychrerythraea* grown at 8 and -2°C.

The species at 1876.78 Da differs from the previous one for the lack of a phosphate group. Therefore, the partially deacylated LOS (LOS-OH) revealed the identical composition with the LOS from *Colwellia* at 4°C.

5.2 Capsular polysaccharide CPS_2

5.2.1 CPS extraction and purification

The remaining PCP pellets were extracted by phenol/water method (*Westphal et al., 1965*); water extracts were dialyzed against water and treated with DNAse, RNAse and protease enzymatic digestion. The purified samples were analyzed by 14% DOC-PAGE and the gel visualized with Alcian blue staining revealing additional bands at high molecular masses (Figure 5.3).

Figure 5.3: Analysis of the CPS fraction from *C. psychrerythraea* 34H grown at 8 and -2°C by 14% DOC-PAGE. The gel was stained with Alcian blue dye.

The sugar analysis confirmed the presence of all the monosaccharidic components belonging to the CPS and EPS; furthermore, in *Colwellia* grown at 8 and -2°C, the occurrence of 2-amino-2-deoxy-D-glucuronic acid (GlcNA) was observed. In order to purify the polysaccharidic components from LPS aggregates, samples were subjected to hydrolysis with 1% acetic acid and centrifugation. The supernatant mixture was separated on a Biogel P-10 chromatography column, using pyridinium acetate buffer as eluent. The first fraction, eluted in the void volume contained the higher molecular mass material; a further purification of this fraction was performed by using a Sephacryl S-400HR chromatography column, followed by a Q-Sepharose fast flow ion exchange chromatography column, eluting with a gradient of NaCl. Two main fractions were obtained: the first one containing a new polysaccharide named CPS_2, and the second corresponding to CPS and EPS, even if in very low amount. The monosaccharides composition of CPS_2 displayed the presence of 2-amino-2-deoxy-galactose (GalN) and 2-amino-2-deoxy-glucuronic acid (GlcNA). A D configuration was identified for these two monosaccharides by the GC-MS analysis of the acetylated (S)-2-octyl glycosides. (*Leontein et al., 1978*).

5.2.2 NMR characterization

The capsular polysaccharide was then analyzed by mono- and two-dimensional NMR spectroscopy. In particular, ^{1}H-^{1}H DQF-COSY (double quantum-filtered correlation spectroscopy), ^{1}H-^{1}H TOCSY (total correlation spectroscopy), ^{1}H-^{1}H NOESY (Nuclear Overhauser enhancement spectroscopy), ^{1}H-^{13}C DEPT-HSQC (distortionless enhancement by polarization transfer-heteronuclear single quantum coherence), ^{1}H-^{13}C HMBC (heteronuclear multiple bond correlation), and BSCT-HMBC (band-selective constant time- HMBC) experiments were performed. ^{1}H-NMR chemical shifts were referred to external 3-trimethylsilyl-propanoate (TSP, δ_H 0.00) and those in ^{13}C NMR to 1,4-dioxane in D_2O (δ_C 67.40). The temperature was calibrated to 310 K with a neat deuterated methanol sample (*Findeisen 2007*) prior to all the experiments.

The ^{1}H spectrum of the CPS_2 fraction, recorded at 310 K, is shown in Figure 5.4. Three anomeric proton signals (**A-C**), attributable to CPS monosaccharide units, were present in the region between δ 4.6 and δ 4.4 ppm (Table 5.1). In addition, four signals of acetyl groups occurred between δ 1.9 and δ 2.1 ppm, and a methyl signal, identified at δ 1.21 ppm, suggested the presence of a deoxy sugar.

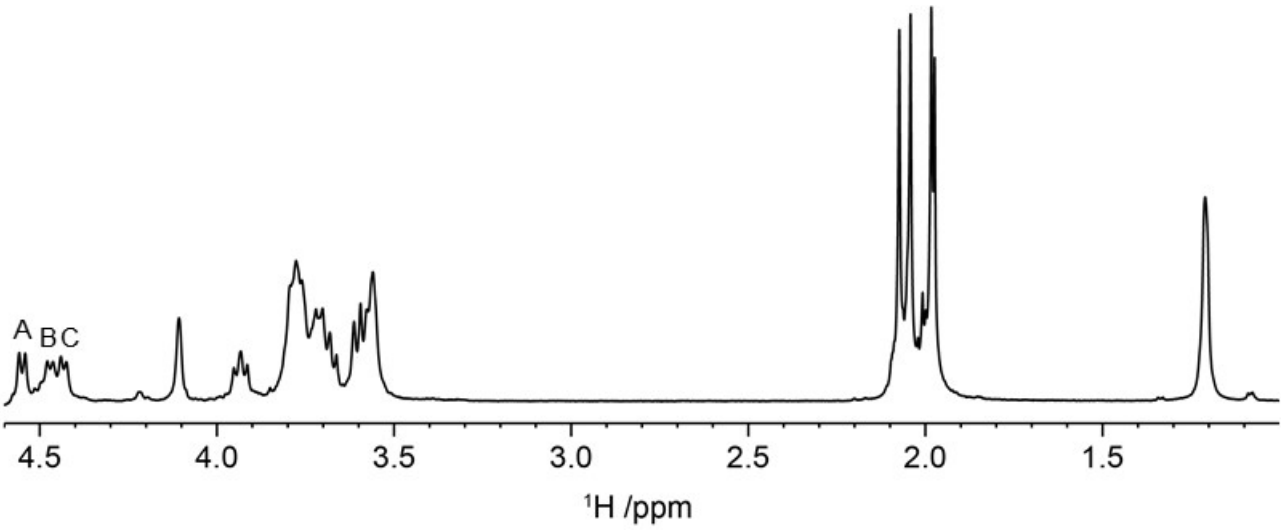

Figure 5.4: ^{1}H NMR spectrum recorded at 310 K and a spectrometer frequency of 500.

Table 5.1: ^{1}H and ^{13}C NMR assignments of the CPS_2 from *C. psychrerythraea* 34H. Spectra were acquired in D_2O at 310 K using as external standard 1,4-dioxane in D_2O (δ_C 67.40).

Sugar residue		**$^{1}H/^{13}C$**											**Correlation to atom (from anomeric atom)**	
		1	2	3	4	5	6	C*H*$_3$CO *N*-2	CH$_3$*C*O *N*-2	C*H*$_3$CO *N*-4	CH$_3$*C*O *N*-4	NH[a]	NOE	HMBC
→3)-β-D-Gal*p*NAc-(1→	**A**	4.55[8.4]	3.93	3.79	4.11	3.70	3.76, 3.78	2.07				8.13(*N*-2)	H4, **C**	C4, **C**
		(-0.13)	(0.03)	(0.02)		(-0.02)		(-0.01)					H3, **A**	H4, **C**
		102.5	51.8	79.7	68.8	75.6	61.9	23.6	175.1					
		(6.2)	(-3.0)	(7.7)	(-0.1)	(-0.4)	(0.0)	(0.5)	(-0.7)					
→3)-β-D-QUINAc4NAc-(1→	**B**	4.47[8.0]	3.78	3.73	3.56	3.55	1.21	2.04		1.96		8.47(*N*-2)	H3, **A**	
		103.1	56.3	78.9	56.5	71.5	17.9	23.3	174.6	23.3	175.9	8.11(*N*-4)		
→4)-β-D-Glc*p*NAcA-(1→	**C**	4.43[7.3]	3.58	3.68	3.77	3.60		1.97				8.28(*N*-2)	H3, **B**	C3, **B**
		(-0.30)	(-0.12)	(0.10)	(0.19)	(-0.12)							H3, **C**	
		103.3	56.0	72.3	81.6	77.6	174.3	23.3	175.5					
		(7.5)	(-1.7)	(-2.3)	(8.0)	(0.6)	(-1.2)	(0.2)	(-1.9)					

[a]Assignment based on $^{1}H,^{1}H$-NOESY experiment at 5°C with τ_m=300 ms using H_2O:D_2O solvent mixture at 95:5.

$^{3}J_{H1,H2}$ values are given in Hertz in square brackets. Differences of chemical shifts compared to those of corresponding monosaccharides are given in parentheses.

The ^{1}H and ^{13}C resonances of the sugar residues in the repeating unit of the polysaccharide were assigned by considering all the 2D NMR experiments (Table 5.1) and subsequently predicted by the CASPER program.

Residue **A** with H-1/C-1 signals at δ 4.55/102.5 ppm was identified as *galacto*-configured residue, based on the presence of cross-peaks from H-1 up to H-4; then, in the NOESY spectrum, starting from H-4 signal, H-5 and H-6 were assigned. Residue **A** was assigned to a 3-substituted β-D-galactosamine as suggested by the high $^{3}J_{H\text{-}1,H\text{-}2}$ value (8.4 Hz) and since in the ^{1}H-^{13}C DEPT-HSQC (Figure 5.5) its H-2 proton at δ 3.93 ppm correlated with a nitrogen-bearing carbon at δ 51.8 ppm. The downfield shift of the C-3 resonance at δ 79.7 ppm identified its substitution (*Bock et al., 1983*). Its H-2 proton was also downfield shifted indicating the presence of an acyl substituent on the amino group, identified as an *N*-acetyl group.

Residue **B** with H-1/C-1 signals at δ 4.47/103.1 ppm was assigned to a 2,4-diamino-2,4,6-trideoxy-β-glucopyranose (bacillosamine) as suggested by the high $^{3}J_{H\text{-}1,H\text{-}2}$ value (8.0 Hz) and the occurrence in the HSQC spectrum of correlations of H-2 and H-4 signals at δ 3.78 and 3.56 ppm with nitrogen-bearing carbons at δ 56.3 and 56.5 ppm, respectively. The correlation peaks from H-1 to H-6 in the TOCSY spectrum provided evidence for the *gluco*-configuration for this ring system. The downfield shift of the C-3 resonance at δ 78.9 ppm with respect to the unsubstituted residue (*Corsaro et al., 1999*) identified its substitution. Moreover, H-2 and H-4 signals were also shifted downfield indicating the presence of acyl substituents on amino groups, that were found to be *N*-acetyl groups. The absolute configuration of the BacN was established on the basis of the glycosylation effect upon the values of ^{13}C NMR chemical shifts (*Lipkind et al., 1988*).

Residue **C,** with H-1/C-1 signals at δ 4.43/103.3 ppm, was identified as an O-4 substituted GlcNAcA residue. The *gluco* stereochemistry was suggested by the occurrence of strong scalar correlations in both COSY and TOCSY experiments; the β-configuration was identified from the large $^{3}J_{H\text{-}1,H\text{-}2}$ value (5.3 Hz), and the downfield shift of the C-4 resonance at δ 77.6 ppm identified its substitution (*Bock et al., 1983*). The ^{1}H-^{13}C HSQC experiment (Figure 5.5) revealed that the H-2 signal at δ 3.58 ppm correlated with a nitrogen-bearing carbon at δ 56.0 ppm, which was N-acetylated as proven by the H-2 downfield chemical shift. Finally, the presence of long-range scalar correlations between both signals of H-5 and H-4 and the carboxyl group at δ 174.3 ppm in the ^{1}H-^{13}C HMBC spectrum confirmed the uronic acid residue.

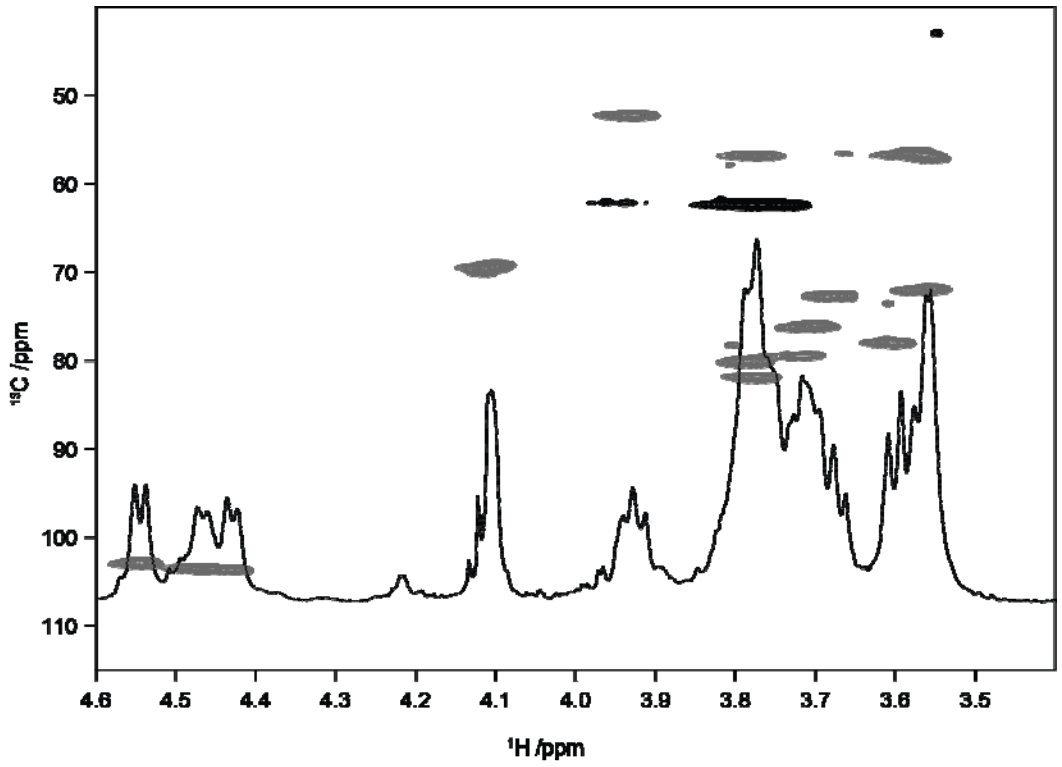

Figure 5.5: Anomeric and carbinolic region of HSQC of CPS_2 from *C. psychrerythraea* 34H grown at 8 and -2 °C. The spectrum was recorded in D_2O at 310 K and 600 MHz.

The substitution of all the residues by acetyl groups was confirmed by a ^1H-^1H NOESY experiment, acquired in H_2O:D_2O (Figure 5.6), and BSCT-HMBC. In particular four additional spin systems, attributed to NH, CH_3 and COOH groups, were founded. Cross peak correlations corresponding to NH/CH_3 at δ 8.47/2.04 ppm, 8.28/1.97 ppm, 8.13/2.07 ppm were attributed to C*H*$_3$CO(*N*-2) of **B**, C*H*$_3$CO(*N*-2) of C, C*H*$_3$CO(*N*-2) of **A**; instead the signal at δ 8.11/1.96 ppm showed correlation with H6-**B**, therefore attributed to C*H*$_3$CO(*N*-4) of residue **B**.

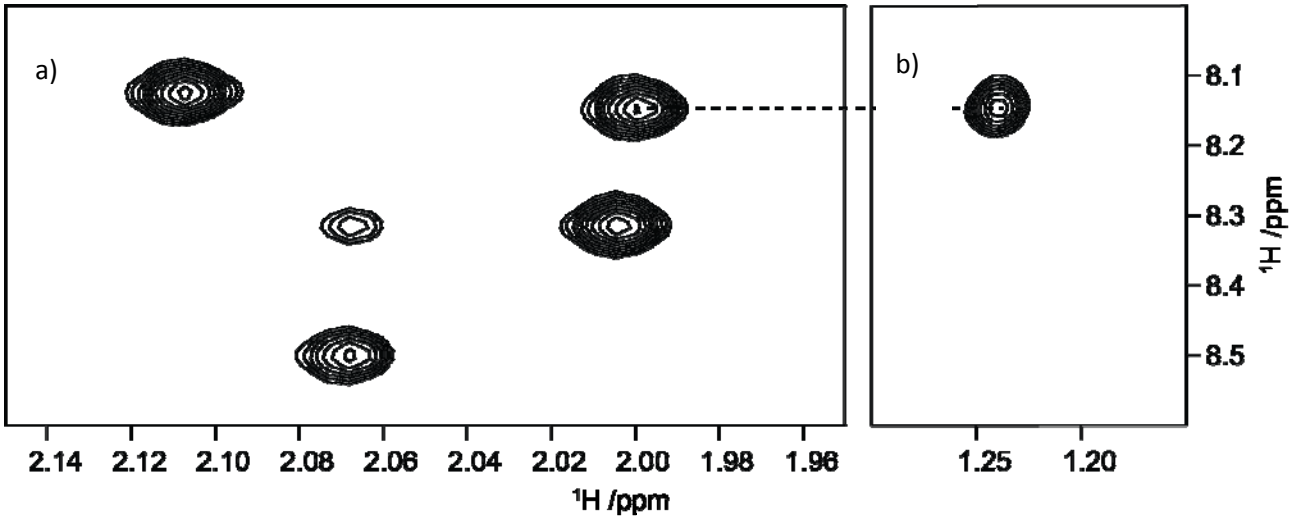

Figure 5.6: Relevant sections of ^{1}H-^{1}H NOESY from the *C. psychrerythraea* CPS_2. Correlations between the amido protons in F1 dimension and acetamido methyl groups protons in F2 dimension are present. The spectrum was recorded in H_2O:D_2O (95:5) at 278 K and 600 MHz using a 300 ms mixing time.

5.2.3 Conformational analysis by NOESY

During my internship at Stockholm University, in the research group of Prof. Goran Widmalm, preliminary conformational analysis was performed. In particular, twelve 2D ^{1}H, ^{1}H-NOESY experiments, with mixing times between 30 and 300 ms, were performed in order to study the conformation of CPS in solution. NOE buildup curves were constructed by the PANIC approach (*Macura et al., 1986*), in which the spin-lattice relaxation is taken under consideration by normalization of cross-peak volumes with the diagonal peak from the same experiment. This procedure has the advantage over a classical approach of compensating for error due to the experimental variation between the measurements.

By utilizing the same fitting procedure as for the classical buildup curve, σ_{PANIC} were calculated (Table 5.2)

Table 5.2: Proton-proton cross relaxation rates (σ in s^{-1}) and effective proton-proton distances (in Å) calculated from σ_{PANIC} (r_{NMR})and CarbBuilder 3D model (r_{CB}).

	σ_{PANIC}	r_{NMR}	r_{CB}
A1-C4	3.59	2.35	2.08
C1-C3*	1.59*	2.70	2.71
C1-C5	3.01	2.70	2.59
C1-B3	1.59	2.70	2.54
B1-B5	2.39	2.51	2.62
B1-A3	2.76	2.45	2.07

* proton pair used as reference in the PANIC calculations

Effective ^1H-^1H distances (r_{ij}) can readly be calculated from σ_{ij} if a reference proton pair with known σ_{ref} and r_{ref} is aviableand the ISPA (Isolated spin pair approximation) can be used, by utilizing the equation:

$$r_{ij} = r_{ref} (\sigma_{ref} / \sigma_{ij})^{1/6}$$

Effective ^1H-^1H distances, calculated from σ_{PANIC} are reported in the table together with the r^{-6} average distances from the CarbBuilder 3D model. The deviations between r_{NMR} and r_{CB} are <0.3 Å. The r_{CB} were provided from the CarbBuilder 3D carbohydrate structure, in order to create a simplified model, that is reported below (Figure 5.7).

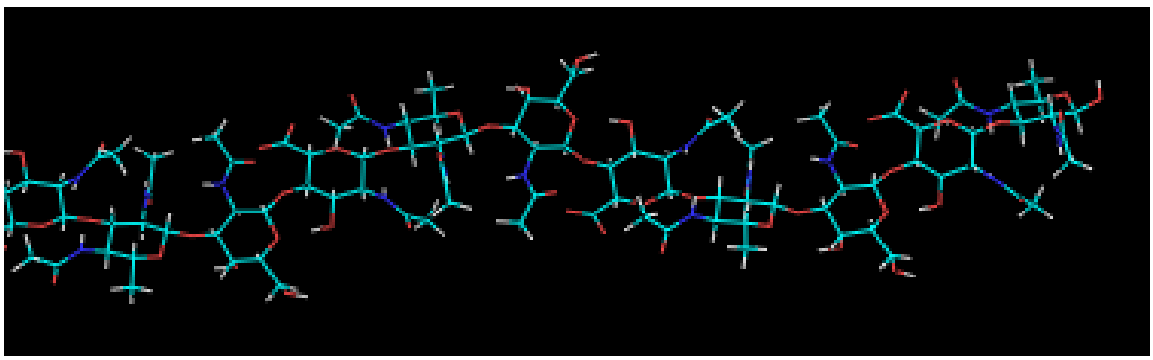

Figure 5.7: CarbBuilder 3D model of CPS_2 from *C. psychrerythraea* 34 H.

Starting from this model, it will be possible to perform 3D structural characterization in order to verify if the 3D conformation is connected with the lack of activity.

5.2.4 Ice recrystalizzation inhibition assay

Quantitative ice recrystallization inhibition (IRI) assays were employed to link the structural characterization of the polysaccharide, its influence on local water structure and ice growth interactions. CPS_2 produced at these temperature, does not display IRI activity in the concentration range of 1.25 – 10 $mg \cdot mL^{-1}$ (Figure 5.8).

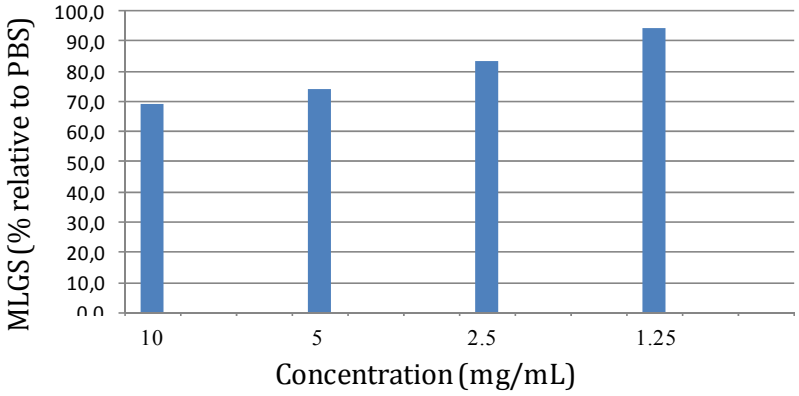

Figure 5.8: Ice recrystallization inhibition activity of CPS_2 from *Colwellia psychrerythraea*.

Conclusion

Colwellia psychrerythraea 34H grown at 8 and -2 °C

C. psychrerythraea has been grown at two temperatures other than 4°C, in order to understand the variations, if any, in the structures of the saccharidic constituents. In particular, 8 and -2°C have been chosen.

The cells extraction confirmed the presence of a rough-LPS (LOS) and sugar analysis suggested that the saccharidic composition is identical to that of the LOS from *Colwellia* grown at 4°C; this result was also confirmed by the MALDI spectrum of the partially deacylated LOS (LOS-OH). In contrast, fatty acid analysis shows a different composition, with a different composition of 3-hydroxy fatty acids, thus suggesting some differences in the lipid A structure.

Furthermore, the presence of the CPS and EPS is confirmed when *Colwellia* grows at 8 and -2°C, even if at these temperatures, the production of an additional polysaccharide (named CPS_2) has been observed. The structure of this polymer has been totally elucidated: it consists of a trisaccharidic repeating unit containing 2,4-diamino-2,4,6-trideoxy-D-glucopyranose (bacillosamine), 2-amino-2-deoxy-D-galactose (GalN) and 2-amino-2-deoxy-D-glucuronic acid (GlcNA). Interestingly, this polysaccharide displays very low ice recrystallization inhibition.

Psychrobacter arcticus 273-4

Permafrost is defined as soils or sediments that are continuously exposed to a temperature of 0°C or less for at least 2 years (*Mueller et al., 1973*). Permafrost temperatures range from -10°C to -20°C in the Arctic and from -10°C to -65°C in the Antarctic, and liquid water occurs as a very thin, salty layer surrounding the soil particles in the frozen layer. Despite the challenges of the permafrost, a variety of microorganisms successfully colonize this environment, and many microorganisms have been isolated from it (*Rivkina et al., 2000; Vishnivetskaya et al., 2000*). *Psychrobacter arcticus* 273-4 is a Gram-negative bacterium isolated from a 20 000–40 000–year-old Kolyma region of Siberian permafrost core (*Vishnivetskaya et al., 2000*). *Psychrobacter arcticus* 273-4 is considered a psychro-tolerant microorganism as it can grow at low, even subzero temperatures and even more than 20°C (*Gilichinsky et al., 2007*). Low temperature is not the only limiting stress within the Siberian permafrost, as ice formation increases solute concentration by decreasing the amount of free available water. This produces an environment with low water activity, similar to desiccated and salt-stressed environments. Low water activity requires an increased amount of turgor pressure to maintain cellular respiration and thus provide the energy necessary for cellular processes.

Furthermore, a capsule layer was visible around all cells of *Psychrobacter arcticus* in 5 osm medium, while no cells showed capsules when incubated in ½ TSB at 4 or 22°C (Figure 6.7). The presence of capsular layers surrounding non-spore-forming bacteria occurs frequently in permafrost soils, and is believed to aid in formation of cyst-like forms (*Soina et al., 2004*).

For all these reasons, *Psychrobacter 273-4* was selected as a model to study cold and salinity adaptation for further understanding further the adaptations of life on other astral bodies.

Chapter VI

Psychrobacter arcticus 273-4

6.1 Lipopolysaccharide structure

6.1.1 LPS extraction and purification

Psychrobacter arcticus strain 273-4 cells were growth at 4 °C and removed from medium by centrifugation. Dried bacteria cells were extracted using phenol/chloroform/light petroleum (PCP) mixture to obtain the crude LPS. Due to the very low amount of LPS_{PCP} (0.03%), cells were extracted by phenol/water method, and the aqueous phase was dialysed and freeze dried. In order to purify LPS_w from other cells contaminants, the sample was treated with DNAse, RNAse and protease followed by dialysis (LPS_W, 3.1 %). The purified sample (LPS_W) was analyzed by DOC-PAGE electrophoresis, and the silver nitrate staining showed bands at low molecular masses, thus revealing a rough LPS (LOS, Figure 6.1).

Figure 6.1. Analysis of the LPS_W (Lane b) fraction from *P. arcticus* strain 273-4 by 14% DOC-PAGE. The gel was stained with silver nitrate and was compared with LPS from *E. coli* O127: B8 (Lane a).

The sugar composition of the intact LOS was obtained by GC-MS analysis of the acetylated methyl glycosides and revealed the occurrence of Rhamnose (Rha), Galactose (Gal), Glucose (Glc), N-Acetylmuramic acid (NAM) and 3-deoxy-D-*manno*-oct-2-ulosonic acid (Kdo). Methylation analysis indicated the presence of 3-substituted Rha, terminal Glc, 4-substituted Glc, 3-substituted Gal, terminal NAM, 3,4,6-trisubstituted Glc, 3,4-disubstituted Glc, terminal Kdo, and 4,5-

disubstituted Kdo. The methylation data also revealed a pyranose ring for all the residues. The absolute configurations of the sugar residues were determined by GC–MS analysis of the corresponding acetylated 2-octyl glycosides; all the hexoses were founded to be in the D-configuration, while rhamnose residue in the L-configuration. The absolute configuration of N-acetylmuramic acid was supported by the NMR data (see below).

Fatty acids analysis revealed the presence of the following main components: 3-hydroxy dodecanoic (C12:0(3OH)), 3-hydroxy tetradecanoic (C14:0(3OH)), tetradecanoic (C14:0), tetradecenoic (C14:1), pentadecanoic (C15:0), and pentadecenoic (C15:1) acids.

6.1.2 Deacylation of the LPS

The LOSw was *O*-deacylated with anhydrous hydrazine and the product obtained (LOS-OH) was analyzed by ESI FT-ICR mass spectrometry. The charge deconvoluted mass spectrum showed various K-adducts [M + n(K – H)] of four main species **M1-M4** (Figure 6.2), the composition of which is reported in Table 6.1. The most abundant species with a mass of 2633.927 u was attributed to the following composition: DeoxyHexHex$_5$Kdo$_2$NAMHexN$_2$P$_2$[C14:0(3OH)][C12:0(3OH)] ([M1 + (K – H)], calculated mass: 2633. 934 u). The signal of **M3**, occurring at 162 u lower than **M1**, suggested the presence of species containing one hexose less. To the species **M2** and **M4** were attributed the same sugar composition as **M1** and **M3**, respectively, whereas the mass difference of 28 u is due to a 3-hydroxy dodecanoic in place of the 3-hydroxy tetradecanoic acid.

In addition, the methylation data revealed that the lack of the hexose residue for the species **M3** and **M4** was from the position O-6 of the 3,4,6-trisubstituted glucose.

Table 6.1. Composition of the main species observed in the charge deconvoluted ESI FT-ICR mass spectrum of the *O*-deacylated LOS from *P. arcticus* 273-4.

Species	Observed mass [u]	Calculated mass [u]	Composition[a]
M1-H+K	2633.927	2633.934	NAMDeoxyHexHex$_5$Kdo$_2$HexN$_2$P$_2$[C14:0(3OH)] [C12:0(3OH)]
M2-H+K	2605.899	2605.903	NAMDeoxyHexHex$_5$Kdo$_2$HexN$_2$P$_2$[C12:0(3OH)] [C12:0(3OH)]
M3-H+K	2471.875	2471.882	NAMDeoxyHexHex$_4$Kdo$_2$HexN$_2$P$_2$[C14:0(3OH)] [C12:0(3OH)]
M4-H+K	2443.845	2443.851	NAMDeoxyHexHex$_4$Kdo$_2$HexN$_2$P$_2$[C12:0(3OH)] [C12:0(3OH)]

[a] All molecular species were revealed as K salts

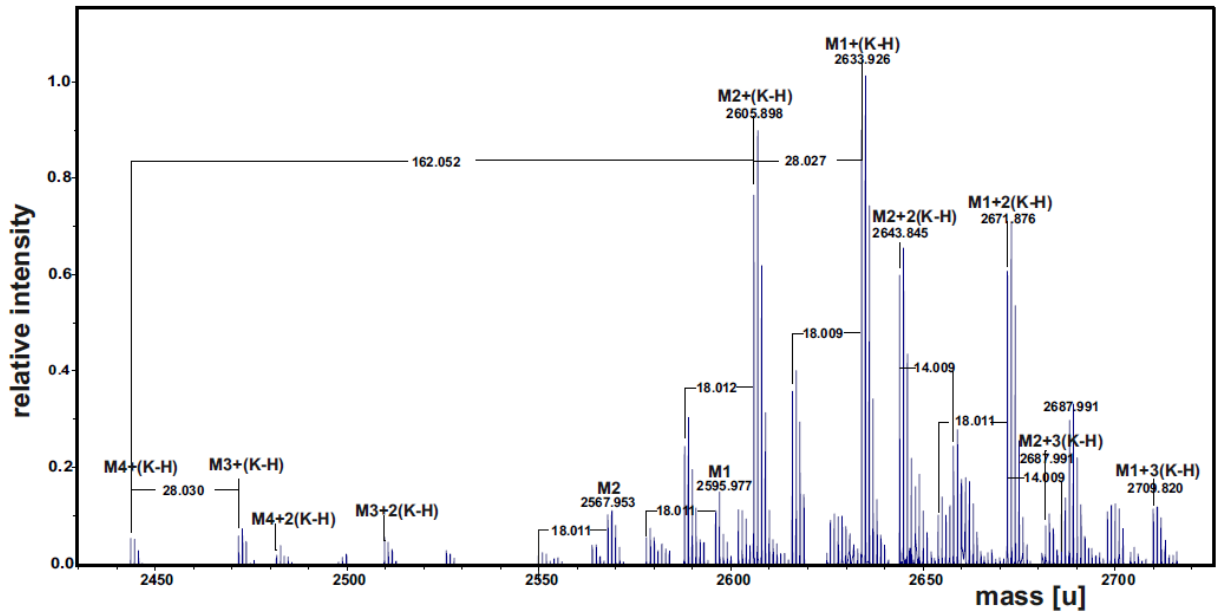

Figure 6.2. Charge deconvoluted ESI FT-ICR mass spectrum of the LOS-OH fraction isolated from *P.arcticus* 273-4. The spectrum was acquired in the negative ion mode.

6.1.3Mild acid hydrolysis of the LPS

The well-known ability of the LOS to form micellar aggregates in aqueous solution did not allow the direct structural NMR analysis. Thus, the LOS was hydrolyzed under mild acidic conditions to cleave the unstable Kdo glycosidic linkage between the lipid A and the saccharidic region. After centrifugation, the supernatant containing the core oligosaccharidic portion of the LOS was

separated from a precipitate constituted by the lipid A. The supernatant was analyzed by ESI FT-ICR MS. The charge deconvoluted mass spectrum displayed the presence of two main species (**N1** and **N2**, Figure 6.3). As expected, for the most abundant species **N1**, occurring at 1469.501 u, (calculated mass: 1469.48 u) it was found the following composition: NAMDeoxyHexHex$_5$Kdo$_1$. Again, the difference of 162 u with **N2** confirmed the presence of a species lacking one hexose residue. No peaks with two Kdo residues were found, since the ketosidic bond is much more acid-labile than the common aldosidic bonds. Signals at 46 and 18 u lower mass values respect to **N1** were both assignable to Kdo artifacts (*Masoud et al., 1994*).

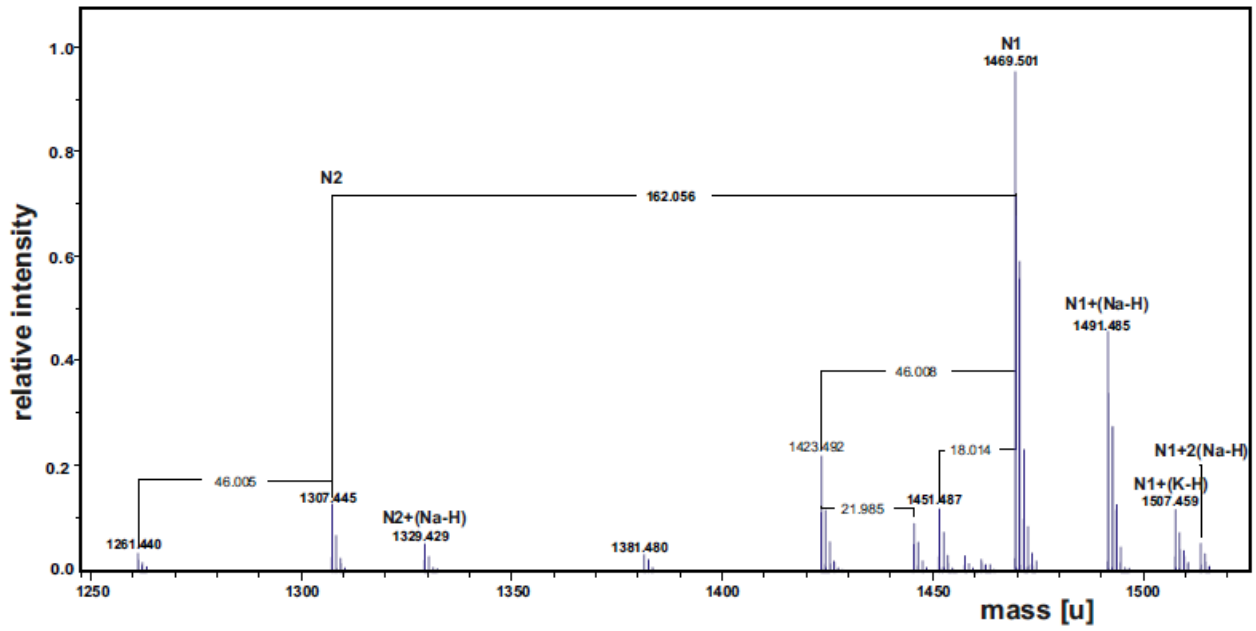

Figure 6.3. Charge deconvoluted ESI FT-ICR mass spectrum of the supernatant of acetic acid hydrolysis of *P.arcticus* 273-4 LOS. The spectrum was acquired in the negative ion mode.

The supernatant mixture was further purified on a Biogel P-10 chromatography column, using pyridinium acetate buffer as eluent. The main obtained fraction, named **OS**, was studied by two-dimensional NMR spectroscopy.

6.1.4 NMR spectroscopic analysis of OS

To characterize the core oligosaccharide **OS** fraction was analyzed by one- and two-dimensional NMR spectroscopy.

The ^{1}H-NMR spectrum of the **OS** fraction, recorded at 310 K, is shown in Figure 6.4. Seven anomeric proton signals (**A-G**), attributable to core monosaccharide units, were present in the region between δ 4.5 and δ 5.4 ppm (Table 6.2).

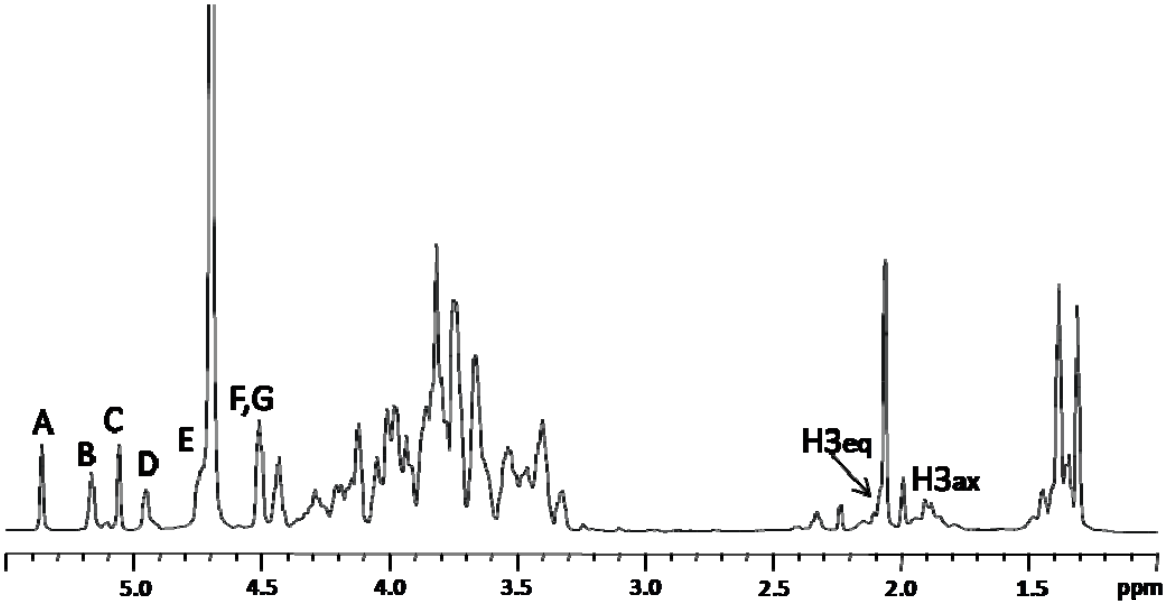

Figure 6.4. ^{1}H NMR spectrum of the oligosaccharide (**OS**) obtained by mild hydrolysis of LOS. The spectrum was recorded in D_2O at 310 K at 600 MHz. The letters refer to the residues as described in Table 3 and Scheme 1.

The ^{1}H-NMR spectrum of **OS** was also recorded at 318 K (data not shown) in order to reduce the anomeric signals overlapping. In this experiment, the anomeric proton signal of **E** was clearly visible. Moreover, the integration of all anomeric signals showed a relative ratio of 1:1 except for the signal at 4.51 ppm. In fact, the peak area for this signal was twice the amount of every other proton anomeric signal, thus indicating the coincidence of H-1 of **F** with H-1 of **G** chemical shifts. By considering all the 2D NMR experiments, the spin systems of all the monosaccharides were identified (Table 6.2).

Table 6.2. ^{1}H and ^{13}C NMR assignments of the oligosaccharide **OS** obtained from acetic acid hydrolysis of the LOS from *P.arcticus* strain 273-4. The spectra were recorded at 310 K at 600 MHz.

Residue	**H1** **C1**	**H2** **C2**	**H3** **C3**	**H4** **C4**	**H5** **C5**	**H6** **C6**	**H7** **C7** **C1'[a]**	**H8** **C8** **H2'[a]** **C2'**	 **H3'** **C3'**
A	5.36	3.72	3.78	3.66	3.98	3.64/3.81	-	4.43	1.40
α-D-MurNAc[b]	95.1	55.0	78.3	71.8	73.5	64.5	183.2	79.8	20.0
B	5.16	3.84	4.28	3.98	4.44	4.19/4.04			
3,4,6-α-D-Glc*p*	100.9	73.6	78.0	75.2	71.4	68.8			
C	5.06	4.12	3.86	3.57	3.82	1.30			
3-α-L-Rha*p*	103.5	68.6	77.2	71.7	70.8	18.8			
D	4.95	3.38	3.52	3.43	3.47	3.93/3.74			
t*-β-D-Glc*p	102.9	74.8	77.2	71.5	77.1	62.2			
E	4.75	3.41	3.67	3.67	3.61	3.82/3.97			
4-β-D-Glc*p*	102.2	74.3	75.6	79.7	76.1	61.5			
F	4.52	3.66	3.72	4.01	3.75	3.92/3.74			
3-β-D-Gal*p*	104.2	71.6	81.6	69.6	76.5	62.2			
G	4.51	3.33	3.52	3.41	3.46	3.92/3.74			
t*-β-D-Glc*p	103.8	74.4	77.1	74.3	77.3				
H	-	-	1.89/2.09	4.16	4.11	3.87	4.06	3.80/3.78	
5-Kdo		97.8	35.5	67.3	77.0	72.8	70.0	64.5	

Additional chemical shifts

[a]All lactyl resonances of MurNAc are labelled prime: 1', carboxylate; 2', linkage point; 3', methyl.

[b]NAc resonances: δ 2.07/23.0 ppm (CH_3), 175.5 ppm (CO)

Residue **A** with H-1/C-1 signals at δ 5.36/95.1 ppm was identified as a 3-*O*-(1-carboxyethyl) ether of 2-acetamido-2-deoxy glucopyranosyl residue [namely N-acetylmuramic acid (NAM)], with an α-

anomeric configuration, as suggested by the low $^{3}J_{H\text{-}1,H\text{-}2}$ value (3.1 Hz). Moreover, its H-2 proton at δ 3.72 ppm was correlated, in the DEPT-HSQC experiment (Figure 6.5), with a C-2 resonance occurring at δ 55.0 ppm, thus indicating a nitrogen-bearing carbon atom. In addition, the HMBC spectrum showed a long range scalar coupling between the signal of H-3 at δ 3.78 ppm with the signal at δ 79.8 ppm, attributed to C-2' of 1-carboxyethyl substituent. The same experiment also revealed a correlation between the signal at δ 4.43 ppm, attributed to H-2', with both the signals of C-1' (δ 183.2 ppm) and C-3' (δ 20.0 ppm), respectively, of 1-carboxyethyl substituent. Finally, a correlation between methyl signal at δ 2.07 ppm (N-acetyl substituent) and CO group at δ 175.5 ppm was also identified.

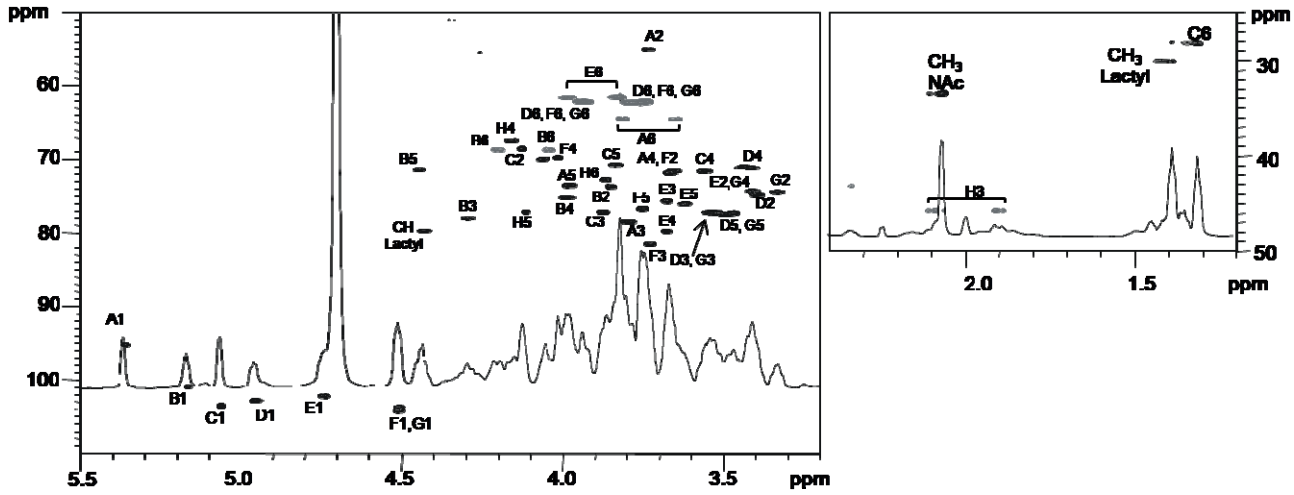

Figure 6.5. Anomeric/carbinolic, (a) and aliphatic regions (b) of ^{1}H-^{13}C DEPT-HSQC spectrum of **OS** core of the LOS from *P. arcticus* strain 273-4. The spectrum was recorded in D_2O at 310 K at 600 MHz.

The correlations of each H-1 to H-6 with all other protons of residues **B**, **D**, **E**, and **G**, in the TOCSY spectrum provided evidence for the *gluco* configuration of all these ring systems.

Residue **B** with H-1/C-1 signals at δ 5.16/100.9 ppm was assigned to a 3,4,6 trisubstituted α-glucose unit on the basis of the small anomeric coupling constant value ($^{3}J_{H\text{-}1,H\text{-}2}$ = 3.7 Hz). The downfield shift of C-3, C-4 and C-6 values of this unit at δ 78.0, 75.2 and 68.8 ppm, respectively (*Carlson et al., 1992*), identified its substitution. This residue was linked to Kdo residue at the O-5 position, as shown by the correlation between H-1 **B** and C-5 of Kdo in the HMBC spectrum (Figure 6.6).

The lack of heptose residue, usually linked in the inner core to the Kdo, has been found so far in *Moraxellaceae* (*Forsberg et al., 1998*) and *Rhizobiaceae* families *(Jansson et al., 1989; CASPER)*. The only example of heptose deficient core region among lipopolysaccharides from psychrophiles was found in *Colwellia psychrerythraea* strain 34H (*Carillo et al., 2013*).

Residues **D** and **G** with H-1/C-1 signals at δ 4.95/102.9 and δ 4.51/103.8 ppm, respectively, were identified as terminal β-glucoses, since none of their carbons were shifted by glycosylation. For both residues the β configuration was inferred by the high $^{3}J_{H\text{-}1,H\text{-}2}$ values (8.1 and 8.0 Hz, for **D** and **G**, respectively). *Intra*-residue NOE contacts of H-1 with H-3 and H-5 (δ 3.52 and 3.47 ppm, and δ 3.52 and 3.46 ppm, for **D** and **G**, respectively) were in agreement with β-anomeric configurations.

A $^{3}J_{H\text{-}1,H\text{-}2}$ coupling constant of 8.0 Hz for residue **E** indicated a β-configuration, which was also confirmed by *intra*-residue NOEs. The C-4 of residue **E** was downfield shifted at δ 79.7 ppm respect to the unsubstituted value (*Agrawal et al., 1994*), thus evidencing that this position was glycosylated. The residue **F** with H-1/C-1 signals at δ 4.52/104.2 was identified as a *galacto* configured residue since the anomeric proton showed only few correlations in the TOCSY experiment; in particular it was identified as a β-galactose ($^{3}J_{H\text{-}1,H\text{-}2}$ = 8.0 Hz). Moreover, the downfield shift of proton resonance of C-3 at δ 81.6 ppm instead of δ 73.8 ppm of an unsubstituted residue (*Agrawal et al., 1994*) indicated glycosylation at this position.

The residue **C** with H-1/C-1 signals at δ 5.06/103.5 ppm was recognized as an α-rhamnose residue, since the TOCSY spectrum showed scalar correlations of the ring protons with methyl signal in the up-field region at δ 1.30 ppm. Its α configuration was suggested by the $^{3}J_{H\text{-}1,H\text{-}2}$ value (< 3 Hz) and by the value of its C-5 chemical shift (http://www. *Casper.organ.su.se/sap/a703.html*). The downfield shift of carbon resonance of C-3 at δ 77.2 ppm respect to the value of δ 71.0 ppm (*Agrawal et al., 1994*) indicated glycosylation at this position.

Finally, the Kdo (residue **H**) proton and carbon chemical shifts were identified starting from the diastereotopic protons $H\text{-}3_{ax}$ and $H\text{-}3_{eq}$ (δ 1.89/2.09 ppm).

The Kdo H-5 proton was identified by vicinal scalar coupling with H-4 in the COSY spectrum. Moreover, the residue resulted to be glycosylated at O-5 position, as suggested by the downfield shift of its C-5 carbon signal at δ 77.0 ppm respect to the value of δ 67.5 ppm for an unsubstituted Kdo (*Agrawal et al., 1994*).

The sequence of the residues was deduced from the HMBC experiment (Figure 6.6), that indicated the following correlations: H-1 of **B** and C-5 of Kdo, H-3 of **B** with C-1 of **D**, H-4 of **B** with C-1 of **E** and H-6 of **B** with C-1 of **G**. In addition, H-1 of rhamnose **C** displayed a correlation with C-3 of residue **F,** while C-1 of residue **A** displayed a correlation with H-3 of **C**. Finally, H-1 of galactose **F** displayed a correlation with C-4 of residue **E**.

Inter-residue NOE contacts, obtained from ROESY experiments, confirmed this sequence, since dipolar couplings were observed between: H-1 of **B** and H-5 of **H**, H-1 of **G** and H-6 of **B**, H-1 of **E**

and H-4 of **B,** H-1 of **F** and H-4 of **E**, H-1 of **D** and H-3 of **B**, H-1 of **A** and H-3 of **C**, H-1 of **C** and H-3 of **F**.

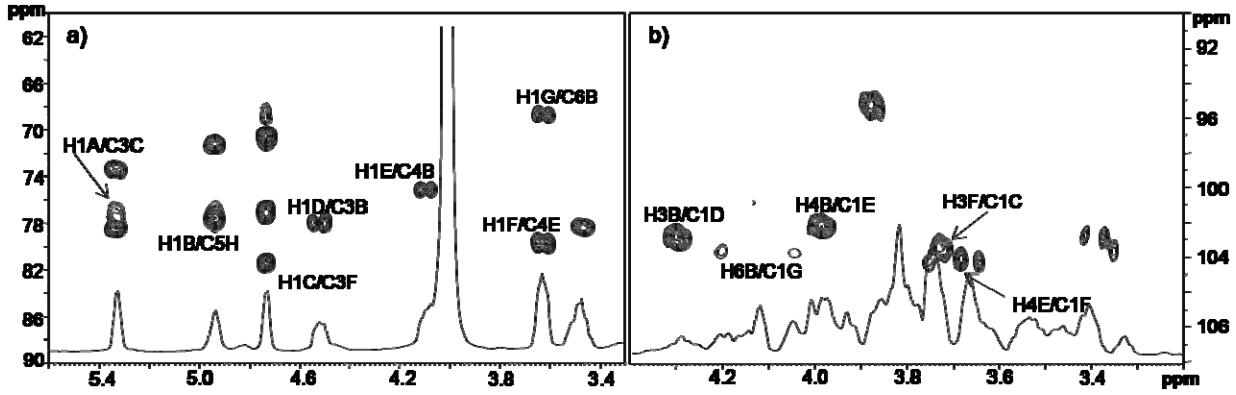

Figure 6.6. Anomeric (a) and carbinolic (b) regions of ^{1}H-^{13}C HMBC spectrum of **OS** core of the LOS from *P. arcticus* 273-4. The spectrum was recorded in D_2O at 310 K at 600 MHz.

The absolute configuration of residue **A** is based on NMR considerations. The chemical shift of C-1 at δ 95.1 ppm indicates that the N-acetylmuramic acid has the opposite configuration of L-rhamnose, since a value of near 103 ppm would be expected for the same absolute configuration of residue **C** (*Lipkind et al., 1988*). As for 1-carboxyethyl substituent, the configuration of (*R*) for C-2' was deduced by comparing both ^{1}H and ^{13}C NMR chemical shifts of residue **A** with those of N-acetylisomuramic acid (*Gunawardena et al., 1998; Knirel et al., 1992*), characterized by a (*S*) configuration at C-2'.

In conclusion, the complete structure of the core saccharidic backbone of the LOS from *Psychrobacter arcticus* 273-4 is reported in the Scheme 6.1.

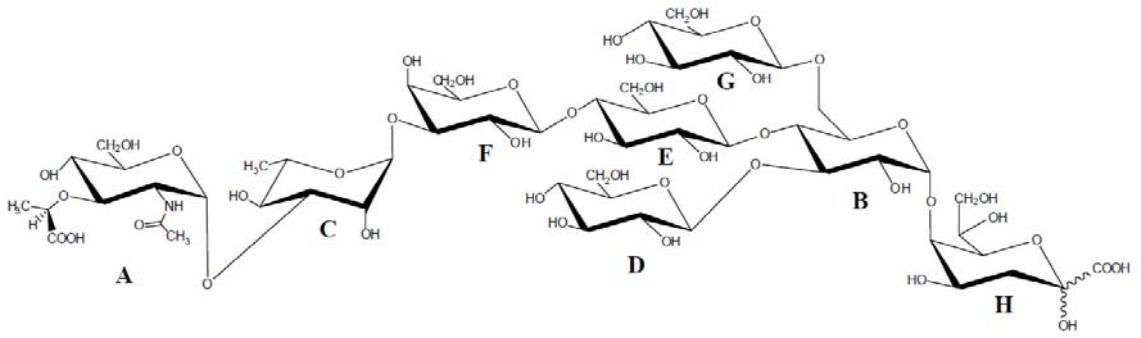

Scheme 6.1. **OS** core structure of the LOS from *Psychrobacter arcticus* strain 273-4.

6.1.5 Discussion

The complete structure of the sugar backbone of the LPS from the permafrost isolate *Psychrobacter arcticus* 273-4 is reported. The structure shows a particular inner core region, with a residue of glucose linked to the Kdo in place of a *manno*-heptose. This structural feature has been found only in another psychrophile, *Colwellia psychrerythrae* 34H, which showed a mannose residue linked to the Kdo.

Generally, the oligo- and polysaccharides produced by marine bacteria are distinguished by the acidic character (*Muldoon et al., 2003*), and by the occurrence of unusual sugars (*Kenne et al., 1983*), non-sugar substituents (*Hanniffy et al., 1999; Komandrova et al., 2010; Carillo et al., 2013*) or structures highly phosphorylated (*Corsaro et al., 2004*). Although *P. arcticus* 273-4 was isolated from Arctic permafrost it displays similar characteristics of cold-adapted marine isolates, due to the presence of the unusual residue of NAM. N-acetylmuramic acid, commonly encountered as a component of bacterial cell-wall peptidoglycan, has been already found in the O-specific polysaccharide of *Yersinia ruckerii* (Beynon et al., 1994), and *Proteus penneri* (*Zych et al., 1998*), but to the best of our knowledge, this is the first time that it has been found in a core oligosaccharide.

It is well known that cold-adapted microorganisms are able to modify the fluidity of the cellular membrane in response to a lowering of temperature by producing a higher content of unsaturated, polyunsaturated and methyl-branched fatty acids (*Driessen et al., 1996; Chintalapati et al., 2004*). Instead, how bacteria modify the LPS structures in response to the cold stress is still poorly understood.

Even though only few LPS structures from cold-adapted bacteria have been characterized (*Corsaro et al., 2001; Corsaro et al., 2008; Carillo et al., 2011; Carillo et al., 2013*), their attractive feature is the production of rough lipopolysaccharides. Moreover, it is worth noting that *Psychrobacter arcticus* 273-4, a permafrost isolate, shares this feature with marine isolates. To the best of our knowledge, only two examples of smooth lipopolysaccharides isolated from psychrophiles has been reported so far (*Kondakova et al., 2012a; Kondakova et al., 2012b*), even if the isolates were grown at 24 °C.

6.2 Capsular structure

6.2.1 CPS extraction and purification

The presence of capsular structure around cells of *Psychrobacter arcticus* 273-4 was reported in a previous paper (*Ponder et al., 2008*) and visualized by TEM images (Figure 6.7).

P. arcticus cells grown in high salinity conditions, were extracted by phenol/water method, dialyzed and then digested with proteases, DNases, and RNases to remove contaminating proteins and nucleic acids.

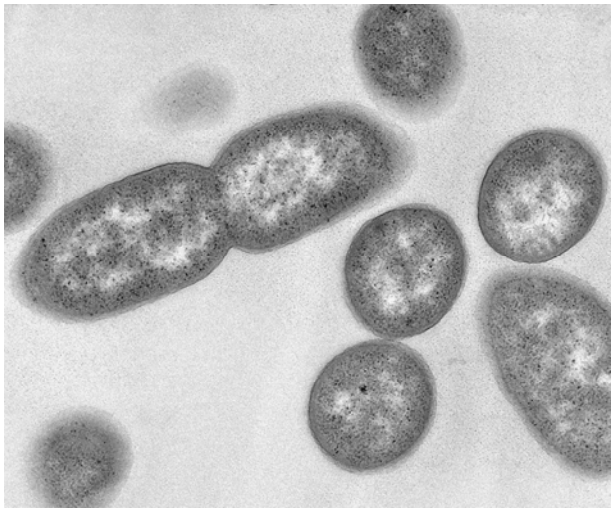

Figure 6.7 : TEM image of *P.arcticus* 273-4 cells

P.arcticus cells were extracted by PCP method to recover the LOS and then by phenol/water method. The water extract was extensively dialyzed against water, and the dyalizate was lyophilized and depleted of nucleic acid proteins through enzymatic digestion. The purified sample was visualized by 14% DOC-PAGE using either silver nitrate or Alcian blue staining methods. The silver nitrate showed the presence of only one band at low molecular masses, corresponding to LOS (*Casillo et al., 2015*). Instead, the sample treated with Alcian blue and then stained with silver allowed us to visualize bands at higher molecular masses, reported in the Figure 6.8, together with that of LOS.

Figure 6.8: Analysis of the purified fraction from *P.arcticus* 273-4 by 14% DOC-PAGE. The sample was stained with and Alcian blue dye and after by silver nitrate staining.

Sugar and fatty acid analysis of the sample showed mainly the presence of glucose (glc), galactose (Gal), rhamnose (Rha), 2-amino-2-deoxy-glucose (GlcN) and N-acetyl-muramic acid (NAM) which belong to the LOS, confirming its presence in the aqueous extract, together with 2-amino-2-deoxy-galactose (GalN), mannose (Man) and amino hexuronic acid (HexNA) probably belonging to the capsule. The molecular masses of CPS and LOS species were expected to be very different on the basis of the DOC-PAGE analysis. Nevertheless, the well-known ability of the LOS to form micellar aggregates in aqueous solution did not allow the separation of the two molecular species by size exclusion chromatography. As an alternative, the sample was hydrolyzed under mild acidic conditions to cleave the glycosidic linkage between the lipid A and the saccharidic region of the LOS. After centrifugation, the supernatant containing the CPS and the core oligosaccharidic portion of the LOS was separated from a precipitate constituted by the lipid A. The supernatant mixture was separated on a Biogel P-10 chromatography column, using pyridinium acetate buffer as eluent. Two fractions were obtained: the first one, eluted in the void volume, contained the higher molecular mass material; the second one (OS) contained species with lower molecular mass, corresponding to the core oligosaccharide of the LOS.

^{1}H NMR experiment showed a too complex mixture due to the presence of several anomeric proton signals (Figure 6.9).

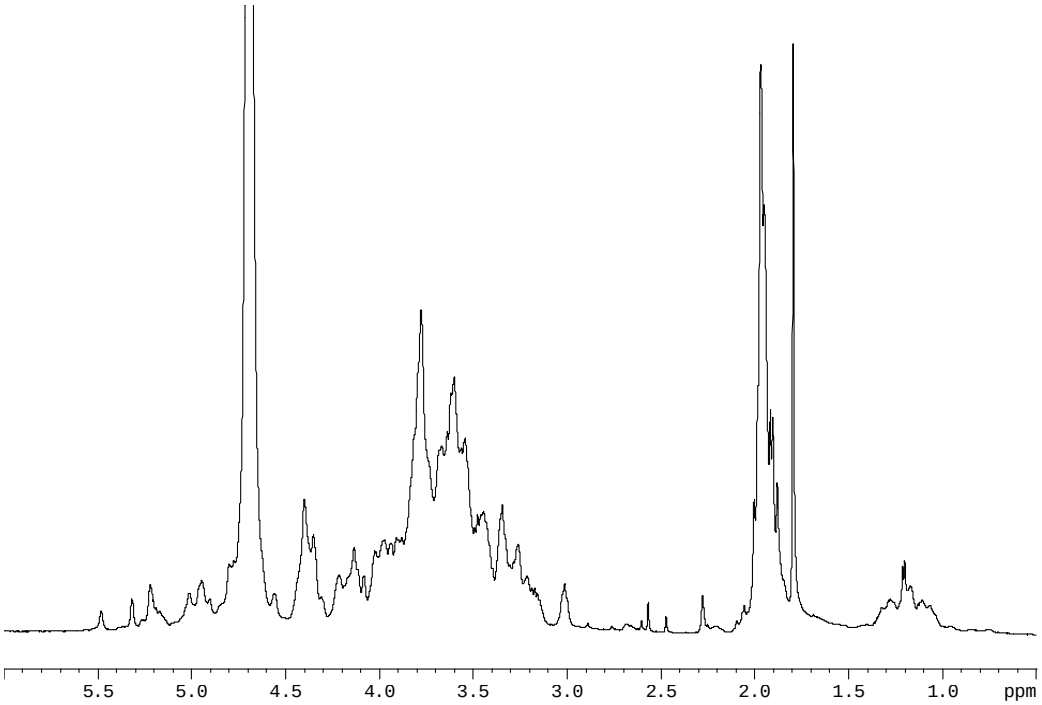

Figure 6.9: ^{1}H NMR spectrum of CPS from P.arcticus; the spectrum was recorded in D_2O at 310K

Due to the very low amount of CPS obtained in this growth condition, it was not possible to characterize it in depth.

6.3 Mannan polysaccharide

6.3.1 Isolation, purification and characterization

Similarly to *Colwellia psychrerythraea*, *Psychrobacter arcticus* releases in the surrounding medium a mannan polysaccharide. The purification of this polysaccharide was performed using the same procedure described for *Colwellia*. After purification, we tested the ice recrystallization inhibition and we found that this exopolysaccharide possesses a significant ice recrystallization inhibition activity, even when the concentration is diluted at 2.5mg/mL. (Figure 6.10).

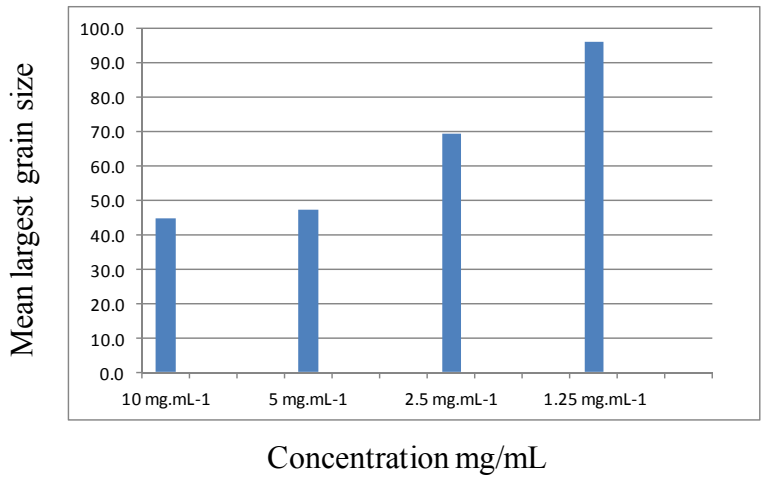

Figure 6.10: Ice Recrystallization Inhibition activity of mannan polysaccharide from *P. arcticus* 273-4. Mean largest grain size is expressed as a percentage of PBS buffer, and small MLGS value indicate increased IRI activity.

The ^{1}H-NMR spectrum of *Psychrobacter* mannan was then compared with that of *Colwellia* (Figure 6.11). Slight differences appeared between the two mannan structures obtained from *P.arcticus* (Figure 6.11a) and *C. psychrerythraea* (Figure 6.11b), thus suggesting the very close similarity of the two polymers. In particular, ^{1}H NMR spectrum from *Colwellia* displayed a most abundant peak of glucose respect of *P.arcticus*, and a weak signal belonging to 6-mannose residue.

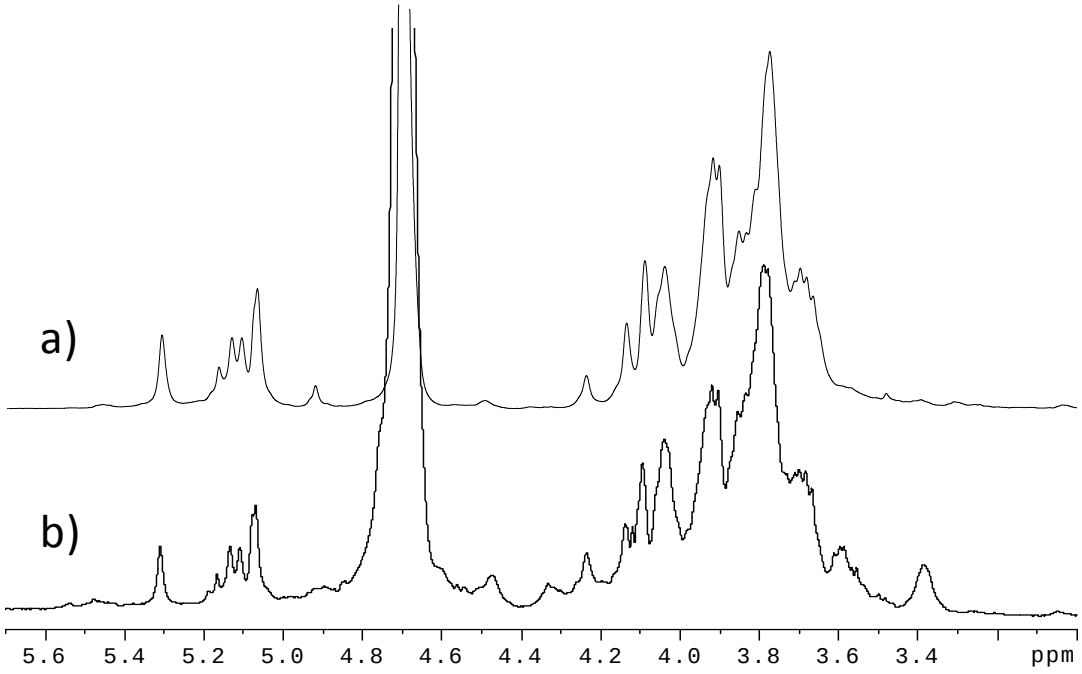

Figure 6.11: ^{1}H NMR spectra of mannan polysaccharide from (a) *Psychrobacter arcticus* and (b) *Colwellia psychrerythraea* 34H.

Conclusion

Psychrobacter arcticus 273-4

Psychrobacter arcticus 273-4 was the first cold-adapted bacterium isolated from a permafrost that possesses genes for a capsular polysaccharide production (*Ayala-del-Rio et al., 2010*). As other cold-adapted microorganisms, *P. arcticus* has evolved different mechanisms to cold-adaptation. To assess if the LPS structure share any common features with those from other psychrophiles, the starting point has been the elucidation of the carbohydrate moiety. After isolation and purification, the LPS produced by this bacterium resulted to be rough-LPS (LOS), in according with others LPSs from psychrophiles already characterized (*Corsaro et al., 2001; Corsaro et al., 2008; Carillo et al., 2011; Carillo et al., 2013*). The LOS from *P.arcticus* displays an α-glucose, in place of heptose residues, linked to the inner core Kdo residue. This structural feature was commonly found in the *Acinetobacter* genus, and in the core region of LOS from *Colwellia psychrerythraea* 34H. Moreover, the LOS was also characterized by the uncommon presence of *N*-acetyl muramic acid, a peptidoglycan sugar constituent (*Casillo et al., 2015*).

Psychrobacter arcticus 273-4 is known in literature for the production of a capsule, when growth in presence of high salt concentration (*Ayala-del-Rio et al., 2010*). The presence of a capsule could be related to a particular adaptation mechanism. In fact, is reported that the brine salinity *in situ,* is approximately 130 to 40 ‰ from the surface of ice to a depth of 160 cm in march, and more than 1% of the volume of the winter sea ice fills with liquid brine with a salinity above 200 ‰ (*Krems et al., 2002*). In addition, freeze-thaw cycles, which tend to damage living cells and reduce viability, are quite common in the sea ice of the Arctic and the Antarctic (*Kim et al., 2007*). Thus, the microorganisms living in the brine channels must have evolved adaptations to tolerate high salinity and repeated freezing and thawing. Therefore, in recent years, increasing attention has been paid to the EPSs produced by the bacteria in sea ice and their ecological roles (*Krems et al., 2002; Junge et al., 2004*).

In order to isolate the CPS, the cells were grown in high salinity condition. The preliminary purification, revealed that the capsule polysaccharide is produced in very low amount, thus suggesting that the growth conditions are not so appropriate as reported . Therefore, in order to fully characterize the CPS, it will be necessary to maximize its production.

Psychrobacter arcticus 273-4 is involved in the production of an exopolyasccharide, a mannan polysaccharide as well as *Colwellia*. The ice recrystallization inhibition activity has been tested for this polymer, and compared to that of mannan produced by *Colwellia* and by the yeast *S. cerevisiae*, a commercial product. Intriguingly, the yeast polymer differs from that of *P. arcticus* and *Colwellia* for the lack of t-Glc residue and phosphates, thus suggesting that these structural features may be connected with the lack of activity.

Pseudoalteromonas haloplanktis TAC 125

Pseudoalteromonas haloplanktis TAC125 is a Gram-negative bacterium isolated from an Antarctic seawater sample collected near Terre Adélie. It can be classified as an eurypsychrophile and it was the first Antarctic Gram-negative bacterium the genome of which was fully sequenced and carefully annotated. *P. haloplanktis* TAC125 is one of the most intensively investigated, as the bacterium is one of the fastest growing cold-adapted characterized so far and it is able to grow in a quite wide temperature range (0-25°C) (*Medigue et al., 2005*)**.** Several exceptional genomic and metabolic features were derived from the genome sequence of this bacterium, showing adaptation in periodic situations of nutrient abundance. The efficiency of cold-adapted expression systems was also validated by the successful production of proteins and biopharmaceutical products (*Corchero et al., 2013; Giuliani et al., 2011; Dragosists et al., 2011; Gasser et al., 2008*).

Furthermore, marine bacteria belonging to the genus *Pseudoalteromonas* produce compounds of biotechnological interest, including anti-biofilm molecules (*Klein et al., 2011*). The interest in the development of new approaches for the prevention and treatment of adhesion and biofilm formation capabilities has increased, in recent years. There is a notable effort towards finding small available molecules that should "break up" the "tangled matrix" of the biofilm.

Previous results (*Papa et al., 2013*) show that the cell-free supernatant of *Pseudoalteromonas haloplanktis* TAC125 grown in static condition strongly inhibits the biofilm of *Staphylococcus epidermidis.*

Chapter VII

Pseudoalteromonas haloplanktis TAC 125: purification and characterization of an anti-biofilm molecule.

7.1 Isolation, purification and characterization

Papa et al., (*Papa et al., 2013*) have been reported that *Pseudoalteromonas haloplanktis* TAC 125, grown in static condition, inhibits the biofilm of *Staphylococcus epidermidis*. This work was carried out in collaboration with Prof. Gilda Parrilli and Prof. Maria Luisa Tutino, Departement of Chemical Sciences. In order to assess whether the anti-biofilm was produced in all the phases of biofilm development cycle, its formation over a 120-h period in BHI at 4°C was evaluated. Biofilm formation was assayed by Christensen method (*Christensen et al., 1985*), and reported data demonstrated that the anti-biofilm molecule is produced in all of *P. haloplanktis* TAC125 biofilm stages, although the best production is obtained at 96 h (Figure 7.1). The supernatant collected at 96 h is able to decrease the biofilm formation of *S. epidermidis* strain O-47 about of 91%, in sessile condition at 4°C for a 96-h period.

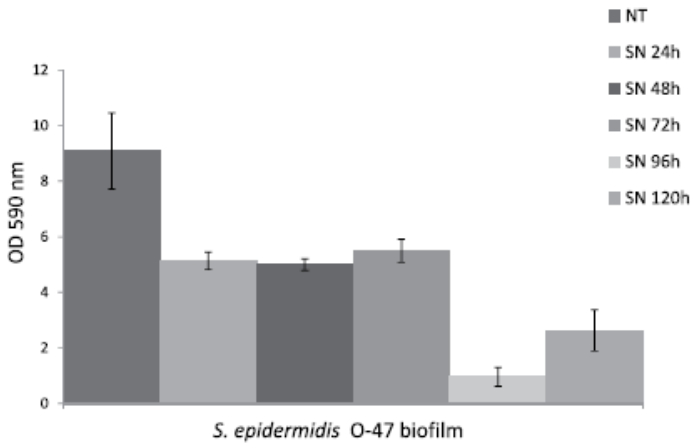

Figure 7.1: Evaluation of *S. epidermidis* biofilm formation in the presence of *P. haloplanktis* supernatant (SN) at different times.

Then, the effect of temperature on anti-biofilm compound production, was evaluated. In particular, the Antarctic bacterium was grown in sessile condition at different temperatures (4°C, 15°C, 20°C). Corresponding supernatants were recovered for each condition after 96 h at 4°C, 96 h at 15°C, and 48 h at 20°C, and their effect on S. *epidermidis* strain O-47 biofilm was evaluated (Figure 7.2). As shown in Figure 7.2 the anti-biofilm compound was produced at all of the tested temperatures (4–20°C), demonstrating that anti-biofilm production is not temperature-dependent.

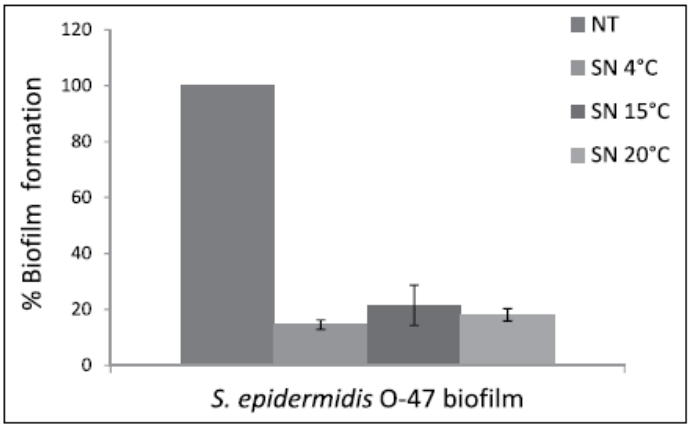

Figure7.2: Biofilm formation of *S. epidermidis* O-47 in the presence (SN) and in the absence of *P. haloplanktis* (NT) supernatant deriving from sessile cultures performed at different temperatures.

P. haloplanktis TAC125 supernatant deriving from sessile growth at 4°C was subject to dialysis treatment using a semipermeable membrane with a cutoff of 3500 Da. Both the retained and the permeate from the dialysis tube were tested for antibiofilm activity and only the second one was shown to be active. The presence of a complex mixture in the permeate was shown by ^{1}H NMR spectrum of the sample (data not shown). Consequently, a liquid chromatography on a Biogel P-2 column was performed to fractionate the dialyszate sample (Figure 7.3a) and the biological activity of each fraction was evaluated (Figure 7.3b). The obtained results indicated for the fraction 6D the best anti-biofilm activity, but once again ^{1}H NMR spectrum revealed the presence of a complex mixture (data not shown). Reverse phase HPLC on a C18 column was used to further purify 6D fraction and, the sub-fractions derived from this procedure were tested to evaluate the anti-biofilm activity on *S. epidermidis* O-47 biofilm.

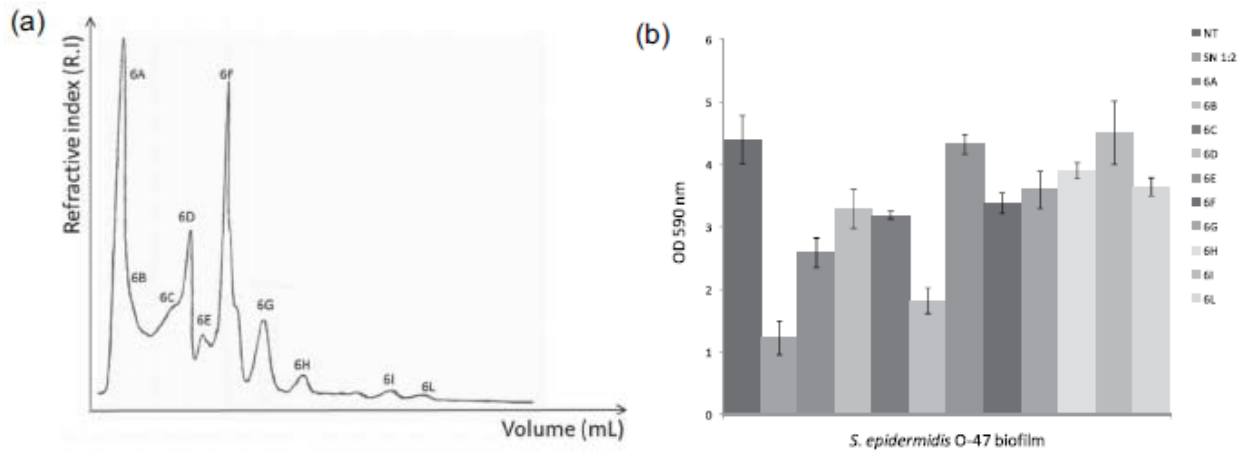

Figure 7.3: Purification of active compound from P.haloplanktis supernatant. (a) Gel filtration chromatographic profile. (b) Biofilm formation by *S.epidermidis* O-47 in the presence and in the absence of exclusion chromatography fractions.

The results (Figure 7.4) clearly showed that the treatment with F fraction induces a decrease of the biofilm formation of *S. epidermidis* strain O-47 about of 90%.

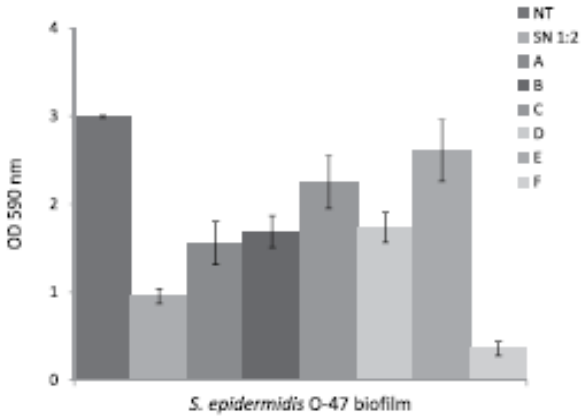

Figure7.4: Biofilm formation by *S.epidermidis* O-47 in the presence and in the absence of HPLC chromatography fractions.

The ^{1}H NMR spectrum suggested that the fraction F is still a mixture, even if the very low amount of the sample did not allow further purification. Therefore, with the aim to get more sample, we decided to improve the purification in terms of amount of product.

Consequently, several Biogel P-2 column were performed to purify 2g of permeated product. The fractions obtained in each gel filtration were tested (Figure 7.5) and assembled on the basis of the presence of the activity.

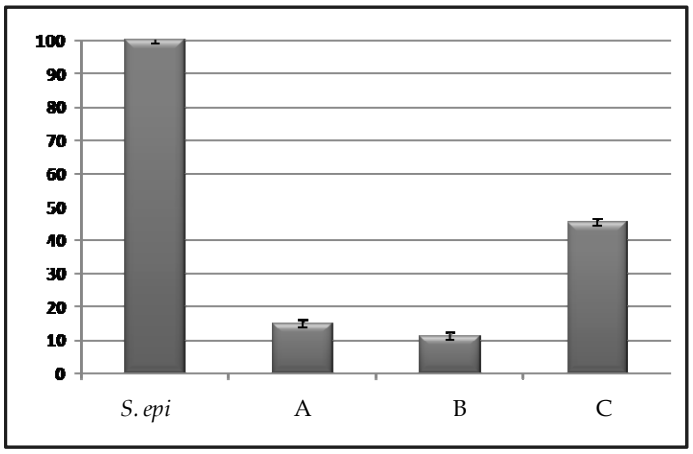

Figure 7.5: Biofilm formation of *S. epidermidis* O-47 in the presence of the purified fractions obtained from one example of Biogel P-2 column.

The fractions B from all the chromatography columns (50mg), were then purified on a C_{18} reverse phase column eluted with acetonitrile and water. The more retained fraction (fraction S) showed the highest inhibition activity (0,1mg). The sub-fractions derived from this procedure were tested to evaluate the anti-biofilm activity on *S. epidermidis* O-47 biofilm. The results (Figure 7.6) clearly showed that the treatment with S fraction induces a decrease of the biofilm formation of *S. epidermidis* strain O-47 about of 90%.

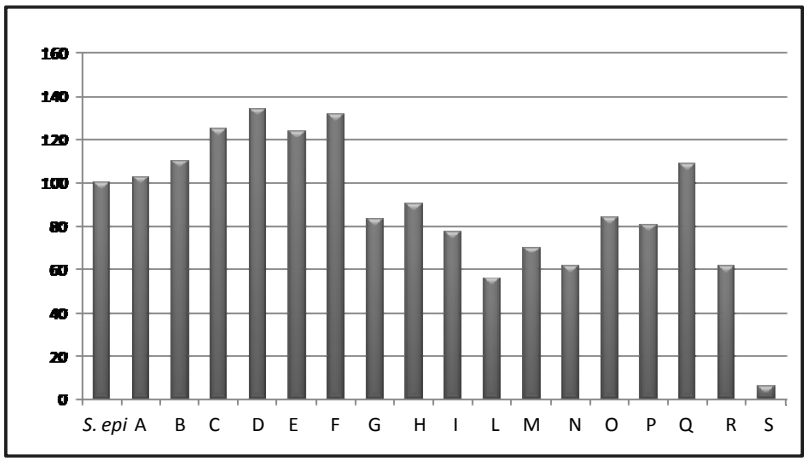

Figure 7.6: Evaluation anti-biofilm activity of different fractions obtained from reverse phase C18 column.

The S fraction was analyzed by ^{1}H NMR experiment and GC-MS analysis; these results displayed that the anti-biofilm activity is due to an aldehyde molecule acting as signal. This molecule has been completely characterized, and the corresponding commercial product was tested, resulting active, too.

Conclusion

Pseudoalteromonas haloplanktis TAC 125: purification and characterization of anti-biofilm molecule.

In a previous paper (*Papa et al., 2013*) we demonstrated that the cell free supernatant of Antarctic bacterium *P. haloplanktis* TAC125 was effective on *S. epidermidis* biofilm even on the mature form. Moreover, the *P.haloplanktis T*AC125 supernatant resulted to have no antibacterial activity against free-living bacteria, and results to be species-specific. (*Papa et al., 2013*) Interestingly *P. haloplanktis* TAC125 produces this activity only when it is grown in sessile condition. This latter result could be explained in consideration that specific environmental conditions prevailing within biofilms, may induce profound genetic and metabolic rewiring of the biofilm-dwelling bacteria, (*Beloin et al., 2006*) which could lead to production of biofilm-specific metabolites. These peculiar features could be compatible with the action of different anti-biofilm molecules, such as polysaccharides (*Valle et al., 2006*), biosurfactants (*Beloin et al., 2006*), quorum sensing inhibitors (*Das et al., 2009; Rasmussen et al., 2006*), or signaling molecule that modulates the gene expression of recipient bacteria (*Estrela et al., 2009*). In this work the kind of anti-biofilm molecule has been characterized. To collect information on anti-biofilm compound characteristics we explored the dependence of bioactive molecule production to growth conditions. Reported results demonstrated that the anti-biofilm compound is produced during all phases of *P. haloplanktis* TAC125 biofilm development with the best production of the molecules corresponding to biofilm detachment steps, and that the production is independent from the specific carbon and nitrogen source, and it is not temperature-dependent. Previously reported data suggested that *P. haloplanktis* TAC 125 anti-biofilm compound is not a surfactant molecule because its action on mature biofilm is not immediate but requires a prolonged time (*Papa et al., 2013*). In this paper we confirmed this hypothesis by surface coating assay, and the reported result demonstrated that *P. haloplanktis* TAC125 supernatant did not modify the surface properties of abiotic substrate. The setting up of a purification protocol allowed us to obtain a fraction (S fraction), that correspond to the active anti-biofilm compound. The proposed purification protocol should to be optimized, since its purification yield is very low. Neverthless, it is interesting to note that the molecule, identified as an aldehyde, is active at a concentration lower than 1 mg/mL. The use of *P. haloplanktis* TAC125 anti-biofilm

molecules during persistent infection sustained by *Staphylococci* in combination therapy with antibiotics could be proposed.

Experimental section

Chapter VIII

8.1 Bacteria growth

All the bacteria growth were performed by by Prof. M.L Tutino and Prof. G. Parrilli research team in Department of Chemical Science, University "Federico II".

8.1.1 Colwellia psychrerythraea 34H

Colwellia psychrerythraea 34H cells were grown aerobically at 4°C, 8°C and -2°C, in Marine Broth medium (DIFCO™ 2216). When the liquid culture reached the late exponential phase (OD_{600}=2), cells were harvested by centrifugation for 20 minutes, 7000 rpm at 4°C.

8.1.2 Psychrobacter arcticus 273-4

P. arcticus strain 273-4, isolated from permafrost soil located in Siberia. Shake flask cultivation were performed in Luria-Bertani broth [37] at 4 °C in aerobic condition. When the liquid cultures reached late exponential phase (about 90 h, OD_{600}= 4) cells were collected by centrifugation for 15 min at 7000 rpm at 4 °C. For the CPS production, *P. arcticus* was grown in LB broth added of 5% of NaCl.

8.1.3 Pseudoalteromonas haloplanktis TAC 125

P. haloplanktis TAC125 was collected in 1992 from seawater (*Medigue et al., 2005*) near the French Antarctic Station Dumont d'Urville. Bacteria were grown in Brain Heart Infusion broth (BHI, Oxoid, UK).

8.2 General and analytical method

8.2.1 LPS extraction

PCP was performed on dried cells as described by Galanos et al (*Galanos et al. 1969*). The cells were extracted three times with a mixture of aqueous phenol 90%/chloroform/light petroleum ether (2:5:8 v/v/v, ~10ml/g of dry cells). After removal of the organic solvents under vacuum, LPS was

precipitated from phenol with drops of water, then washed with cold acetone and then lyophilized. The yields obtained for each bacterium are summarized in Table 8.1.

Table 8.1: Yields obtained from each strain after PCP purification.

Bacterium	Dried cells	LPS_{PCP}
C. psychrerythraea 4°C	4.8	52mg
C. psychrerythraea 8°C	0.7	20mg
C. psychrerythraea -2°C	0.8g	10mg
P.arcticus	3.1g	96mg

8.2.2 CPS extraction and purification

Water/phenol extraction for capsular polysaccharide was performed according to Westphal et al. procedure (*Westphal et al., 1965*). Dried cells or PCP residual were suspended in aqueous phenol 90%/water (1:1 v/v, ~10ml/g of dry cells) at 68°C. After three extraction with hot water the supernatant were collected and the phenol phase diluted with water; both were dialysed against water (cut-off 3500 Da). The fractions were purified from proteic and nucleic material with enzymatic digestion with DNase, RNase and protease K (Sigma-Aldrich) and then dialysed again. The water extract was hydrolyzed with 1% aqueous CH_3COOH (10mg/mL, 100 °C, 3-5 h). The resulting suspension was then centrifuged (7000 rpm,4 °C, 30 min). The pellet was washed twice with water, and the supernatant layers were combined and lyophilized. The supernatant portion was then fractionated on a Biogel P-10 column (Biorad, 1.5 × 110 cm, flow rate 17 mL/h, fraction volume 2.5 mL), eluted with water buffered (pH 5.0) with 0.05 M pyridine, and 0.05 M acetic acid, obtaining two fractions. The polysaccharidic material was further purified on a Sephacryl S-400HR (Sigma, 1 × 110 cm, flow rate 15.6 mL/h, fraction volume 2.5 mL) eluted with 0.05 M ammonium hydrogen carbonate, providing a major fraction containing a fairly pure polysaccharide. The yields obtained for each bacterium are summarized in Table 8.2.

Table 8.2: Yields obtained from each strain after purification.

Bacterium	Water extract	CPS amount
C. psychrerythraea 4°C	300mg	6mg
C. psychrerythraea 8°C	100mg	1mg
C. psychrerythraea -2°C	120mg	1.2mg
P.arcticus	240mg	0.3mg

8.2.3 EPS purification

The supernatant cells free was dialyzed against water (cut off 3500 Da) and lyophilized. The growth broth was hydrolyzed with 5% aqueous CH_3COOH (10mg/mL, 100 °C, 3-5h). The resulting suspension was then centrifuged (7000 rpm, 4 °C, 30 min). The pellet was washed twice with water, and the supernatant layers were combined and lyophilized. The supernatant portion was then fractionated on a Sephacryl S-400 HR column (Sigma, 1.5 × 95 cm, flow 16.8 mL/h, fraction volume 2.5 mL), eluted with 0.05 M ammonium hydrogen carbonate obtaining two fractions. The saccharidic portion was further purified on a Q-Sepharose fast flow ion exchange chromatography (Sigma, 1 × 35 cm, flow rate 23 mL/h, fraction volume 2 mL) eluted with 0.1 to 1 M NaCl. The yields obtained for each bacterium are summarized in Table 8.3.

Table 8.3: Yields obtained from each strain after purification.

Bacterium	Dialyzed growth broth	EPS amount
***C. psychrerythraea* EPS**	1.9g	0.8
***C. psychrerythraea* Mannan**	1.9	0.5
***P. arcticus* Mannan**	0.7g	5mg

8.2.4 Electrophoretic analysis

PAGE was performed using the system of Laemmli (*Laemmli 1970*) with sodium deoxycholate (DOC) as detergent. The separating gel contained final concentrations of 14% acrylamide, 0.1% DOC, and 375 mM Tris/HCl (pH 8.8); the stacking gel contained 4% acrylamide, 0.1% DOC, and 125 mM tris/HCl (pH 6.8). Samples were prepared at a concentration of 0.05% in the sample buffer (2% DOC and 60 mM Tris/HCl [pH 6.8], 25% glycerol, 14.4 mM 2-mercaptoethanol, and 0.1% bromophenol blue). All concentrations are expressed as mass/vol percentage. The electrode buffer was composed of SDS (1 g/L), glycine (14.4 g/L), and Tris (3.0 g/L). Electrophoresis was performed at a constant amperage of 30 mA. Gels were fixed in an aqueous solution of 40% ethanol and 5% acetic acid. Samples were visualized by both silver staining and Alcian blue as described previously (*Tsai 1982; Al-Hakim et al., 1990*).

8.2.5 Chemical analysis

Sugar and fatty acids analysis: Monosaccharides were analyzed as acetylated methyl glycosides obtained from each LPS (0.5 mg) as follows: the methanolysis was performed in 1 M HCl/MeOH (1 mL, 80°C, 20 h). The obtained product was extracted twice with hexane and the methanol layer was dried and acetylated with Ac_2O (50 μL) and Py (50 μL) at 100°C for 30 min. The hexane layer containing fatty acids methyl esters was analysed by GC-MS to obtain fatty acids composition. The monosaccharides were identified by EI mass spectra and GC retention times by comparison with those of authentic standards. When phosphorylated sugars were present 48% HF treatment was performed before. Absolute configuration: The absolute configuration of the sugars was determined by gas-chromatography of the acetylated (*S*)-2-octyl glycosides (*Leontein et al., 1978*). The absolute configuration of amino acids residues was inferred analyzing their butyl esters derivatives (*Leontein et al., 1978*). Linkage analysis: The linkage positions of the monosaccharides were determined by GC-MS analysis of the partially methylated alditol acetates. Briefly, the deacylated LPS (1 mg) was methylated with CH_3I (300 μL) in DMSO (1.0 mL) and NaOH powder (20 h) (*Ciucanu et al., 1984*). The product was hydrolyzed with 2 M TFA (100 μL, 120°C, 2 h), reduced with $NaBD_4$ and finally acetylated with Ac_2O and Py (50 μL each, 100°C, 30 min). If uronic acids were present in the sample, acid hydrolysis was preceded by reduction of carboxymethyl with

$NaBD_4$. When phosphorylated sugars were present 48% HF treatment was performed before. All of these sugar derivatives were analysed on a Agilent Technologies gas chromatograph 6850A equipped with a mass selective detector 5973N and a Zebron ZB-5 capillary column (Phenomenex, 30 m x 0.25 mmi.d., flow rate 1 cm^3/min, He as carrier gas), by using an appropriate temperature program as reported in Table 8.4

Table 8.4: Temperature programs for sugar derivates.

Derivates	**Temperature program**
Acetylated methyl glycosides	150 °C for 3 min, 150 °C → 240 °C at 3 °C/min.
Methylation analysis	90 °C for 1 min, 90 °C → 140 °C at 25 °C/min, 140 °C → 200 °C at 5 °C/min, 200 °C → 280 °C at 10 °C/min, at 280 °C for 10 min.
Methyl esters fatty acids	140 °C for 3 min, 140 °C → 280 °C at 10 °C/min, 280 °C for 20 min.
Octyl glycosides	150 °C for 5 min, then 150 °C → 240 °C at 6 °C/min, and 240 °C for 5 min
Aminoacids acetylated butyl esters	100 °C for 2 min, 100 °C → 180 °C at 3 °C/min, then 180 °C → 300 °C at 15 °C/min.

8.2.6 Mild acid hydrolysis

The LPSs were hydrolysed with 1% or 5% aqueous CH_3COOH (10mg/mL, 100°C, ~3-6h). The obtained suspensions were then centrifuged (7000 rpm, 4°C, 30 min.). The pellet were washed twice with water and the supernatant layers were combined and lyophilized. The precipitate (lipid A) were also lyophilized. The polysaccharide portions were then fractionated on a Biogel P-10 column (Biorad, 1.5 x 130 cm, flow rate 17 mL/h, fraction volume 2.5 mL) eluted with water buffered (pH 5.0) with 0.05 M pyridine and 0.05 M sodium acetate.

8.2.7 De-O and de-N-acylation of LPSs

The LPS were first dried under vacuum over phosphoric anhydride and then incubated with hydrazine (20-30 mg/mL, 37°C, 1.5 h). To precipitate the *O*-deacylated LPSs cold acetone was added. The pellet were recovered after centrifugation (4°C, 7000 rpm, 30 min), washed 3 times with acetone and finally suspended in water and lyophilized.

The *O*-deacylated LPSs were dissolved in 4 M KOH and incubated at 120°C for 16 h. KOH was neutralized with 2 M HCl until pH 6 and the mixtures were extracted three times with $CHCl_3$. The water phases were recovered and desalted on a column Sephadex G-10 (Amersham Biosciences, 2.5 × 43 cm, 35 mLh-1, fraction volume 2.5 mL, eluent NH4HCO3 10 mM). The eluted oligosaccharide mixtures were then lyophilized.

8.2.8 Ammonium hydroxide hydrolysis of lipid A

The lipid A (~1 mg) were incubated with conc. NH_4OH (100 µL), as reported (*Silipo et al., 2002*).The sample was simply dried and analyzed by mass spectrometry.

8.3 Polyhydroxyalkanoates (PHAs) extraction

PHAs were converted to the corresponding monomer-esters by combining 1 ml of chloroform and 1 ml of 15% H_2SO_4 in methanol (v/v) with 2-5 mg of lyophilized cells in a 6 ml pyrex glass tube (*Agnew et al., 2012*). The mixture was heated at 100 °C in a heat block for 3 h followed by neutralization with 2 ml of 100 mg/ml NaHCO3 in water. The mixture was vortexed and centrifuged 1500 rpm for 10min and the aqueous layer was removed by aspiration. The organic phase (1 µL) was analyzed using a Agilent Technologies 6850A gas chromatograph equipped with a mass spectrometer 5973N (Agilent Technologies Italia, Milan, Italy) and a Zebron ZB-5 Phenomenex, 30 x 0.25 mm i.d. column (He 1ml/min) (Phenomenex, Bologna, Italy). The injection was done in splitless mode with Tinjector at 230°C. The temperature programme used was as follows: 40°C → 240°C at 20°C /min, 240°C for 10 min. The MS was operated in scanning mode

between 40 and 360 *m/z*. The identification of compounds was performed by comparison of mass spectra with standard ones. PHA contents (mg/l) were calculated by using calibration curves, which in turn were obtained by using either 3-hydroxybutyrate or 3-hydroxyhexanoate (Larodan Fine Chemicals, Sweden) supplemented with benzoic acid as internal standard. %PHAs was expressed as the ratio between produced PHAs (mg) and CDW (mg) of lyophilized cell material.

8.4 Anti-biofilm molecule purification

The *P. haloplanktis* TAC125 supernatant deriving sessile growth at 4°C was dialyzed against MilliQ water (cut off of 3500 Da). The dialyzate water was subjected to a gel-filtration chromatography on a Biogel P-2 column (Bio-Rad, molecular mass separation range 100–1800 Da, 60 × 0.75 cm, flow rate 15 mL/h, eluent water, fraction volume 1 mL). The fraction resulting as active was further fractionated by high-performance liquid chromatography on a C_{18} column (Kinetex, Phenomenex, 150 × 4.6 mm) eluting with the following program: 1% of B for 10 min (A: H2O, B: AcCN), 1 to 95% of B in 10 min, 95% of B for 10 min, flow rate 1 mL/min). For the scale up, the dialyzate water (1.5 g) was subjected to a gel-filtration chromatography on a ten Biogel P-2 column (Bio-Rad, 45 × 1.5 cm, flow rate 28.8 mL/h, eluent water, fraction volume 3 mL). The fractions resulting active were collected (50 mg) and further fractionated by C_{18} reversed phase sylica gel (Sigma, 0.5 × 38 cm, fraction volume 4 mL), eluting with AcCN:H_2O (from 10% AcCN to 100% AcCN).

8.5 Mass spectrometry

Electrospray ionization Fourier transform ion cyclotron (ESI FT-ICR) mass spectrometry was performed by Dott. Buko Lindner from research Centre in Borstel. Mass spectra were performed in negative ion mode using an APEX QE (Bruker Daltonics GmbH, Bremen, Germany),equipped with a 7 Tesla actively shielded magnet. The samples were dissolved in a 50:50:0.001 (v/v/v) mixture of 2-propanol, water and triethylamine at a concentration of ~10 ng/μL, sprayed at a flow rate of 2 μL/min, and analyzed as described previously (*Pieretti et al., 2012*).

The MS and MS/MS spectra of lipid A from *C.psychrerythraea* were also measured in the positive ions mode on a Q Exactive Hybrid Quadrupol Orbitrap (Thermo Scientific). The MS/MS lipid species were analyzed in the positive ion mode; precursor ions were isolated in the ICR-cell and then fragmented by infrared multiphoton dissociation (IRMPD).

Negative ions reflectron MALDI-TOF mass spectra were acquired on a Voyager DE-PRO instrument (Applied Biosystems). Mass calibration was obtained with a hyaluronan oligosaccharides mixture. A solution of 2,5-dihydroxybenzoic acid acid in 20% CH_3CN in water at concentration of 20 mg/mLwas used as the MALDI matrix. Spectra were calibrated and processed under computer control by using the Applied Biosystems Data Explorer software.

8.6 Nuclear Magnetic Resonance (NMR)

^{1}H and ^{13}C NMR spectra were recorded using a Bruker Avance 600 MHz spectrometer equipped with a cryoprobe. All two-dimensional homo- and heteronuclear experiments (double quantum-filtered correlation spectroscopy, DQF-COSY; total correlation spectroscopy TOCSY; rotating-frame nuclear Overhauser enhancement spectroscopy, ROESY; nuclear Overhauser effect spectroscopy, NOESY; distortionless enhancement by polarization transfer−heteronuclear single quantum coherence, $^{1}H–^{13}C$ DEPTHSQC; heteronuclear multiple bond correlation, $^{1}H–^{13}C$ HMBC; and 2D F2-coupled HSQC) were performed using standard pulse sequences available in the Bruker software. The mixing time for TOCSY and ROESY experiments was 100 ms. ^{31}P and ^{1}H-^{31}P spectra were recorded at 298 K using a Bruker Ascend 400 MHz spectrometer. To identify genuine NOEs effects of CPS and EPS from *Colwellia* at 4°C, NOESY experiments were performed at mixing times of 70, 100, 150, and 200 ms, in order. Chemical shifts were measured at 298 K for CPS and 310 K fro EPS, in D_2O. TOCSY (mixing time 100 ms) and NOESY (mixing time 200 ms) experiments were also performed in H_2O/D_2O 9:1. Diffusion-edited proton NMR spectrum was recorded at 310 K by using a Bruker 500 MHz equipped with cryoprobe. ^{1}H, ^{1}H NOESY keeler filter experiments were performed at mixing times from 30 to 300 ms in order to identify genuine NOEs effects. Spectra were recorded in D_2O at 303 K, by using a Bruker Avance 700 MHz spectrometer equipped with a cryo-probe. BSCT-HMBC (band-selective constant time- HMBC) experiments were performed by using a Bruker Avance 700 MHz spectrometer equipped with a cryo-probe. The temperature was calibrated to 310 K with a neat deuterated methanol sample (5) prior to all the experiments. TOCSY (mixing time 100 ms) and NOESY (mixing time 200 ms) experiments were also performed in H_2O/D_2O 9:1.

8.7 Ice Recrystallization Inhibition Assay (IRI)

Two different assays were performed to test the ice recrystallization inhibition activity.

8.7.1 IRI assay for CPS Colwellia psychrerythraea 4°C

Ice recrystallization was measured using an Optical Recrystallometer (Otago Osmometers, New Zealand) as reported elsewhere.44,45 The solutions were prepared in ultrapure Milli-Q water with 9‰ NaCl. We measured the CPS sample (10 mg/mL = 6.6 μM) and positive and negative controls. As a positive control we used a recombinant AFP from the sea-ice diatom Fragilariopsis cylindrus. The protein was provided by M. Bayer-Giraldi and produced recombinantly in E. coli as described previously.44 As a negative control we used chondroitin, a CPS produced by an engineered E. coli K4.46 All particle solutions (CPS, AFP, and chondroitin) were measured at the same concentration of 6.6 μM. Furthermore, we measured a particle-free solution of Milli-Q water with 9 ‰ NaCl. We injected 200 μL solution in a cold, thin glass sample tube and shock-froze the sample at −80 °C. Ice was annealed in the Optical Recrystallometer for 1.5 h at −4 °C. The device was cooled by a refrigerated circulating fluid and connected to a dry air (nitrogen gas) source to avoid condensation on the sample tube surface. The intensity of the light transmitted through the sample was recorded over time, where its increase is a measure for recrystallization. The increase was reported as It − I0, where It is the intensity at a moment t and I0 is the initial intensity. The procedure was repeated three times for each sample.

8.7.2 Ice Recrystallization Inhibition assay

Ice recrystallization inhibition was measured using a modified splay assay (*Congdon et al., 2013*). A 10 μL sample of hydrogel dissolved in PBS buffer (pH 7.4) was dropped 1.40 m onto a chilled glass coverslip sat on a piece of polished aluminium placed on dry ice. Upon hitting the chilled glass coverslip, a wafer with diameter of approximately 10 mm and thickness 10 μm was formed instantaneously. The glass coverslip was transferred onto the Linkam cryostage and held at −6 °C under N_2 for 30 minutes. Photographs were obtained using an Olympus CX 41 microscope with a UIS-2 20×/0.45/∞/0–2/FN22 lens and crossed polarizers (Olympus Ltd, Southend on sea, UK),

equipped with a Canon DSLR 500D digital camera. Images were taken of the initial wafer (to ensure that a polycrystalline sample had been obtained) and after 30 minutes. Image processing was conducted using Image J (http://imagej.net/), which is freely available. In brief, ten of the largest ice crystals in the field of view were measured and the single largest length in any axis recorded. This was repeated for at least three wafers and the average (mean) value was calculated to find the largest grain dimension along any axis. The average of this value from three individual wafers was calculated to give the mean largest grain size (MLGS). This average value was then compared to that of a PBS buffer negative control providing a way of quantifying the amount of IRI activity.

Bibliography

Al-Hakim A. et al., Isolation and recovery of acidic oligosaccharides from polyacrylamide gels by semi-dry electrotransfer *Electrophoresis* **1990**, 11, 23−28

Agnew D.E., Stevermer, A.K., Youngquist, J.T., Pfleger, B.F., Engineering *Escherichia coli* for production of C12–C14 polyhydroxyalkanoate from glucose. Metabolic Engineering. 2012, 14, 705-713.

Agrawal P.K. et al., Structural analysis of lipid A and Re-lipopolysaccharides by NMR spectroscopic methods. *Adv. Biophys. Chem.* **1994**, 4, 179–236.

Alvarez H. M et al., Triacylglycelors in prokaryotic microorganims. *Appl. Microbiol. Biothecnol*.**2002** 60, 367-376

Anderson A.J et al., Occurrence, metabolism, metabolic role, and industrial use of bacterial polyhydroxyalkanoates. *Microbiol. Rev.* **1990** 54, 450-472.

Ayala-del-Río H.L, et al., The Genome Sequence of *Psychrobacter arcticus*273-4, a Psychroactive Siberian Permafrost Bacterium, Reveals Mechanisms for Adaptation to Low-Temperature Growth. *Appl. Environ. Microbiol*. **2010**. 76 , 7 2304-2312

Bakermans C. and Nealson, K. H. Relationship of critical temperature to macromolecular synthesis and growth yield in *Psychrobacter cryopegella*. *J. Bacteriol.* **2004** 186, 2340–2345.

Bayer-Giraldi M. et al., Characterization of an antifreeze protein from the polar diatom *Fragilariopsis cylindrus* and its relevance in sea ice *Cryobiology* **2011**, *63*, 210-219

Beloin C. et al., The transcriptional antiterminator RfaH represses biofilm formation in *Escherichia coli. Journal of Bacteriology* **2006**188: 1316–1331.

Ben N. R. Antifreeze glycoproteins preventing the growth of ice *Chem biochem* **2001**, *2*, 161-166

Beveridge T.J and Graham L.L. **Surface layers of** bacteria**.** *Microbiol. Mol. Biol. Rev*. **1991**, 55, 4684-705

Beynon L.M. et al.,The structure of the lipopolysaccharide O-antigen of *Yersinia ruckeri* serotype O1. *Carbohyd. Res*. **1994**, *256*,303–317

Bianciotto V. et al., Extracellular polysaccharides are involved in the attachment of Azospirillum brasilense and Rhizobium leguminosarum to arbuscular mycorrhizal structures.. *Eur J Histochem* **2001** 45: 39–49

Bock K. et al., Carbon-13 nuclear magnetic resonance spectroscopy of monosaccharides *Carbohydr. Chem. Biochem*. **1983**, *41*, 27-66.

Bowman J.P . The family *Colwelliaceae*. In The prokaryotes-*Gammaproteobacteria.* **2014** Rosenberg et al., (Ed.s) Chapter 10.

Bowman J.P Bioactive compound synthetic capacity and ecological significance of marine bacterial genus Pseudoalteromonas *Marine drugs* **2007** *5*(4), 220-241

Bung J.K et al., Antifreeze Peptides and Glycopeptides, and Their Derivatives: Potential Uses in Biotechnology, *Marine drugs* **2013**, 11(6), 2013-2041.

Carillo S, et al., A unique capsular polysaccharide structure from the psychrophilic marine bacterium *Colwellia psychrerythraea* 34H that mimics antifreeze (Glyco)proteins. *JACS* **2015** 137: 179-189.

Carillo S. et al., Structural characterization of the core oligosaccharide isolated from the lipopolysaccharide of the psychrophilic bacterium *Colwellia psychrerythraea* strain 34H. *Eur J Org Chem* **2013** 18: 3771-3779.

Carillo S. et al., Structural investigation and biological activity of the lipooligosaccharide from the psychrophilic bacterium *Pseudoalteromonas haloplanktis* TAB 23. *Chemistry* **2011** 17: 7053-7060.

Carlson R.W. et al., Structures of the oligosaccharides obtained from the core regions of the lipopolysaccharides of *Bradyhizobium japonicum*61A101c and its symbiotically defective lipopolysaccharide mutant, JS314. *Carbohyd. Res*. **1992**, 231, 205–219.

Casanueva A. et al., Molecular adaptations to psychrophily: the impact of 'omic' technologies. *Trends Microbiol* **2010** 18: 374-381.

Casillo A. et al., Structural investigation of the oligosaccharide portion isolated from the lipooligosaccharide of the permafrost psychrophile *Psychrobacter arcticus* 273-4. *Mar Drugs* **2015**13: 4539-4555.

CASPER. Available online: http://www.casper.organ.su.se/casper/ (accessed on 31 January 2011)

Cavicchioli R Cold-adapted archaea *Nat Rev Microbiol*. **2006** 4: 331-343.

Chattopadhyay K. et al., Psychrophilic Bacteria: Biodiversity, Molecular Basis of Cold Adaptation and Biotechnological Implications *Current Biotechnology* **2014**, 3, 100-116.

Chattopadhyay K. Mechanism of bacterial adaptation to low temperature *J. Biosci.* **2006** 31(1) 157-165

Chin J.P. et al., Solutes determine the temperature windows for microbial survival and growth. *PNAS* **2010** 107, 7835-7840.

Chintalapati, S. et al., Role of membrane lipid fatty acids in cold adaptation. *Cell. Mol. Biol.* **2004**, *50,* 631–642.

Christensen G.D. et al., Adherence of coagulase-negative staphylococci to plastic tissue culture plates: a quantitative model for the adherence of staphylococci to medical devices. *J Clin Microbiol*. **1985** 22,6, 996–1006

Ciucanu I. et al., A simple and rapid method for the permethylation of carbohydrates *Carbohydrate Research* **1984**, 131, 2 209–217.

Collins R.E. et al., Persistence of bacterial and archaeal communities in sea ice through an Arctic winter. *Environ Microbiol* **2010** 12:1828–1841

Congdon T.C. et al., Antifreeze (Glyco)protein mimetic behavior of poly(vinyl alcohol): detailed structure ice recrystallization inhibition activity study. *Biomacromolecules* **2013** 14(5): 1578-1586

Corbett D. Capsular polysaccharides in Escherichia coli. *Adv Appl Microbiol* **2008** 65:1–26

Corbett D. et al., Bacterial polysaccharide capsules. In Prokaryotic cell wall compound, Chapter 3. 2010.

Corchero J.L. et al., Unconventional microbial systems for the cost-efficient production of high-quality protein therapeutics. *Biotechnol. Adv*., **2013**, 31:140–153.

Corsaro M.M. et al., Structure determination of an exopolysaccharide from an alkaliphilic bacterium closely related to *Bacillus* spp. *Eur. J. Biochem.* 1999, *264*, 554–561.

Corsaro M.M et al., Lipid A structure of *Pseudoalteromonas haloplanktis* TAC 125: use of electrospray ionization tandem mass spectrometry for the determination of fatty acid distribution. *Journal of Mass Spectrometry* **2002** 37, 5 481-488

Corsaro M.M. et al., Highly phosphorylated core oligosaccaride structures from cold-adapted *Psychromonas arctica. Chemistry* **2008** 14: 9368-9376.

Corsaro M.M. et al., Influence of growth temperature on lipid and phosphate contents of surface polysaccharides from the Antarctic bacterium *Pseudoalteromonas haloplanktis* TAC 125. *J Bacteriol* **2004** 186: 29-34.

Corsaro M.M. et al., Structural determination of the O-Chain polysaccharide from the lipopolysaccharide of the haloalkaliphilic *Halomonas pantelleriensis* bacterium. *Eur J Org Chem* **2006** 7:1801-1808

Corsaro M.M. et al., Structural investigation on the lipooligosaccharide fraction of psychrophilic *Pseudoalteromonas haloplanktis* TAC 125 bacterium. *Eur. J. Biochem*. **2001**, *268*, 5092-5097.

Costerton JW. et al., Microbial biofilms. *Annu Rev Microbiol* **1995** 49: 711–745

Daley M.E. et al., The role of side chain conformational flexibility in surface recognition by Tenebrio molitor antifreeze protein *Protein Science* **2003**, *12*, 1323-1331.

Das P. et al., Antiadhesive action of a marine microbial surfactant. *Colloids and Surfaces B: Biointerfaces* **2009** 71: 183–186.

De Maayer et al., Some like it cold: understanding the survival strategies of psychophiles. *EMBO reports* **2014** 15, 5 508-517.

Debbab A. et al., Bioactive Compounds from Marine Bacteria and Fungi. *Microbial technology* **2010** 3,5, 544–563

Decho, A.W. and Herndl, G.J. Microbial activities and the transformation of organic matter within mucilaginous material. *Sci. Total Environ.* **1995**, *165*, 33–42

Decho, A.W. Microbial exopolymer secretions in ocean environments: their role(s) in food webs and marine processes. In *Oceanography and Marine Biology: an Annual Review*; Barnes, M., Ed.; Aberdeen Univ Press: Aberdeen, UK, **1990**; pp. 73–153.

Deller R.C. et al., Ice recrystallisation inhibition by polyols: comparison of molecular and macromolecular inhibitors and role of hydrophobic units. *Biomater Sci* **2013** 1: 478-485.

Demchick P. and Koch A.L The permeability of the wall fabric of Escherichia coli and Bacillus subtilis. *J. Bacteriol.* **1996** , 3 768-773.

Deming J.W. et al., Isolation of an obligately barophilic bacterium and description of a new genus *Colwellia* gen. nov. *Syst Appl Microbiol* **1988** 10:152–160

Deming J.W. Extremophiles: cold environments. *Encyclopedia of Microbiology,* eds. Schaechter M, (Elsevier), pp. 147-158 **2009**.

Domon B. et al., A systematic nomenclature for carbohydrate fragmentations in FABMS/MS of glycoconjugates *Glycoconj. J.* **1988** 5: 397-409.

Dragosists M. et al., Influence of growth temperature on the production of antibody Fab fragments in different microbes: a host comparative analysis. *Biotechnol. Prog*., **2011**, 27:38–46.

Driessen, J.M. et al., Membrane composition and ion-permeability in extremophiles. *Fems Microbiol. Rev.* **1996**, *18*, 139-148.

Errington J.R. et al., Relationship between structural order and the anomalies of liquid water. *Nature* **2001** 409: 318-321.

Estrela A.B. et al., Novel approaches to control biofilm infections. *Current Medicinal Chemistry* **2009** 16: 1512–1530.

Ewert M. et al., Sea Ice microorganisms: environmental constraints and extracellular response. *Biology* **2013** 2: 603-628.

Feller G. and Gerday C. Psychrophilic enzymes: hot topics in cold adaptation. *Nature Reviews Microbiology* **2003** 1,200-208.

Findeisen M. A ^{1}H NMR thermometer suitable for cryoprobes. *Magn reson chem*. **2007**, 45: 175-178

Forsberg, L.S. et al., The Structures of the Lipopolysaccharides from *Rhizobium etli* Strains CE358 and CE359. *J. Biol. Chem.* **1998**, 273, 2747–2757.

Francolini I. and Donelli G. Prevention and control of biofilm-based medical-device-related infections *FEMS immunology and medical microbiology* **2010** 59, 3 227 - 238.

Freitas F. et al., Advances in bacterial exopolysaccharides: from production to biotechnological applications. *Trends in microbiology* **2011**, 29, 8, 388–398.

Fuller B.J Cryoprotectants: the essential antifreezes to protect life in the frozen state. *Cryoletters* **2004** 25,6, 375-388.

Fux C.A, et al., Bacterial biofilms: a diagnostic and therapeutic challenge. *Expert Rev Anti Infect Ther* **2003** 1: 667–683

Galanos C. et al., A new method for the extraction of R lipopolysaccharides. *Eur. J. Biochem.* **1969**, 9, 245-249.

Gao H et al., Global transcriptome analysis of the cold shock response of Shewanella oneidensis Mr-1 and mutational analysis of its classic cold shock proteins . *J bacterial* **2006** 188: 4560-4569

Gasser B. et al., Protein folding and conformational stress in microbial cells producing recombinant proteins: a host comparative overview. *Microb. Cell Fact.*, **2008**, 7:11.

Gilichinsky D.A. et al., Microbial Populations in Antarctic Permafrost: Biodiversity, State, Age, and Implication for Astrobiology *Astrobiology* **2007** 7, 275-311.

Giuliani M. et al., Process optimization for recombinant protein production in the psychrophilic bacterium *Pseudoalteromonas haloplanktis***.** *Process. Biochem.* **2011**, 46:953–959.

Goh Y.S et al. Polyhydroxyalkanoate production by antarctic soil bacteria isolated from Casey Station and Signy Island *Microbiological Research* **2012**, 167, 211-219.

Graether S.P. et al., β-Helix structure and ice-binding properties of a hyperactive antifreeze protein from an insect. *Nature*, **2000** 406, 325.

Gunawardena, S. et al., Structure of a muramic acid containing capsular polysaccharide from the pathogenic strain of *Vibrio vulnificus* ATCC 27562. *Carbohyd. Res.* **1998**, *309*, 65–76.

Hakomori S., A rapid permethylation of glycolipid, and polysaccharide catalyzed by methylsulfinyl carbanion in dimethyl sulfoxide. *J. Biochem.* **1964**, 55, 205-208.

Hanniffy, O.M. et al., Structure of an acidic O-specific polysaccharide of *Pseudoalteromonas haloplanktis* type strain ATCC 14393 containing 2-acetamido-2-deoxy-D- and -L-galacturonic acids and 3-(N-acetyl-D-alanyl) amino-3,6-dideoxy-D-glucose. *Carbohyd. Res*. **1999**, *321* , 132–138.

Hazer B, et al., Increased diversification of polyhydroxyalkanoates by modification reactions for industrial and medical applications. *Appl Microbiol Biotechnol* **2007**;74:1–12.

Helmke E. and Weyland H. Psychrophilic versus psychrotolerant bacteria: occurrence and significance in polar and temperate marine habitats. *Cellular and Molecular Biology* **2004** 50 (5), 553-561

Henrichsen J, Six newly recognized types of Streptococcus pneumoniae. *J Clin Microbiol* **1995**

Ho Y.H, et al., Biodegradation of a medium-chain-length polyhydroxyalkanoate in tropical river water. *Appl Biochem Biotechnol* **2002**; 10, 337-347.

Holmstrom et al., Antifouling activities expressed by marine surface associated *Pseudoalteromonas* species *FEMS Microbiology Ecology* **2002** 41, 1 47-58

Holst O., Deacylation of lipopolysaccharides and isolation of oligosaccharide phosphates., *Methods Mol. Biol.*, **2000** 145, 345 –353.

Huston A.L. et al., Purification, characterization, and sequencing of an extracellular cold-active aminopeptidase produced by marine psychrophile *Colwellia psychrerythraea* strain 34H. *Appl Environ Microbiol* **2004** 70: 3321-3328

Jansson, P.-E. et al., Computer-assisted structural analysis of polysaccharides with an extended version of CASPER using 1H- and13C-NMR data. *Carbohydr. Res.* **1989**, 188, 169–171.

Jay Z. et al., Antifreeze proteins: an unusual receptor–ligand interaction *Trends Biochem. Sci*. **2002**, *27*, 101-110.

Junge K. et al., Bacterial activity at-2 to-20 degrees C in Arctic wintertime sea ice. *Appl. Environ. Microbiol.* **2004** 70:550–557.

Kamio Y. and Nikaido H. Outer membrane of Salmonella typhimurium: accessibility of phospholipid head groups to phospholipase C and cyanogen bromide activated dextran in the external medium *Biochemistry* **1976 ,** *15*(12), 2561–2570.

Kaplan J.B. Biofilm Dispersal: Mechanisms, Clinical Implications, and Potential Therapeutic Uses. *Journal of Dental Research* **2010**, 89, 3 205-218.

Kenne, L. et al., In *The Polysaccharides*. Aspinall, G. O., Ed.; Vol. 2; Academic Press: New York, 1983; Volume 2, pp 287-363.

Kenyon J.J. et al., O-chain yersinia tubercolosis *Glycobiology* **2011** 21, 9,1131 –1139

Kim S.J. et al., Cryoprotective properties of exopolysaccharide (P-21653) produced by the Antarctic bacterium, Pseudoalteromonas arctica KOPRI 21653. *J. Microbiol*. **2007** 45:510 – 514.

Kiran G.S et al., Optimization and characterization of a new lipopeptide biosurfactant produced by marine *Brevibacterium aureum* MSA13 in solid state culture **2010** 101, 7, 2389–2396.

Klein G.L. et al., The anti-biofilm activity secreted by a marine *Pseudoalteromonas* strain. *Biofouling* **2011** 27: 931–940.

Knight C.A et al., Inhibition of recrystallization of ice by insect thermal hysteresis proteins: a possible cryoprotective role *Cryobiology* **1986**, *23*, 256-262

Knirel YA, et al., Somatic antigens of *Pseudomonas aeruginosa* The structure of the O-specific polysaccharide chain of the lipopolysaccharide from *P. aeruginosa* O13. *Eur. J. Biochem* **1987** 163: 627-637.

Knirel, Y.A. et al., Structure of the *O*-specific polysaccharide of *Proteus penneri* 62 containing 2-ace tamido-3-*O*-[(*S*)-1-carboxye thyl]-2-deoxy-D-glucose (*N*-acetylisomuramic acid). *Carbohyd. Res.* **1992**, 235, C19–C23.

Komandrova N.A et al., Structure of an acidic O-specific polysaccharide of the marine bacterium *Pseudoalteromonas agarivorans* KMM 232 (R-form) *Biochemistry (Moscow),* **2010**, *75*, 623-628.

Kondakov A. et al., Application of electrospray ionization with Fourier transform ion cyclotron resonance mass spectrometry for structural screening of core oligosaccharides from lipopolysaccharides of the bacteria *Rapid Communication in Mass Spectrometry* **2005** 19,16 2343–2349

Kondakova, A.N. et al., Structure of the O-polysaccharide chain of the lipopolysaccharide of *Psychrobacter muricolla* 2pST isolated from overcooled water brines within permafrost. *Carbohyd. Res.* **2012b**, *349*, 78–81.

Kondakova, A.N. et al., Structure of the O-Specific Polysaccharide from the Lipopolysaccharide of *Psychrobacter cryohalolentis* $K5^T$ Containing a 2,3,4-Triacetamido-2,3,4-trideoxy-L-arabinose Moiety. *J. Nat. Prod*. **2012a**, *75*, 2236−2240

Krembs C. et al., Exopolymer alteration of physical properties of sea ice and implications for ice habitability and biogeochemistry in a warmer Arctic. *Proc Natl Acad Sci USA* **2011** 108: 3653-3658.

Krembs C. et al., High concentrations of exopolymeric substances in Arctic winter sea ice: implications for the polar ocean carbon cycle and cryoprotection of diatoms. *Deep Res Part I Oceanogr Res Pap* **2002** 49: 2163-2181.

Kristjansson J.K et al., Ecology and habitats of extremophiles *World Journal of Microbiology and Biotechnology* **1995**, 11, 1, 17-25.

Kumar A.S et al., Evaluation of Biosurfactant/Bioemulsifier Production by a Marine Bacterium *Bulletin of Environmental Contamination and Toxicology* **2007**, 79,6, 217-221.

Kumar G.S, et al., Low-temperature-induced changes in composition and fluidity of lipopolysaccharides in the Antarctic psychrotrophic bacterium *Pseudomonas syringae J bacteriol* **2002,** 184(23) 6746-6749

Laemmli U.K. Most commonly used discontinuous buffer system for SDS electrophoresis. Nature **1970**, 227, 680−685.

Laucks M.L et al., Comparison of Psychro-active Arctic Marine Bacteria and Common Mesophillic Bacteria Using Surface-Enhanced Raman Spectroscopy *Applied Spectroscopy* **2005** 59, 10, 1222-1228

Lee G.C et al., Virulence Studies, in Mice, of Transposon-Induced Mutants of Staphylococcus aureus Differing in Capsule Size *J Infect Dis.* **1987** 156(5):741-750.

Lemoigne M. Produits de deshydration et de polymerisation de lacide β-oxybutyrique. *Bull. Soc. Chim. Biol*. **1926** 8, 770-782

Lenz R.W, et al., Bacterial polyesters: biosynthesis, biodegradable plastics and biotechnology. *Biomacromolecules* **2005**;6:1–8.

Leontein K. et al., Determination of the absolute configuration of sugars by Gas-Liquid Chromatography of their acetylated 2-octyl glycosides. *Carbohydrate Research.* **1978**, 62, 359-362.

Lequette L. et al., Using enzymes to remove biofilms of bacterial isolates sampled in the food-industry *Biofouling* **2010**, 26, 4 421-431.

Lim S.P, et al., Degradation of medium-chain-length polyhydroxyalkanoates in tropical forest and mangrove soils. *Appl Biochem Biotechnol* **2005**;126:23–33.

Lipkind, G.M. et al., A computer-assisted structural analysis of regular polysaccharides on the basis of 13C-NMR data. *Carbohyd. Res.* **1988**, 175, 59–75.

Logan, B.E.; Hunt, J.R. Advantages to microbes of growth in permeable aggregates in marine systems. *Limnol. Oceanogr.* **1987**, *32*, 1034–1048

Lüderitz O., et al., Structural relationship of *Salmonella* O and R antigens., *J. Ann. NY Acad. Sci.*, **1966** 133, 347-349.

M. Carty S., et al., Effect of cold shock on lipid A biosynthesis in E.coli. J*ournal of biological chemistry* **1999** 274, 14, 9677-9685.

Macura S. et al.,An improved method for the determination of cross-relaxation rates from NOE data *J. Magnetic Reson*. **1986**, 70, 493

Mallajosyula S.S. et al., Perturbation of long-range water dynamics as the mechanism for the antifreeze activity of antifreeze glycoprotein. *J Phys Chem* B **2014** 118(40):11696-706.

Mancuso Nichols C. et al., Bacterial Exopolysaccharides from Extreme Marine Environments with Special Consideration of the Southern Ocean, Sea Ice, and Deep-Sea Hydrothermal Vents: A Review. *Mar. Biotechnol.* **2005a,** *7*, 253-271.

Mancuso Nichols C. et al., Chemical Characterization of Exopolysaccharides from Antarctic Marine Bacteria *Microbial ecology* **2005b**, *49*, 578-589.

Margesin R. et al., Cold-loving microbes, plants, and animals fundamental and applied aspects. *Naturwissenschaften* **2007,** 94,2, 77-99.

Martin D. et al., Solute accumulation in the deep-sea bacterium *Photobacterium profundum. Extremophiles* **2002**, 6, 6, 507-514.

Marx JG, et al., Production of cryoprotectant extracellular polysaccharide substances (EPS) by the marine psychrophilic bacterium *Colwellia psychrerythraea* strain 34H under extreme conditions. *Can J Microbiol* **2009** 55: 63-72.

Masoud, H. et al., Structural elucidation of the backbone oligosaccharide from the lipopolysaccharide of *Moraxella catarrhalis* serotype A. *Can. J. Chem*. **1994**, *72*, 1466–1477.

Medigue C. et al., Coping with cold: the genome of the versatile marine Antarctica bacterium Pseudoalteromonas haloplanktis TAC125. *Genome Res*., **2005**, 15:1325-1335.

Methé, B. A. et al., .The psychrophilic lifestyle as revealed by the genome sequence of Colwellia psychrerythraea 34H through genomic and proteomic analyses *Proc. Natl. Acad. Sci*. U.S.A**.** **2005**, 102, 10913−10918

Mitchell D.E. et al., Rational, yet simple, design and synthesis of an antifreeze-protein inspired polymer for cellular cryopreservation. *Chem Commun* **2015** 51: 12977-12980.

Mooibroek H, et al., Assessment of technological options and economical feasibility for cyanophycin biopolymer and high-value amino acid production*. Appl Microbiol Biotechnol* **2007** 77:257–267

Morita R.Y Psychrophilic bacteria. *Bacteriol Rev.* **1975** 39(2): 144–167.

Mueller S. Permafrost or permanently frozen ground and related engineering problems. **1973** United States Army, Washington, DC.

Muldoon, J. et al., Structure of an acidic polysaccharide from the marine bacterium *Pseudoalteromonas flavipulchra* NCIMB 2033T. *Carbohyd. Res.* **2003**, 338, 459-462

Navarro–Gonzales R. et al., Mars-Like Soils in the Atacama Desert, Chile, and the Dry Limit of Microbial Life *Science* **2003** . 302, Issue 5647, 1018-1021

Nguyen C.N. et al., Grid inhomogeneous solvation theory: Hydration structure and thermodynamics of the miniature receptor cucurbituril. *J Chem Phys* **2012** 137: 044101

Nicolaus B. et al., Exopolysaccharides from extremophiles: from fundamentals to biotechnology. *Environmental Technology*. **2010**, 31, 10, 1145–1158

Otto M. Staphylococcal Biofilms. In Bacteria biofilm. *Current Topics in Microbiology and Immunology* **2008** 322, 207-228

Palusiak A. et al., Immunochemical properties of *Proteus penneri* lipopolysaccharides—one of the major Proteus sp. virulence factors *Carbohydr. Res*. **2013**, *380*, 16-22.

Papa R. et al., Anti-biofilm activity of the Antarctic marine bacterium*Pseudoalteromonas haloplanktis* TAC125 *Research in Microbiology* **2013** 164: 450–456.

Pertaya N. et al., Direct Visualization of Spruce Budworm Antifreeze Protein Interacting with Ice Crystals: Basal Plane Affinity Confers Hyperactivity *Biophys. J*. **2008**, *95*, 333-341.

Philips N. et al., The lipid A from Vibrio fischeri lipopolysaccharide. A unique structure bearing a phosphoglycerol mojety. *Journal of Biological Chemistry*. **2011** 286,24, 21203-21219.

Pieretti, G. et al., Characterization of the Core Oligosaccharide and the O-Antigen Biological Repeating Unit from *Halomonas stevensii* Lipopolysaccharide: The First Case of O-Antigen Linked to the Inner Core. *Chem. Eur. J.* **2012**, *18,* 3729-3735

Pikuta E.V. et al., Microbial Extremophiles at the Limits of Life *Critical Reviews in Microbiology* **2007** 33, 3 183-209.

Plotz B. M. et al., Characterization of a novel lipid A containing D-galacturonic acid that replaces phosphate residues. The structure of the lipid a of the lipopolysaccharide from the hyperthermophilic bacterium Aquifex pyrophilus. Journal of Biological Chemistry, **2000**, 275, 15 11222 -11228.

Poli A. et al., Bacterial exopolysaccharides from extreme marine habitats: production, characterization and biological activitie. *Marine drugs* **2010**, 8, 1779-1802.

Pommerville J.C., Alcamo's fundamentals of microbiology 9th Edition, Chapter 4. (Eds.: Jones & Bartlett Publishers), Burlington, MA, **2010**.

Ponder M.A. et al., Metabolic activity of Siberian permafrost isolates, *Psychrobacter arcticus* and *Exiguobacterium sibiricum*, at low water activities. *Extremophiles* **2008**, 12,4, 481-490

Qin G., et al., Structural characterization and ecological roles of a novel exopolysaccharide from the deep-sea psychrotolerant bacterium Pseudoalteromonas sp. SM9913, *Microbiology* **2007**, 153, 1566–1572.

Que N.L.S., et al., Purification and mass spectrometry of six lipid A species from the bacterial endosymbiont *Rhizobium etli*. Demonstration of a conserved distal unit and a variable proximal portion. *J. Biol. Chem*., **2000** 275, 28006-28016.

Quin Z. et al., *Pseudomonas aeruginosa* extracellular products inhibit staphylococcal growth, and disrupt established biofilms produced by *Staphylococcus epidermidis Microbiology* **2009** 155, 2148-2156.

Raetz C.R. et al., Lipopolysaccharide endotoxins. *Annu. Rev. Biochem.*, **2002** 71: 635–700

Ramos M.L.D. et al., NMR Study of uronic acids and their complexation with molybdenum (VI) and tungsten (VI) oxoions *Carbohydr. Res*. **1996**, 286, 1-15.

Rasmussen T.B. et al., Quorum-sensing inhibitors as anti-pathogenic drugs. *International Journal of Medical Microbiology* **2006** 296: 149–161.

Raven P.H., Johnson G.B., Biology 9th Edition, Chapter 34 (Ed.: McGraw Hill), **2011**.

Raymond J.A. et al., An ice-binding protein from an Antarctic sea ice bacterium *FEMS Microbiol.Ecol.* **2007**, *61*, 214-221.

Rendueles O. Antibiofilm polysaccharides *Environmental microbiology* **2013** 5, 2, 334–346.

Rivkina E. M. et al., Metabolic activity of permafrost bacteria below the freezing point. *Appl. Environ. Microbiol* **2000**. 66:3230–3233.

Rothshild L.J and Mancinelli R. Life in extreme environments *Nature* **2001** 409, 1092-1101

Rothwell, J. *Microbiology of Frozen Dairy Products*; Elsevier Applied Science Publishers: London, UK, 1985.

Scotter A.J et al., The basis for hyperactivity of antifreeze proteins *Cryobiology*, **2006**, *53*, 229-239.

Siddiqui K.S. et al., Psychrophiles *Annu. Rev. Earth Planet. Sci.* **2013** 41, 87-115.

Sidorczyk Z. et al., Structure and Epitope Specificity of the O-specific Polysaccharide of *Proteus penneri* Strain 12 (ATCC 33519) Containing the Amide of D-Galacturonic Acid with L-threonine *Eur. J. Biochem*. **1995**, *230*, 713-721

Silhavy T.J. et al., The Bacterial Cell Envelope. *Cold Spring Harb Perspect Biol* **2010**, 2:a000414.

Silipo A. et al., Full structural characterization of the lipid A components from the Agrobacterium tumefaciens strain C58 lipopolysaccharide fraction. *Glycobiology* **2004** 14, 9 805±815.

Silipo A. et al., Full structural characterization of the lipid A components from the *Agrobacterium tumefaciens* strain C58 lipopolysaccharide fraction., *Glycobiology* **2004** 14, 805-815.

Silipo A. et al., The O-chain structure from the LPS of marine halophilic bacterium Pseudoalteromonas carrageenovora -type strain IAM 12662 *Carb. Research* **2005** 340, 2693–2697

Singh O.V. In Extremophiles: sustainable resources and biotechnological implications Singh Ed. Wiley-Blackwell publication

Soina V.R. et al., The Structure of Resting Bacterial Populations in Soil and Subsoil Permafrost. *Astrobiology* **2004** 4, 345-358

Spina E. et al., New fragmentation mechanisms in matrix-assisted laser desorption/ionization time-of-flight/time-of-flight tandem mass spectrometry of carbohydrates *Rapid Comm. Mass Spec.* **2004** 18: 392-398.

Steinbuchel A. Perspective for biotechnological production and utilisation of biopolymers: metabolic engineering of polyhydroxyalkanoates biosynthesis pathways as a successful example. *Macromol. Biosci*. **2001** 1, 1-24

Sun T. et al., An antifreeze protein folds with an interior network of more than 400 semi-clathrate waters. *Science* **2014** 343(6172): 795-798.

Sutherland I.W The biofilm matrix – an immobilized but dynamic microbial environment. *Trends in microbiology* **2001,** 9,1 222–227

Sutherland I.W. The exopolysaccharides of Klebsiella serotype 2 strains as substrates for phage-induced polysaccharide depolymerases *Journal of General Microbiology* **1972**, 70, 331-338

Sweet C.R. et al., Endotoxin Structures in the Psychrophiles *Psychromonas marina* and*Psychrobacter cryohalolentis* Contain Distinctive Acyl Features *Marine drugs* **2014**, 12, 4126-4147

Tachibana Y. et al., Antifreeze glycoproteins: elucidation of the structural motifs that are essential for antifreeze activity. *Angew Chem Int Ed Engl* **2004** 43(7):856-62.

Takeuchi A. et al., Oral administration of xanthan gum enhances antitumor activity through Toll-like receptor 4 *International Immunopharmacology* **2009** 9, 13 1562–1567.

Tsai C.M. et al., A sensitive silver stain for detecting lipopolysaccharides in polyacrylamide gels. *Anal Biochem* **1982** 119: 115-119.

Ummarino S. et al., Determination of phosphorylation sites in lipooligosaccharides from *Pseudoalteromonas haloplanktis* TAC 125 grown at 15°C and 25°C by nano-electrospray ionization quadrupole time-of-flight tandem mass spectrometry. *Rapid Commun Mass Sp* **2003** 17: 2226-2232.

Valle J. et al., Broad-spectrum biofilm inhibition by a secreted bacterial polysaccharide. *PNAS* **2006** 103, 33, 12558–12563

Vaughan D.G., et al. Observations: Cryosphere. *Climate Change 2013: The Physical Science Basis*. Contribution of Working Group I to the Fifth Assessment Report of the Intergovernmental Panel on Climate Change, eds Stocker TF, et al.(Cambridge University Press, Cambridge), **2013** pp. 317-382.

Vinogradov E. et al., Structural analysis of the intact polysaccharide mannan from Saccharomyces cerevisiae yeast using 1H and 13C NMR spectroscopy at 750 MHz *Carbohydrate Res*. 1998, 307, 177-183

Vishnivetskaya, T. et al.,. Low-temperature recovery strategies for the isolation of bacteria from ancient permafrost sediments. *Extremophiles* **2000** 4**:**165–173.

Walters K.R. et al., A nonprotein thermal hysteresis-producing xylomannan antifreeze in the freeze-tolerant Alaskan beetle *Upis ceramboides*. *Proc. Natl. Acad. Sci.* **2009**, *106*, 20210-20215.

Westphal O., et al., Bacterial lipopolysaccharides: extraction with phenol-water and further applications of the procedure. *Methods Carbohydr. Chem*., **1965**, 5, 83–91.

Whitfield C. Biosynthesis and assembly of capsular polysaccharides in Escherichia coli. *Annu Rev Biochem* **2006** 75:39–68

Wiggins P. Life depends upon two kinds of water. *PLoS One* **2008** 9:e1406

Woese C.R. Towards a natural system of organisms: proposal for the domains Archaea, Bacteria, and Eucarya. *PNAS* **1990** 87, 12, 4576–4579

Yeh, Y. et al., Antifreeze proteins: Structures and mechanisms of function. *Chem. Rev.* **1996**, *96*, 601–618.

Zinn M, et al., Occurrence, synthesis and medical application of bacterial polyhydroxyalkanoate. *Adv Drug Deliv Rev* **2001**;53:5–21.

Zych, K. et al., Structure of the O-specific polysaccharide of *Proteus penneri* strain 41 from a new proposed serogroup O62. *Fems Immunol. Med. Mic.* **1998**, *21*, 1-9